Wave effect mitigation on floating offshore wind turbines through feedforward data-driven predictive control

Alexandra Ministeru

Master of Science Thesis

TU Delft Delft University of Technology

Delft Center for Systems and Control

Wave effect mitigation on floating offshore wind turbines through feedforward data-driven predictive control

Master of Science Thesis

Alexandra Ministeru

February 19, 2024

Faculty of Mechanical Engineering (ME) · Delft University of Technology

Delft Center for
Systems and Control

Delft University of Technology
Department of
Delft Center for Systems and Control

The undersigned hereby certify that they have read and recommend to the Faculty of Mechanical Engineering (ME) for acceptance a thesis entitled

Wave effect mitigation on floating offshore wind turbines through feedforward data-driven predictive control

by

Alexandra Ministeru

in partial fulfillment of the requirements for the degree of

Master of Science Systems & Control

Dated: February 19, 2024

Supervisor(s):

Prof. dr. ir. J.W. van Wingerden

A.R.M. Hegazy

Reader(s):

Dr. M. Guo

Ir. R.T.O. Dinkla

Abstract

Floating offshore Wind Turbines (FOWTs) pave the way to accessing deep water regions with abundant wind resources that are unreachable to bottom-fixed turbines. This technology is not widely deployed due to the increased cost of producing energy. A suitable control strategy can improve the power quality and extend the lifespan of the FOWT, resulting in a reduction of the final cost of energy. However, FOWTs face a specific set of control challenges in the above-rated operational region, such as the negative damping issue, rough environmental conditions, and increased model complexity due to both the floating structure and the increase in wind turbine size. Advanced control strategies are the most suited to resolve the negative damping problem, but obtaining a control model that balances low complexity with good accuracy is an increasingly difficult task. To mitigate the effect of environmental disturbances, feedforward control using wind preview is most commonly employed. Although waves have been shown to increase rotor speed oscillations and turbine loads, wave preview-based methods remain scarce.

This thesis implements a model-free, feedforward controller based on wave preview for the above-rated region of a FOWT. The controller uses a preview of wave forces acting on the floating platform and aims for simultaneous rotor speed regulation and platform motion reduction using collective blade pitch control. As a model-free approach, a modified Data-enabled Predictive Control (DeePC) formulation that considers past and future information about measurable disturbances is proposed. The controller is implemented with a linear model of the NREL 5-MW wind turbine installed on the OC3-Hywind spar-buoy platform and tested in several cases. The effectiveness of the wave feedforward data-driven controller is evaluated in a high-fidelity environment using the QBlade simulator. A decrease in rotor speed variance of 67% and platform pitching motions of 71% is obtained, at the cost of a 7-fold increase in blade pitching effort compared to the baseline controller. In turbulent wind conditions, the wind proved to be the dominant disturbance, and including both wind and wave previews in the controller is recommended. This work demonstrated the feasibility of a model-free feedforward control strategy for wave effect mitigation in FOWTs. Further efforts are required to adapt this strategy to closed-loop operation and to validate its effectiveness across the entirety of the above-rated region.

Table of Contents

List of Figures

List of Tables

Acknowledgements

Although wind turbines are a topic that is very close to my heart, working on this thesis proved to be a challenging journey. I am grateful for all the encouragement and support I have received from the people around me.

Firstly, I would like to thank my daily supervisor, Amr Hegazy, for all the time and invaluable guidance he offered me during the course of this thesis. The expertise and creative suggestions he shared during our regular meetings were crucial for my progress. Furthermore, I would like to express my gratitude towards my main supervisor, prof. dr. ir. Jan-Willem van Wingerden, for his patience, constructive ideas, and feedback that kept me on the right track. I would also like to thank ir. Rogier Dinkla for his insights on data-driven control, his feedback on my implementation, and his valuable remarks. My thanks also go out to ir. Daniel van den Berg for his help with QBlade.

I am grateful to my friends Sachin, Knut, and Liam. Thank you for all the times we shared our challenges and attempted to solve them together. Our countless discussions inspired me and taught me how to keep an open mind.

Finally, I would like to thank my family: my mother, Luminița, for being a model of courage and decisiveness, my father, Iulian, for nurturing my curiosity and for his thoughtfulness, my sister, Sabina, for her incessant support and encouragement, and my cousin, Alice, for being an incredible pillar of support.

Delft, University of Technology
February 19, 2024

Alexandra Ministeru

Chapter 1

Introduction

Energy is crucial for human life and development, and ensuring a reliable source is of high priority. Currently, fossil fuels are still the primary energy source, accounting for 83% of the global energy consumption in 2020 [5]. Aside from the imminent depletion [6], the greenhouse gases that result from fossil fuel combustion pose numerous threats, with two of the most prominent being air pollution-related health issues [7] and climate change. The risks associated with climate change are manifold: local species loss, extreme meteorological phenomena, water scarcity, decrease of food availability, ocean warming and acidification, and sea-level increase threatening coastal and low-lying regions [8]. The effect of climate change is often summarized by the evolution of the global mean temperature. Compared to pre-industrial times, an increase of 1.2 °C is currently observed [9]. Limiting the temperature increase to 1.5 °C, as advised by the Intergovernmental Panel on Climate Change, would require achieving net zero carbon dioxide global emissions by 2050 [8].

It is thus essential to act towards a transition from conventional fuel to alternative sources, and renewable energy plays a key role in this process. A 6-fold increase in renewable energy production would be required to achieve carbon neutrality by 2050 [5]. Wind and solar energy already account for a large share of the current clean energy production and are expected to be the main contributors to the decarbonization challenge [10, 11]. Wind represents a reliable and secure source of energy [12] that is currently moving to the broad market. At present, there is a 255 GW wind power capacity installed in Europe, out of which 19.1 GW were installed in 2022. The majority of this figure is covered by onshore wind energy, which amounted to 87% of the new installations [13].

Despite the popularity of onshore wind turbines, the visual impact and noise pollution are two frequent objections of neighboring communities. As a solution, the wind energy sector expanded to offshore locations. This is highly beneficial for energy extraction: the earth's irregular surface, which lowers the speed of wind due to friction, is significantly reduced at sea. Recently, it was concluded that the average power of new offshore turbines is almost double compared to their onshore counterparts [13] since deploying at sea allows for larger-scale wind turbine installation. Additionally, the environmental impact of offshore wind farms proved to have a lower magnitude compared to the onshore farms [14]. However, a fixed-bottom offshore wind turbine can only be placed in shallow waters, up to a depth of 60 meters [15], and is thus often still visible from the shore. Offshore wind turbines become economically unfeasible in deep water due to the costs associated with the seabed foundation. In

addition, appropriate locations that do not intersect with navigation routes must be identified. Consequently, a new solution was introduced, namely Floating offshore Wind Turbines (FOWTs), which enable extracting resources from sites that are not accessible to fixed-bottom offshore wind turbines. Nevertheless, despite being an attractive concept, FOWTs are yet to gain popularity in industry [12].

The technology behind FOWTs is considered young relative to other clean energy sources, with high associated risks, hence the investment hesitation. The Levelized Cost of Energy (LCOE) is often used as a standardized cost comparison metric across different sources of energy. In the case of a wind turbine, the LCOE represents the energy production cost over its lifetime [16]. Currently, the LCOE of onshore wind energy reached a similar or even lower level compared to conventional energy, making it a competitive alternative [17]. The LCOE of offshore wind energy is still higher and would need further reduction to become an attractive choice. Floating offshore wind energy has an even larger cost. Nevertheless, it has the potential to be lowered through technological advancements: the estimated cost reduction for floating wind energy is predicted to reach up to 50% by 2050 [18].

Control design plays a key role in FOWT development that may eventually lead to commercial deployment. From a control engineering point of view, LCOE reduction may be achieved by decreasing operational and maintenance costs and/or increasing the lifetime energy production [16]. Reducing maintenance expenditures can be done by lowering the loads on the wind turbine components, which in turn leads to less maintenance and downtime necessary, along with an extended lifespan. The lifetime energy production can be increased by controlling the wind turbine such that optimal power output is obtained, meaning power maximization below the rated wind speed and fluctuation reduction above-rated wind speed.

The remainder of the chapter is structured as follows. Section 1-1 gives a definition of FOWTs, along with a short description of conventional wind turbine control. The control challenges posed by FOWTs are then discussed in Section 1-2, followed by a short literature review of state-of-the-art control solutions in Section 1-3. The knowledge gap is outlined and translated into a research question in Section 1-4. Finally, Section 1-5 outlines the main structure of this thesis.

1-1 Background

1-1-1 Definition of a FOWT

A FOWT consists of a regular wind turbine installed on top of a floating platform. Commonly employed floating platforms are inspired by the ones found in the offshore oil and gas industry [19]. They fall into four categories: spar-buoy, Tension Leg Platform (TLP), barge, and semi-submersible, as illustrated in Figure 1-1. All of them achieve stability using a combination of the three floating principles: ballast, mooring lines, and buoyancy [20]. Spar-buoys are ballast stabilized, TLPs rely on mooring line tension, the barge uses buoyancy as the main floating principle, while the semi-submersible is a blend of buoyancy and mooring line stabilization. Each design type has its advantages and trade-offs. Wave sensitivity, water depth independence, and onsite installation complexity are only a few of the challenges that affect the platform choice [19, 20].

1-1-2 Wind turbine control notions

Wind turbines come in a variety of configurations with specific control schemes. This thesis considers a category often encountered among utility-scale modern wind turbines: a 3-bladed variable-speed horizontal-axis variable-pitch wind turbine.

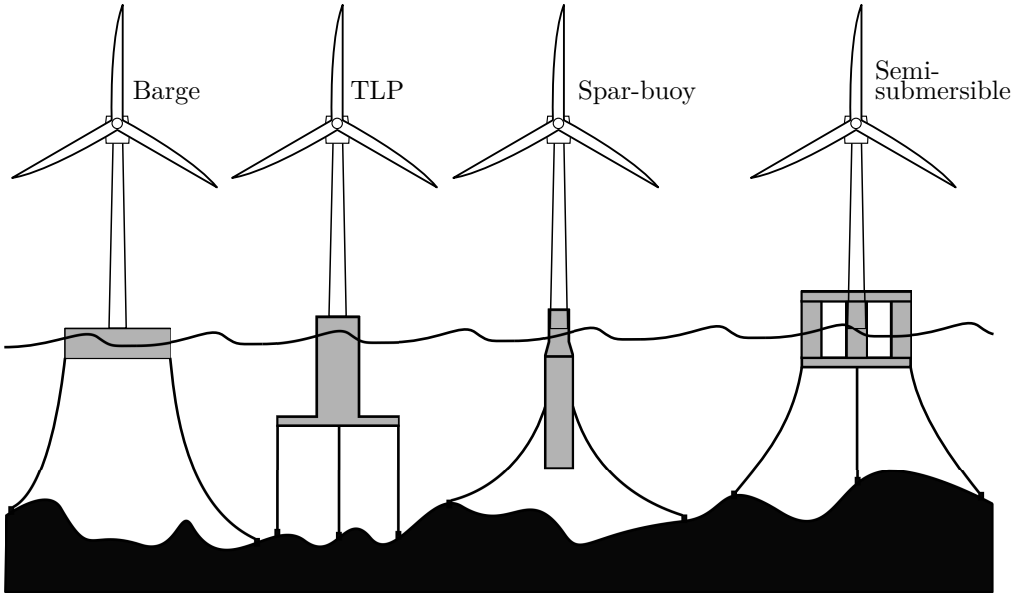

Figure 1-1: The four types of FOWT platforms.

Currently, the control strategy used for FOWTs is often an adapted version of the onshore wind turbine controller [21]. An overview of the baseline controller of onshore wind turbines is therefore given first.

A wind turbine usually has three hierarchical levels of control [22]. Firstly, supervisory control represents the highest level of control and is responsible for wind turbine startup and shutdown. Secondly, turbine control, the middle level, ensures that the control objectives are fulfilled and it includes generator torque control, blade pitch control, and yaw control. Lastly, on the lowest level, subsystem control is concerned with pitch and nacelle yaw actuators and the internal generator. In what follows, the turbine (or operational) control is of interest because this is where control objectives such as reference tracking or load mitigation are approached.

Two main types of control are used in the operational wind speed range of a wind turbine, namely generator torque control and blade pitch control. Yaw control is not discussed here, but its main purpose is to ensure that the nacelle is aligned with the wind direction. The baseline controller implements these as two separate Single-Input Single-Output (SISO) control loops, illustrated in Figure 1-3. The loops are active in separate regions and are, thus, decoupled. A switching strategy is used to change controllers between the operational regions [21].

The dependency of power production on the incoming wind speed is usually represented as a power curve. The typical shape of the power curve for a wind turbine can be seen in Figure 1-2. Both control loops are based on the expression of power given in

$$P = \tau_{\mathrm{g}} \cdot \omega_g, \tag{1-1}$$

where P is the power, τ_{g} is the generator torque, and ω_g is the generator speed. Before being fed back to the control loops, the generator speed is filtered with a low pass filter to prevent high-frequency excitation of the control system [1].

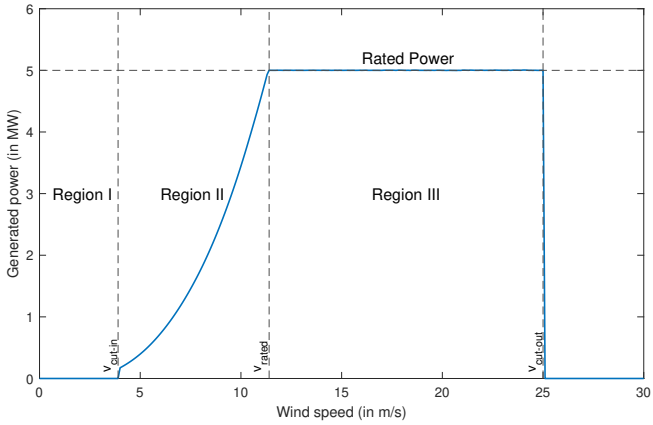

Figure 1-2: Power curve and operation regions of the reference 5 MW NREL wind turbine [1], where $v_{\text{cut-in}}$, v_{rated} and $v_{\text{cut-out}}$ represent the cut-in, rated, and cut-out wind speed respectively. In Region I, the wind turbine is inactive due to the losses outweighing the potential power production [2]. In Region II or partial load region, the wind turbine maximizes wind power extraction. In the full load region or Region III, the power production is limited to the rated value such that safety loading thresholds are not surpassed.

The generator torque control loop aims for optimal energy production by maximizing power. This is achieved by setting the generator torque whilst keeping the blade pitch angle θ constant at the value corresponding to the optimal tip-speed ratio and, consequently, to the optimal power coefficient [2]. To this end, a nonlinear controller such as $\tau_{\text{g}} = k_{\text{opt}}\omega_g^2$ is used, where the constant k_{opt} is known as the optimal mode gain.

In the full load region, the generator torque has already reached the rated value and must be kept constant. This is done by pitching the blades to reduce aerodynamic thrust and track the reference generator speed.

There are two types of pitching strategies: Collective Pitch Control (CPC) or Individual Pitch Control (IPC). With CPC, every blade pitch actuator receives the same command. In the case of IPC, a different pitch angle is computed for each of the blades. A proportional-integrative (PI) controller with collective blade pitching is commonly employed [2]. The pitch command is computed as

$$\theta_c(t) = k_{\text{P}}\omega_e(t) + k_{\text{I}}\int_0^t \omega_e(\tau)\text{d}\tau, \tag{1-2}$$

where $\omega_e = \omega_g - \omega_{g,\text{ref}}$ is the generator speed error, k_{P} is the proportional gain, and k_{I} is the integral gain. It is important to mention that a wind turbine has a nonlinear behavior that changes with the incoming wind speed. As a consequence, the baseline above-rated controller is a scheduled PI, where each operating point has appropriately tuned gains. So far, generator speed tracking has been considered to be the main control objective. However, the focus can be also shifted to explicit load mitigation [23], case in which a Gain Scheduled PI (GSPI) controller with collective blade pitching is the usually employed technique [24] as well.

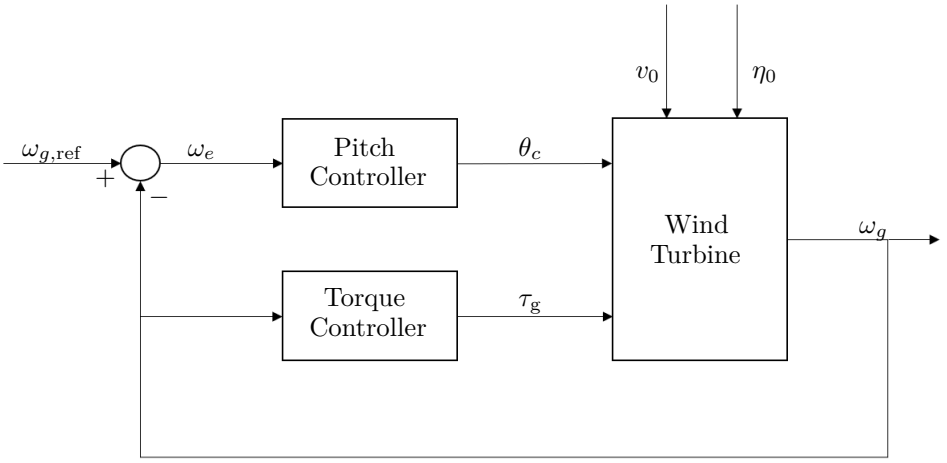

Figure 1-3: The two control loops of the baseline wind turbine controller. Wind disturbance v_0 and wave disturbance η_0 act on the wind turbine system, but are not explicitly taken into account in the control loops.

1-2 FOWT control challenges

Due to their nature and placement in environments with harsh environmental conditions, FOWTs face distinctive issues compared to fixed-bottom wind turbines, which makes the control of such plants a non-trivial challenge. These control issues can be categorized as follows.

Platform dynamics and model complexity The floating platform introduces complexity to the dynamical behavior of the wind turbine due to the extra Degrees of Freedom (DoFs), namely, the three translations along the axes (surge, sway, heave) and their corresponding rotations (pitch, roll, yaw) [25]. This has two consequences: first, instability for all types of platforms [19], which ensues the challenge of developing stabilizing control systems for each platform typology [21]. Second, an increase in model complexity due to additional rotor motions [26], and the growing size of FOWTs [27]. Numerous advanced control strategies, such as Linear Quadratic Regulator (LQR) or Model Predictive Control (MPC) require a model of the controlled system. The model must balance between accuracy and reasonable complexity since the control algorithm must have a feasible computation time. Therefore, the increase in complexity represents a challenge that requires consideration during control system design.

Negative damping Mounting a wind turbine on top of a floating platform lowers the natural frequencies of the system compared to the fixed-bottom counterparts, in particular the pitch eigenfrequency. As a consequence, using a traditional onshore wind turbine controller for a FOWT in the above-rated region leads to a coupling between the platform pitching motion and blade pitch control due to pitch regulation becoming too fast compared to the tower movement. This is a control challenge known as negative damping, illustrated in Figure 1-4.

From a control theory point of view, the issue is caused by a pair of right-half plane zeros that limit the bandwidth of the blade pitch controller [28]. Increasing the gain of the control system causes the poles of the closed-loop to migrate towards the open-loop zeros, which eventually leads to instability [29].

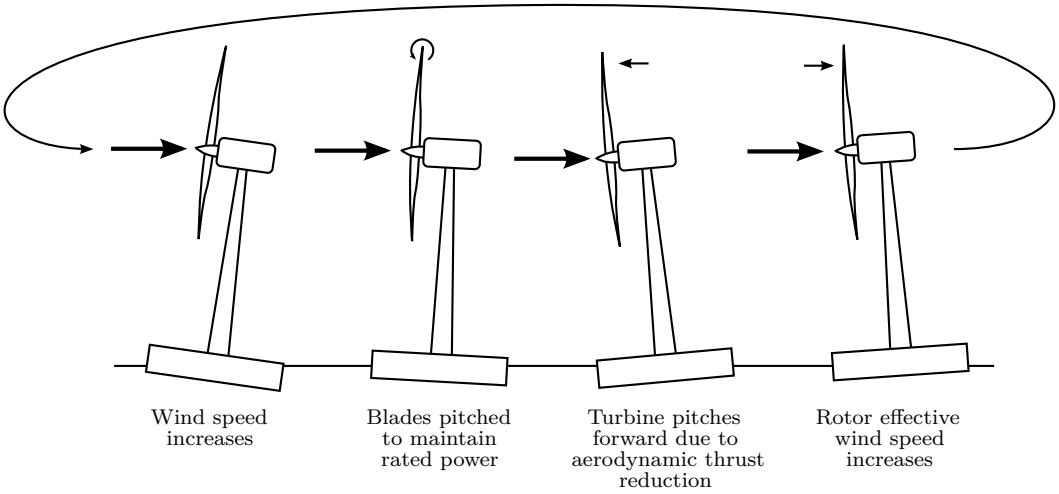

Figure 1-4: Physical representation of the negative damping phenomenon, the central arrows indicate the evolution from left to right: when the Rotor-Nacelle Assembly (RNA) moves forward, the rotor is subjected to a higher relative wind speed. Consequently, the blades are pitched out of the wind direction to slow the rotor. The aerodynamic thrust is then reduced, causing further forward motion of the RNA, triggering once again the same course of events. This results in negative aerodynamic damping, with the converse phenomenon happening when the platform is pitching downwind [3].

This non-minimum phase behavior induces larger generator speed oscillations and increased tower base bending moments relative to fixed-bottom wind turbines [30, 31]. A control authority conflict is therefore present in the above-rated region for FOWTs due to the trade-off between rotor speed regulation and platform pitching motion reduction [32]. This highlights the necessity of a multi-objective controller.

Disturbances FOWTs operate in locations with complex environmental disturbances which can be separated into two categories: aerodynamic and hydrodynamic [21]. Aerodynamic perturbations include turbulent wind, wind shear (an issue accentuated by increasing rotor diameters), and tower shadow. Hydrodynamic loads on the floating platform are caused by radiation and diffraction effects due to incident waves, along with currents [25, 33].

These two types of disturbances have a combined effect on the wind turbine, resulting in stability issues, decreased performance due to oscillations, and higher structural loads in the tower and blades compared to non-floating structures [19] that eventually negatively impact the lifespan of the wind turbine. Among the wave-induced effects, increased tower-base load cycles and blade pitch actuation are found to be of significant importance [34]. The baseline fixed-bottom wind turbine controller is not designed to consider these issues. Thus, the control challenge resides in accounting for the added external factors during the control design stage, and potentially including future knowledge of incoming disturbances [35–37].

1-3 State-of-the-art control strategies

This section gives an overview of state-of-the-art FOWT control strategies with CPC in the above-rated region. Another category of solutions relies on additional actuation: blades may also be pitched

individually, a strategy known as IPC. IPC is commonly used to lower 1P (once per revolution) loads [38], but power regulation and platform motion reduction can also be achieved [39, 40]. However, IPC leads to increased load cycles on the pitching system [40], which can further result in a shortened lifetime of the wind turbine. Additionally, pitching the blades individually may introduce a destabilizing roll moment [38, 39], which must be accounted for. In FOWTs, the reduction in 1P blade loads is overshadowed by the magnitude of blade loads caused by thrust variations due to platform motions. As a consequence, the use of IPC is less effective on individual floating turbines compared to the fixed-bottom counterparts [38]. Thus, IPC is not further discussed.

1-3-1 Baseline controller adaptations

There are numerous attempts at adapting the conventional controller of a fixed-bottom wind turbine for challenges specific to FOWTs. Many of these modifications are made in an attempt to solve the negative damping issue. There are three main approaches: introducing additional control loops, pitching-to-stall, and gain detuning. Alternatively, the traditional feedback (FB) controller can be extended with a feedforward (FF) block to combat delayed compensation.

Additional control loops Using additional sensor measurements is one of the explored possibilities, which is often referred to as the "parallel compensation approach". Control loops using tower-top acceleration measurements [29, 30], or even both platform pitch and nacelle velocity [41] are appended to the baseline controller. The method is found to lead to a conflict between the two blade pitch control systems, and degradation in generator speed tracking [29]. Additionally, the proximity of the platform's natural frequencies to the wave frequency range points out the imminent coupling between these control loops and, consequently, the difficulty in counteracting wave disturbances using feedback control.

Pitch-to-stall In the full-load region, the control system is usually pitching-to-feather. A briefly researched idea is to use pitch-to-stall instead. Although Larsen and Hanson show promising results [3], this method proved to be ineffective in the simulations carried out by Jonkman, where, even if turbine power tracking improved, platform motions were amplified [30]. This discrepancy, however, may be caused by the different types of floating platforms used.

Gain detuning Lastly and the most effective of the three is gain detuning. The GSPI can be modified by lowering the gains in an attempt to lower the bandwidth of the blade pitch controller such that it falls below the natural frequency of the tower (and wave-excitation frequency) [30]. This approach results in a platform pitching motion reduction at the cost of generator speed tracking degradation.

Several variations of gain detuning have been explored: non-static generator speed tracking [38], scheduled detuning [31, 42, 43], and robust gain scheduling ensuring a stability margin around each operating point [44]. In all cases, platform stability comes at the cost of large rotor speed and power oscillations. Therefore, gain detuning alone does not represent an effective solution and advanced control strategies are deemed necessary to deal with this control challenge.

Feedforward control The industry-standard controller only relies on output feedback. As a consequence, disturbances can only be counteracted once they have occurred. However, methods of measuring and estimating perturbations are available. For control purposes, the use of nacelle-mounted

LIght Detection And Ranging (LIDAR) systems gained popularity [35]. Wave excitation forces can be estimated based on data from water elevation sensors through wave prediction models [36]. Given that control performance can be significantly improved by using future information of exogenous signals [45], the FOWT baseline controller can be enriched with an additional FF controller based on incoming wind and/or wave disturbances (Figure 1-5).

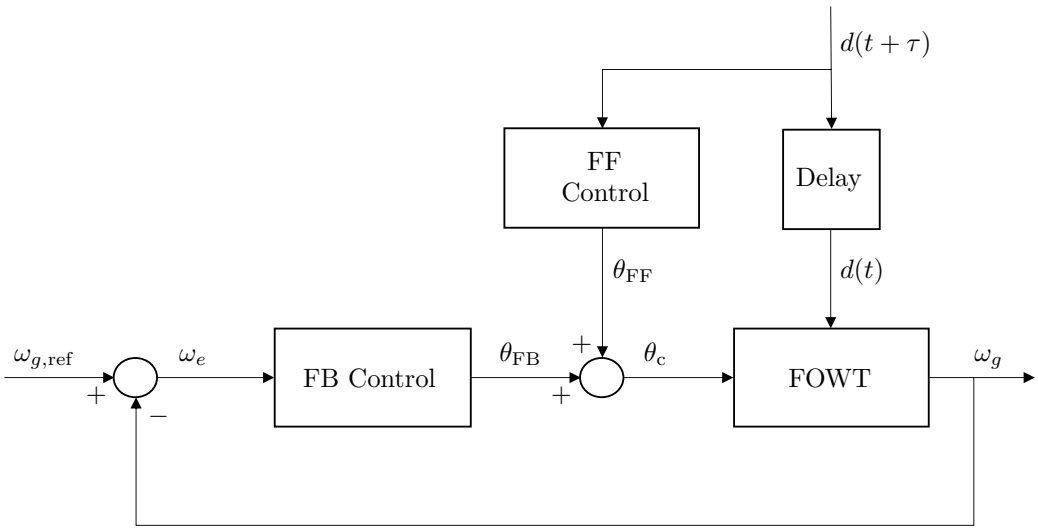

Figure 1-5: FF-FB blade pitch controller with disturbance preview. The disturbance is available to the FF controller τ seconds before it affects the FOWT.

Future wind disturbance is most often employed [46, 47]. The strategy is based on inversion FF control and it shows great potential in reducing both platform pitching motion and rotor speed fluctuation.

The topic of wave disturbance-oriented FF control is, however, scarcely approached, despite the considerable impact of waves on the FOWT. Traditional FB turbine control has been shown to not be sufficient for wave disturbance mitigation [48]. Model-inversion based FF control leads to increased performance and lower turbine loads, at the cost of increased blade-pitch activity, along with higher mooring line loads, highlighting the challenge of multi-objective control in a SISO setting [34].

1-3-2 Advanced control methods

Ultimately, SISO control is deemed insufficient [30, 49], and advanced Multiple-Input Multiple-Output (MIMO) control strategies are largely recommended. Thus, a multitude of advanced control methods have been explored for FOWTs, including LQR [39, 50, 51], $\mathcal{H}_\infty$ control [52–54], mixed $\mathcal{H}_2$ /$\mathcal{H}_\infty$ control [55], as well as Disturbance Accommodating Control (DAC) [56], and Linear Parameter Varying (LPV) control [51, 57]. Advanced control strategies are also combined with FF control, which usually relies on LIDAR-based wind measurements [54, 58, 59]. Again, research on wave preview control is quite rare [36, 60], and it is even stated that LQR can not effectively cancel out wave disturbances, despite the improvements it brings [49].

The model-based advanced control strategies mentioned so far can set and prioritize control objectives but are not able to explicitly consider constraints. However, a wind turbine is an inherently constrained system: the power output must be kept within safety intervals, blade pitch angles are physically

limited, and loads must also be accounted for (e.g. the blade pitching rate should be bounded to prevent fatigue damage).

Of particular interest is the MPC framework, which can handle constrained MIMO systems while also including preview information. MPC is a well-researched topic for non-floating wind turbines and has also been implemented for floating structures with good results [61–63].

Since MPC entails an optimization process over a finite time horizon, it was a natural step to include preview information of incoming disturbances in the framework. Wakui et al. integrated both wind and wave disturbance knowledge into an MPC for a FOWT. Including both signals led to higher performance in terms of platform stabilization and load reduction than an MPC that only uses wind preview [64].

Along with all advanced control methods, MPC requires a good model of the system. A high-fidelity representation of a FOWT is too complex to be used during control design. As a solution, control-oriented Reduced-Order Models (ROMs) derived from the first principles of physics were developed [25, 61, 65]. However, capturing the complex behavior of a FOWT within a Linear Time-Invariant (LTI) model is turning into a challenge. Thus, Nonlinear Model Predictive Control (NMPC) is attempted as well: wind and wave preview have been included in such a setting with excellent results [66]. However, the nonlinear model also induced increased computational complexity, making the controller infeasible for real-life usage.

1-3-3 Model-free control

Two issues arise during the modeling stage of a wind turbine. First, the increase in size leads to an accentuation of nonlinear phenomena, along with difficulty in deriving a control-oriented model with a sufficient level of fidelity [27]. Second, obtaining an accurate model of a process is a costly process that requires considerable effort and expert knowledge [67]. The assumptions and simplifications made during the modeling stage, along with manufacturing differences and unmodeled sensor or actuator dynamics can lead to model mismatch, which, in turn, affects the robustness and the safety of the closed-loop control system [67]. Thus, circumventing the need for a system model during control design is a topic of interest, which leads to the field of model-free control.

A considerable amount of data can be collected from wind turbine sensors and used for controller design, without requiring a system model beforehand. These methods fall under the Data-Driven Control (DDC) approach. Since a process model is never used, issues such as model uncertainty, unmodeled dynamics, model complexity, or nonlinearity no longer present a limitation [67].

Direct DDC methods use input-output data to obtain future control commands without explicitly computing a system realization in the process [68]. Among direct DDC approaches, Subspace Predictive Control (SPC) and Data-enabled Predictive Control (DeePC) propose frameworks similar to that of MPC, allowing for a constrained optimization criterion applied in a receding horizon manner. These methods can be straightforwardly used in a reference tracking setting, but SPC has also been successfully adapted for periodic load mitigation [69]. Regarding disturbance preview, LIDAR wind knowledge has been recently integrated into the SPC algorithm [70].

1-4 Research question

The previous sections outlined the main challenges of controlling a FOWT and presented how they have been addressed in the literature. Despite the abundance of both SISO and model-based MIMO

approaches, two aspects have been only scarcely addressed: the model complexity and the inclusion of wave preview information. A summary of proposed controller features along with the corresponding issues they solve would therefore be:

1. Multi-objective optimal control: a solution to the control authority conflict caused by the negative damping problem that was not resolved through SISO methods.
2. Feedforward action based on wave preview knowledge: early mitigation of the negative effects of wave disturbances.
3. Data-driven approach: circumvention of the modelling stage and the subsequent challenges posed by the increase in model complexity.

Concerning the data-driven approach, a direct method is preferred because no system realization is obtained in the process [29]. Additionally, current formulations of DeePC often approach the challenge of non-measurable process and output noise, while measurable disturbances are not considered. Therefore, including measurements of past and future disturbances in the mathematical framework of DeePC represents an open research opportunity. Providing a disturbance preview is expected to result in a better prediction of the system response and a subsequent feedforward control action that has the potential to mitigate the effect of hydrodynamic disturbances in the context of floating wind turbine control.

It is hypothesized that a controller that combines these characteristics results in a framework that addresses the proposed control objectives, challenges, and shortcomings. The question then resides in how these elements can be assembled into a FOWT control structure. This paves the way for a formulation of the research question:

Can a data-driven, feedforward, predictive controller that includes wave disturbance preview be synthesized for a floating offshore wind turbine?

To answer this question, the following four sub-questions will be considered:

1. How may the DeePC algorithm be extended to include knowledge about incoming disturbances?
2. What adaptations are necessary to implement this algorithm on a FOWT using wave preview?
3. Can this data-driven control method be integrated with a high-fidelity wind turbine simulator?
4. How does the developed control strategy perform compared to a conventional controller?

1-5 Report Structure

This thesis consists of six chapters. The first chapter provided an introduction to FOWT control strategies and outlined the research question. Chapter 2 aims to answer the first research sub-question by proposing an adaptation of the DeePC framework present in literature that includes both past and future disturbance knowledge.

In Chapter 3, the wind turbine and floating platform type used throughout this thesis are defined. A linearization of the plant at an operating point in the above-rated region is first obtained using OpenFAST [71] to enable a simplified environment for controller design and implementation.

Chapter 4 focuses on the second research sub-question. Two control goals are considered, rotor speed tracking and platform motion reduction. The wind turbine linear model is first adapted for control purposes. Then, appropriate sampling time, data window sizes, and parameter tuning are identified. The multi-objective controller is tested in several load cases with various wind and waves scenarios. A baseline PI controller is used for comparison purposes, both in overall performance and frequency response. In this chapter, the simulation of the baseline controller is carried out using OpenFAST.

Chapter 5 addresses the third research sub-question. The data-driven feedforward controller is evaluated in a high-fidelity environment using the QBlade simulator [72]. The wind turbine is subjected to the same load cases as in the linear setting. A baseline controller is used as a benchmark to evaluate the performance of the controller. Along with Chapter 4, this chapter provides an answer to the last sub-question.

Finally, Chapter 6 revisits the research question and draws a general conclusion of this thesis. Future research directions and recommendations are suggested.

Chapter 2

Disturbance feedforward DeePC

The Data-enabled Predictive Control (DeePC) framework notably resembles the one of Model Predictive Control (MPC): it is based on solving an optimal control problem in real-time at each time step over a prediction horizon. An optimal input sequence is obtained by minimizing a cost that is usually defined by an objective function consisting of terms that quantify the control goals. These terms are penalized using tuned weights. The optimization problem is constrained by system dynamics, as well as user-defined bounds. Then, only the first computed input is applied to the controlled system, and the optimization starts over with a newly obtained set of measurements.

DeePC falls into the category of direct Data-Driven Control (DDC) methods, meaning that no system matrices are explicitly computed from the data, and the state of the system is not recovered. Therefore, no system description is available to restrict the optimization problem to dynamics specific to the controlled plant. Instead, DeePC relies on behavioral systems theory [73] and is based on Willems' fundamental Lemma [74]. The dynamical system is described in terms of the signal subspace in which its trajectories live. If given a sufficiently persistently exciting input signal, future input-output trajectories are fully parameterized by this one past input-output trajectory. Thus, the system behavior is described as a linear relation between past and future data.

A few aspects must be considered. First, in a real setting, noise affects the process and the measurements. To this end, regularizations [68] or instrumental variables [4] are proposed to mitigate the effect of noise. Next, model-independent stability and robustness analysis methods specific to the DDC algorithm are necessary [67] and are actively researched [75]. Lastly, the controller may eventually rely on closed-loop data, which leads to a bias when noise is present [76].

The purpose of this chapter is to propose a DeePC derivation that considers a measurable disturbance input. Section 2-1 describes the problem formulation, the notations, and the assumptions used. In Section 2-2, the characteristic equation of DeePC with disturbance information is derived, starting from the data equations. Instrumental variables are also included as a method of dealing with noise-corrupted data. Section 2-3 presents the disturbance DeePC algorithm, along with constraints and optimization approach.

The following is based on and closely follows the derivation of van Wingerden et al. [4]. Moreover, Dinkla et al. present a similar approach to the wind turbine disturbance feedforward problem focused on Subspace Predictive Control (SPC) [70].

2-1 Setup and assumptions

The setup consists of an unknown system with access to input, output, and disturbance signals. The system may have multiple input and output channels. However, no other system description is available. The DeePC problem can be primarily described as follows:

Problem formulation Starting from a set of input, output, and disturbance data points generated by an unknown system, find a relation between future system outputs over a given prediction horizon, future inputs, and previously collected data.

2-1-1 Model structure

The underlying process assumed to generate the input-output data sets is a discrete-time Linear Time-Invariant (LTI) system described by a state-space model in innovation form:

$$x_{k+1} = Ax_k + B_u u_k + B_w w_k + Ke_k, \tag{2-1a}$$
$$y_k = Cx_k + D_u u_k + D_w w_k + e_k, \tag{2-1b}$$

where $x_k \in \mathbb{R}^n$, $u_k \in \mathbb{R}^r$, $w_k \in \mathbb{R}^q$, $y_k \in \mathbb{R}^\ell$, represent the state, input, disturbance, and output vectors respectively, while $k \in \mathbb{Z}_{\geq 0}$ indicates the discrete time index. The system is subject to measurement and/or process noise, $e_k \in \mathbb{R}^\ell$ representing an ergodic white noise signal with zero mean and covariance matrix $\mathbb{E}\{e_j e_k^{\mathrm{T}}\} = S\delta_{ij}$, with $S \succ 0$ and δ_{ij} being the Kronecker delta function. Matrices $A, B_u, B_w, K, C, D_u, D_w$ are the state, control input, disturbance input, Kalman, output, direct feedthrough, and disturbance direct feedthrough matrices respectively of appropriate dimensions. Although the disturbance acts as an input to the plant, it is represented separately from the control input because it is not controllable.

By eliminating e_k from Equation 2-1a, the system can be alternatively represented in the predictor form

$$x_{k+1} = \tilde{A}x_k + \tilde{B}_u u_k + \tilde{B}_w w_k + Ky_k, \tag{2-2a}$$
$$y_k = Cx_k + D_u u_k + D_w w_k + e_k, \tag{2-2b}$$

with $\tilde{A} = A - KC$, $\tilde{B}_u = B_u - KD_u$, $\tilde{B}_w = B_w - KD_w$. In what comes next, the ‘ $\tilde{}$ ’notation refers to the matrices of the predictor form of the system.

2-1-2 Notations

Several notations of frequently used matrices will be introduced before proceeding to the derivation of the DeePC framework that includes disturbance knowledge. A block-Hankel matrix is defined as:

$$U_{i,s,\bar{N}} = \begin{bmatrix} u_i & u_{i+1} & \cdots & u_{i+\bar{N}-1} \\ u_{i+1} & u_{i+2} & \cdots & u_{i+\bar{N}} \\ \vdots & \vdots & \ddots & \vdots \\ u_{i+s-1} & u_{i+s} & \cdots & u_{i+\bar{N}+s-2} \end{bmatrix}, \tag{2-3}$$

where $U_{i,s,\bar{N}} \in \mathbb{R}^{rs\times\bar{N}}$, $i \in \mathbb{Z}$, and $\{s,\bar{N}\} \in \mathbb{Z}_{>0}$. For clarity, i indicates the index of the first element of the matrix, s represents the block size, while $\bar{N}$ indicates the number of columns. To construct this block-Hankel matrix, $\bar{N}+s-1$ data samples are necessary. Similarly, the block matrices $Y_{i,s,\bar{N}} \in \mathbb{R}^{\ell s\times\bar{N}}$, $E_{i,s,\bar{N}} \in \mathbb{R}^{\ell s\times\bar{N}}$, and $W_{i,s,\bar{N}} \in \mathbb{R}^{qs\times\bar{N}}$ are defined, using output, noise and disturbance data respectively. In the case of block-Hankel matrices that have only one block-row ($s = 1$), the second index is omitted. This is the case for state sequences, with $X_{i,\bar{N}} \in \mathbb{R}^{n\times\bar{N}}$:

$$X_{i,\bar{N}} = \begin{bmatrix} x_i & x_{i+1} & \cdots & x_{i+\bar{N}-1} \end{bmatrix} \tag{2-4}$$

Block-Toeplitz matrices are defined as:

$$H^{(f)}_{(\tilde{B}_u,D_u)} = \begin{bmatrix} D_u & 0 & 0 & \cdots & 0 \\ C\tilde{B}_u & D_u & 0 & \cdots & 0 \\ \vdots & \vdots & \ddots & \ddots & \vdots \\ C\tilde{A}^{f-2}\tilde{B}_u & C\tilde{A}^{f-3}\tilde{B}_u & \cdots & C\tilde{B}_u & D_u \end{bmatrix}, \tag{2-5}$$

where $H^{(f)}_{(\tilde{B}_u,D_u)} \in \mathbb{R}^{\ell f\times rf}$. Similarly, $H^{(f)}_{(\tilde{B}_d,D_d)} \in \mathbb{R}^{\ell f\times qf}$ and $H^{(f)}_{(K,I)} \in \mathbb{R}^{\ell f\times\ell f}$ are defined, where I represents the identity matrix of appropriate size, and $f \in \mathbb{Z}_{>0}$ is the length of the prediction window.

Next, the extended controllability matrix is defined as:

$$\mathcal{K}^{(p)}_{(\tilde{B}_u)} = \begin{bmatrix} \tilde{A}^{p-1}\tilde{B}_u & \tilde{A}^{p-2}\tilde{B}_u & \cdots & \tilde{B}_u \end{bmatrix}, \tag{2-6}$$

with $\mathcal{K}^{(p)}_{(\tilde{B}_u)} \in \mathbb{R}^{n\times rp}$. Additionally, $\mathcal{K}^{(p)}_{(\tilde{B}_d)} \in \mathbb{R}^{n\times qp}$, and $\mathcal{K}^{(p)}_{(K)} \in \mathbb{R}^{n\times\ell p}$ are introduced, with $p \in \mathbb{Z}_{>0}$ being the length of the past data window. For conciseness, the controllability matrices are collected in $\mathcal{K} = \begin{bmatrix} \mathcal{K}^{(p)}_{(\tilde{B}_u)} & \mathcal{K}^{(p)}_{(\tilde{B}_d)} & \mathcal{K}^{(p)}_{(K)} \end{bmatrix} \in \mathbb{R}^{n\times(r+q+\ell)p}$.

Moreover, the extended observability matrix is given as:

$$\Gamma^{(f)} = \begin{bmatrix} C \\ C\tilde{A} \\ C\tilde{A}^2 \\ \vdots \\ C\tilde{A}^{f-1} \end{bmatrix}, \tag{2-7}$$

where $\Gamma^{(f)} \in \mathbb{R}^{\ell f\times n}$. Additionally, $\mathbf{1}_n = \begin{bmatrix} 1 & 1 & \cdots & 1 \end{bmatrix}^{\mathrm{T}} \in \mathbb{R}^n$. The identity matrix is denoted by I, while O and o stand for the zero matrix and vector respectively, all of suitable dimensions.

2-1-3 Assumptions

The following assumptions are used throughout the remainder of the chapter:

1. The input, output, and disturbance signals are measurable.
2. Disturbance preview of length f is available at any given point during the control stage.
3. e_k is a zero-mean white noise, uncorrelated to the input and disturbance signals.

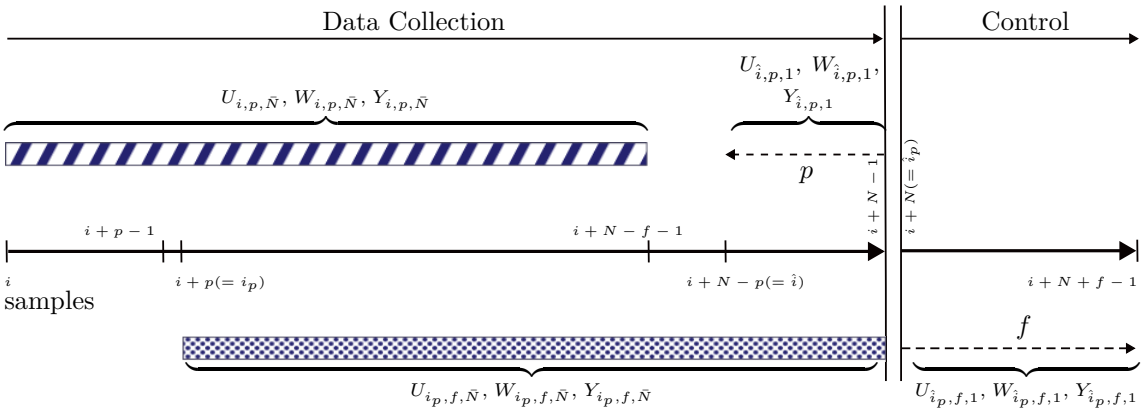

Figure 2-1: Partition of the data set used by the DeePC algorithm. The batch gathered during the offline data collection stage is split into two sets and used to derive the characteristic equation. During the online control stage, the last p measurements initialize the optimal controller and enable the prediction of the evolution of the future input-output trajectories over a future horizon of length f. Figure adapted from [4].

4. (2-1) is a controllable system in a minimal realization.
5. $\tilde{A} = A - KC$ has all the eigenvalues inside the open unit circle.
6. The length of the past window p is high enough to remove the bias given by initial states.
7. The length of the data set N is large enough to remove the influence of measurement noise.
8. The input sequence is persistently exciting of order at least $p + f + n$, where n is the order of the minimal representation in (2-1) [73].
9. The disturbance is also persistently exciting of at least order $p + f + n$.

2-2 The characteristic equation

2-2-1 The data equation

DeePC is based on the MPC framework [73]. However, in a data-driven approach, the system matrices are not available to constrain the search for an optimal command to a feasible region specific to the plant's dynamics. Instead, the plant behavior must be derived starting from available input-output trajectories. In other words, it is necessary to obtain a future output predictor over a finite time horizon based on previously collected input-output data, along with future inputs.

Synthesizing the DeePC controller requires a data collection stage. The length of the data set is N, and is typically chosen such that the number of columns of the block-Hankel matrices is significantly larger (100 times) than p and f [77]. Figure 2-1 illustrates the partitioning of the data used to derive the control algorithm.

The batch of data from the data collection step is first partitioned into two overlapping sets, the so-called past and the so-called future, represented in Figure 2-1 by the striped and the dotted bar,

respectively. The data points from the striped segment are organized in the $U_{i,p,\bar{N}}$ input, $W_{i,p,\bar{N}}$ disturbances, and $Y_{i,p,\bar{N}}$ outputs block-Hankel matrices, where $\bar{N} = N-p-f+1$. Similarly, matrices $U_{i_p,f,\bar{N}}$, $W_{i_p,f,\bar{N}}$, and $Y_{i_p,f,\bar{N}}$ are constructed using data from the dotted segment, where $i_p = i+p$. To derive the DeePC algorithm, a few additional data matrices are used. First, corresponding to the dashed arrow pointing to the left, the last p input-output samples of the data set are gathered in $U_{\hat{i},p,1}$, $W_{\hat{i},p,1}$, and $Y_{\hat{i},p,1}$, with $\hat{i} = i+N-p$. Then, starting from $\hat{i}_p = i+N$, the vectors $U_{\hat{i}_p,f,1}$, $W_{\hat{i}_p,f,1}$ and $Y_{\hat{i}_p,f,1}$ are employed. These vectors correspond to the dashed arrow pointing toward the right of the sample axis, which is outside of the collected data set. It is important to note that $U_{\hat{i}_p,f,1}$ and $Y_{\hat{i}_p,f,1}$ contain unknown samples, while $W_{\hat{i}_p,f,1}$ is fully known since the disturbance is assumed to be measurable and preview is available.

The aim of the disturbance feedforward DeePC is to find an optimal future input command $U_{\hat{i}_p,f,1}$ such that $Y_{\hat{i}_p,f,1}$ follows a prescribed reference r_f in the presence of a known disturbance $W_{\hat{i}_p,f,1}$, based on a connection between the known and unknown data trajectories.

To derive this connection, first a relationship between the striped, or so-called past, and dotted, or so-called future, data sets is sought out. That is, expressing the output data in the dotted set in terms of all the data available in the striped set along with input and disturbance data from the striped set.

By using the predictor form in Equation 2-2, the output at any time index k can be expressed in terms of the initial state, previous inputs, disturbances, and noise:

$$\begin{aligned} y_k = C\tilde{A}^k x_0 + \sum_{i=0}^{k-1} C\tilde{A}^{k-1-i}\tilde{B}_u u_i + \sum_{j=0}^{k-1} C\tilde{A}^{k-1-j}\tilde{B}_w w_j + \sum_{m=0}^{k-1} C\tilde{A}^{k-1-m} K e_m \\ + D_u u_k + D_w w_k + e_k \end{aligned} \tag{2-8}$$

Starting from $k = i_p$ with an initial state x_{i_p}, Equation 2-2 is propagated for $f-1$ steps forward in time and the resulting outputs are concatenated in the vector $y^{\mathrm{T}}_{i_p,f,1} = \begin{bmatrix} y^{\mathrm{T}}_{i_p} & y^{\mathrm{T}}_{i_p+1} & \cdots & y^{\mathrm{T}}_{i_p+f-1} \end{bmatrix}$. To cover the entire set of so-called future outputs, this process is repeated for a total of $\bar{N}$ for each time index of the remaining data batch and the resulting vectors are stacked in a block-Hankel matrix, which can be compactly described as:

$$Y_{i_p,f,\bar{N}} = \Gamma^{(f)} X_{i_p,\bar{N}} + H^{(f)}_{(\tilde{B}_u,D_u)} U_{i_p,f,\bar{N}} + H^{(f)}_{(\tilde{B}_w,D_w)} W_{i_p,f,\bar{N}} + H^{(f)}_{(K,I)} E_{i_p,f,\bar{N}}. \tag{2-9}$$

The sequence of initial states $X_{i_p,\bar{N}}$ is, however, unknown. As a consequence, $Y_{i_p,f,\bar{N}}$ does not yet solely rely on measured input-output data. To this end, DeePC utilizes a result that is often encountered in subspace identification methods [78]: a state x_k can be iteratively propagated forward using Equation 2-2a over p time samples. The resulting x_{k+p} state will depend only on the initial state x_k and input-output data:

$$x_{k+p} = \tilde{A}^p x_k + \mathcal{K} \begin{bmatrix} U_{k,p,1} \\ W_{k,p,1} \\ Y_{k,p,1} \end{bmatrix}. \tag{2-10}$$

Therefore, the unknown state sequence can be rewritten using input, output, and disturbance data from the striped set, along with another set of initial conditions $X_{i,\bar{N}}$:

$$\begin{aligned} X_{i_p,\bar{N}} &= \tilde{A}^p X_{i,\bar{N}} + \mathcal{K} \begin{bmatrix} U_{i,p,\bar{N}} \\ W_{i,p,\bar{N}} \\ Y_{i,p,\bar{N}} \end{bmatrix} \\ &\approx \mathcal{K} \begin{bmatrix} U_{i,p,\bar{N}} \\ W_{i,p,\bar{N}} \\ Y_{i,p,\bar{N}} \end{bmatrix} \Leftarrow p \gg 0. \end{aligned} \tag{2-11}$$

Since all eigenvalues of $\tilde{A}$ are situated inside the open unit circle and the size of the past window p is assumed to be chosen high enough, $||\tilde{A}^p||_F$ becomes arbitrarily small and the influence of the initial states term becomes negligible. Thus, introducing the approximation in Equation 2-11 in Equation 2-9 leads to the data equation:

$$Y_{i_p,f,\bar{N}} = \Gamma^{(f)} \mathcal{K} \begin{bmatrix} U_{i,p,\bar{N}} \\ W_{i,p,\bar{N}} \\ Y_{i,p,\bar{N}} \end{bmatrix} + H^{(f)}_{(\tilde{B}_u,D_u)} U_{i_p,f,\bar{N}} + H^{(f)}_{(\tilde{B}_w,D_w)} W_{i_p,f,\bar{N}} + H^{(f)}_{(K,I)} E_{i_p,f,\bar{N}}. \tag{2-12}$$

This equation only depends on input, output, and disturbance trajectories, along with system matrices, and it is further used for the derivation of the disturbance feedforward DeePC algorithm. Before proceeding to the characteristic equation, a similar relation must be expressed between the past and future data corresponding to the dashed arrows:

$$Y_{\hat{i}_p,f,1} = \Gamma^{(f)} \mathcal{K} \begin{bmatrix} U_{\hat{i},p,1} \\ W_{\hat{i},p,1} \\ Y_{\hat{i},p,1} \end{bmatrix} + H^{(f)}_{(\tilde{B}_u,D_u)} U_{\hat{i}_p,f,1} + H^{(f)}_{(\tilde{B}_w,D_w)} W_{\hat{i}_p,f,1} + H^{(f)}_{(K,I)} E_{\hat{i}_p,f,1}. \tag{2-13}$$

2-2-2 The disturbance DeePC characteristic equation

As an intermediary step of the derivation of the disturbance DeePC characteristic equation, the noiseless case is considered. Equation 2-12 and Equation 2-13 are rewritten as:

$$\begin{bmatrix} \Gamma^{(f)}\mathcal{K} & H^{(f)}_{(\tilde{B}_u,D_u)} & H^{(f)}_{(\tilde{B}_w,D_w)} & -I \end{bmatrix} \begin{bmatrix} \begin{bmatrix} U_{i,p,\bar{N}} \\ W_{i,p,\bar{N}} \\ Y_{i,p,\bar{N}} \end{bmatrix} \\ U_{i_p,f,\bar{N}} \\ W_{i_p,f,\bar{N}} \\ Y_{i_p,f,\bar{N}} \end{bmatrix} = O, \tag{2-14}$$

$$\begin{bmatrix} \Gamma^{(f)}\mathcal{K} & H^{(f)}_{(\tilde{B}_u,D_u)} & H^{(f)}_{(\tilde{B}_w,D_w)} & -I \end{bmatrix} \begin{bmatrix} \begin{bmatrix} U_{\hat{i},p,1} \\ W_{\hat{i},p,1} \\ Y_{\hat{i},p,1} \end{bmatrix} \\ U_{\hat{i}_p,f,1} \\ W_{\hat{i}_p,f,1} \\ Y_{\hat{i}_p,f,1} \end{bmatrix} = o. \tag{2-15}$$

Following the derivation in [4], Equation 2-14 is multiplied at the right hand side with a vector $g \in \mathbb{R}^{\bar{N}\times 1}$, followed by subtracting Equation 2-15 from Equation 2-14:

$$\begin{bmatrix}\Gamma^{(f)}\mathcal{K} & H^{(f)}_{(\tilde{B}_u,D_u)} & H^{(f)}_{(\tilde{B}_w,D_w)} & -I\end{bmatrix}\left(\begin{bmatrix}\begin{bmatrix}U_{i,p,\bar{N}}\\W_{i,p,\bar{N}}\\Y_{i,p,\bar{N}}\end{bmatrix}\\U_{i_p,f,\bar{N}}\\W_{i_p,f,\bar{N}}\\Y_{i_p,f,\bar{N}}\end{bmatrix}g-\begin{bmatrix}\begin{bmatrix}U_{\hat{i},p,1}\\W_{\hat{i},p,1}\\Y_{\hat{i},p,1}\end{bmatrix}\\U_{\hat{i}_p,f,1}\\W_{\hat{i}_p,f,1}\\Y_{\hat{i}_p,f,1}\end{bmatrix}\right)=o. \tag{2-16}$$

Given that the first block-matrix has full rank, it remains that:

$$\begin{bmatrix}\begin{bmatrix}U_{i,p,\bar{N}}\\W_{i,p,\bar{N}}\\Y_{i,p,\bar{N}}\end{bmatrix}\\U_{i_p,f,\bar{N}}\\W_{i_p,f,\bar{N}}\\Y_{i_p,f,\bar{N}}\end{bmatrix}g=\begin{bmatrix}\begin{bmatrix}U_{\hat{i},p,1}\\W_{\hat{i},p,1}\\Y_{\hat{i},p,1}\end{bmatrix}\\U_{\hat{i}_p,f,1}\\W_{\hat{i}_p,f,1}\\Y_{\hat{i}_p,f,1}\end{bmatrix}. \tag{2-17}$$

This is in accordance with the findings presented in [73], which outline that any future trajectory of a system can be expressed as linear combinations of past input-output trajectories, given that the input sequence was persistently exciting enough. Moreover, Equation 2-17 can be further split [79]:

$$\begin{bmatrix}\begin{bmatrix}U_{i,p,\bar{N}}\\W_{i,p,\bar{N}}\\Y_{i,p,\bar{N}}\end{bmatrix}\\U_{i_p,f,\bar{N}}\\W_{i_p,f,\bar{N}}\end{bmatrix}g=\begin{bmatrix}\begin{bmatrix}U_{\hat{i},p,1}\\W_{\hat{i},p,1}\\Y_{\hat{i},p,1}\end{bmatrix}\\U_{\hat{i}_p,f,1}\\W_{\hat{i}_p,f,1}\end{bmatrix} \tag{2-18}$$

$$Y_{i_p,f,\bar{N}}g=Y_{\hat{i}_p,f,1}. \tag{2-19}$$

Due to the condition on the persistency of excitation, the data matrix on the left-hand side of Equation 2-18 should have full row rank. This also requires that $\bar{N}\geq(r+q+\ell)p+(r+q)f$. If this matrix contains noisy data or trajectories generated by a nonlinear system, a deterministic DeePC does not ensure the feasibility of the predicted future trajectories for the real system [80]. To mitigate the effect of process or measurement noise, an instrumental variable $Z_{\bar{N}}$ is used, similar to [4]. First, Equation 2-14 is considered including noise:

$$\begin{bmatrix}\Gamma^{(f)}\mathcal{K} & H^{(f)}_{(\tilde{B}_u,D_u)} & H^{(f)}_{(\tilde{B}_w,D_w)} & -I\end{bmatrix}\begin{bmatrix}\begin{bmatrix}U_{i,p,\bar{N}}\\W_{i,p,\bar{N}}\\Y_{i,p,\bar{N}}\end{bmatrix}\\U_{i_p,f,\bar{N}}\\W_{i_p,f,\bar{N}}\\Y_{i_p,f,\bar{N}}\end{bmatrix}=-H^{(f)}_{(K,I)}E_{i_p,f,\bar{N}}, \tag{2-20}$$

while Equation 2-19 is preserved to suggest a noise-free prediction. It is then desirable to remove the effect of the noise from Equation 2-20, which is done through the use of the instrumental variable. A $Z_{\bar{N}}$ candidate must satisfy two properties [78]. First, the future noise term must be uncorrelated to $Z_{\bar{N}}$, such that when taking the limit for $\bar{N}\to\infty$, its bias is removed:

$$\lim_{\bar{N}\to\infty} \frac{1}{\bar{N}} \left(E_{i_p,f,\bar{N}} Z_{\bar{N}}^{\mathrm{T}} \right) = O. \tag{2-21}$$

The second property ensures that the introduction of the instrumental variable does not change the rank of the data matrix, and thus the subspace spanned by the trajectories in the data matrix is not reduced:

$$\operatorname{rank} \left(\lim_{\bar{N}\to\infty} \frac{1}{\bar{N}} \begin{bmatrix} U_{i,p,\bar{N}} \\ W_{i,p,\bar{N}} \\ Y_{i,p,\bar{N}} \\ U_{i_p,f,\bar{N}} \\ W_{i_p,f,\bar{N}} \end{bmatrix} Z_{\bar{N}}^{\mathrm{T}} \right) = \operatorname{rank} \left(\begin{bmatrix} U_{i,p,\bar{N}} \\ W_{i,p,\bar{N}} \\ Y_{i,p,\bar{N}} \\ U_{i_p,f,\bar{N}} \\ W_{i_p,f,\bar{N}} \end{bmatrix} \right). \tag{2-22}$$

A candidate matrix that satisfies these properties is given below, where $Z_{\bar{N}} \in \mathbb{R}^{(r+q+\ell)p+(r+q)f\times\bar{N}}$:

$$Z_{\bar{N}} = \begin{bmatrix} U_{i,p,\bar{N}} \\ W_{i,p,\bar{N}} \\ Y_{i,p,\bar{N}} \\ U_{i_p,f,\bar{N}} \\ W_{i_p,f,\bar{N}} \end{bmatrix} \tag{2-23}$$

By multiplying Equation 2-20 with $Z_{\bar{N}}^{\mathrm{T}}$, and both Equation 2-20 and Equation 2-15 with a vector $\hat{g} \in \mathbb{R}^{(r+q+\ell)p+(r+q)f}$, the following are obtained:

$$\lim_{\bar{N}\to\infty} \left(\begin{bmatrix} \begin{bmatrix} U_{i,p,\bar{N}} \\ W_{i,p,\bar{N}} \\ Y_{i,p,\bar{N}} \end{bmatrix} \\ U_{i_p,f,\bar{N}} \\ W_{i_p,f,\bar{N}} \end{bmatrix} Z_{\bar{N}}^{\mathrm{T}} \hat{g} \right) = \begin{bmatrix} \begin{bmatrix} U_{\hat{i},p,1} \\ W_{\hat{i},p,1} \\ Y_{\hat{i},p,1} \end{bmatrix} \\ U_{\hat{i}_p,f,1} \\ W_{\hat{i}_p,f,1} \end{bmatrix} \tag{2-24}$$

$$\lim_{\bar{N}\to\infty} Y_{i_p,f,\bar{N}} Z_{\bar{N}}^{\mathrm{T}} \hat{g} = Y_{\hat{i}_p,f,1}. \tag{2-25}$$

With this formulation, the effect of noise is asymptotically removed. In practice, $\bar{N}$ should be chosen high enough to ensure this property is sufficiently satisfied. Even though this translates to a necessity for a high amount of data points, the introduction of the instrumental variable leads to an important reduction in the size of the DeePC problem: the optimization vector variable $\hat{g}$ decreases from a size of $\bar{N}$ in the deterministic case, to $(r+q+\ell)p+(r+q)f$.

2-3 Disturbance feedforward DeePC

The behavior of the underlying process is captured by equations (2-24)-(2-25), which replace the need for an explicit model representation. The formulation of the DeePC optimization problem extended with disturbance preview follows as:

$$
\begin{aligned}
\min_{U_{\hat{i}_p,f,1},\hat{g}} \quad & \left(Y_{i_p,f,\bar{N}} Z_{\bar{N}}^{\mathrm{T}} \hat{g} - r_f\right)^{\mathrm{T}} Q \left(Y_{i_p,f,\bar{N}} Z_{\bar{N}}^{\mathrm{T}} \hat{g} - r_f\right) + U_{\hat{i}_p,f,1}^{\mathrm{T}} R U_{\hat{i}_p,f,1} \\
\text{s.t.} \quad & \begin{bmatrix} U_{i,p,\bar{N}} \\ W_{i,p,\bar{N}} \\ Y_{i,p,\bar{N}} \\ U_{i_p,f,\bar{N}} \\ W_{i_p,f,\bar{N}} \end{bmatrix} Z_{\bar{N}}^{\mathrm{T}} \hat{g} = \begin{bmatrix} U_{\hat{i},p,1} \\ W_{\hat{i},p,1} \\ Y_{\hat{i},p,1} \\ U_{\hat{i}_p,f,1} \\ W_{\hat{i}_p,f,1} \end{bmatrix}, \\
& Y_{i_p,f,\bar{N}} Z_{\bar{N}}^{\mathrm{T}} \hat{g} = Y_{\hat{i}_p,f,1}, \\
& u_k \in \mathcal{U}, \forall k \in \{0, \cdots, f-1\}, \\
& y_k \in \mathcal{Y}, \forall k \in \{0, \cdots, f-1\},
\end{aligned}
\tag{2-26}
$$

where $Q \in \mathbb{R}^{\ell f \times \ell f}$ and $R \in \mathbb{R}^{rf \times rf}$ are the output and input block diagonal weight matrices respectively. The output weighting matrix Q is considered to be positive semi-definite, while R is positive definite. The desired reference over the future horizon is given by $r_f \in \mathbb{R}^{\ell f}$. $\mathcal{U} \in \mathbb{R}^r$ and $\mathcal{Y} \in \mathbb{R}^\ell$ are the sets of admissible inputs and outputs, while u_k and y_k represent a shorthand notation for any element of the unknown future input and output vectors, $U_{\hat{i}_p,f,1}$ and $Y_{\hat{i}_p,f,1}$ respectively. After the data collection stage is complete and control is activated, the optimal control input is found by solving this optimization problem in a receding horizon manner at each time step and applying only the first element of the sequence to the system. The first part of the cost function penalizes the reference tracking error or corresponds to the disturbance rejection scenario if the reference is missing. Large amplitudes of the control input are prevented through the second part of the objective function.

2-3-1 Constraints

Since it is a data-driven framework, only the inputs and the available outputs of a system can be constrained. In the context of wind turbine control, the usual control inputs, namely the generator torque and the collective blade pitch angle, need a lower and an upper bound due to physical restrictions. Depending on the control objectives, bounds on selected outputs are also specified. The disturbance is not controllable, so no constraint can be imposed on it. Therefore, for wind turbine control purposes, the sets $\mathcal{U}$ and $\mathcal{Y}$ can be generally described as:

$$
\begin{aligned}
u_{min} \leq u_k \leq u_{max}, \forall k \in \{0, \cdots, f-1\}, \\
y_{min} \leq y_k \leq y_{max}, \forall k \in \{0, \cdots, f-1\}.
\end{aligned}
\tag{2-27}
$$

Moreover, the wind turbine's blade pitch actuators have pitching speed limitations. The rate of change of the control input command must also be constrained:

$$
|\dot{u}_k| \leq \dot{u}_{max}, \forall k \in \{0, \cdots, f-1\}. \tag{2-28}
$$

This can be rewritten as a set of linear inequations:

$$
\begin{aligned}
T U_{\hat{i}_p,f,1} \leq \bar{\dot{u}}_{max} \otimes \mathbf{1}_{r(f-1)} + T_0 U_{\hat{i},p,1}, \\
T = \begin{bmatrix} I & 0 & \cdots & 0 \\ -I & I & \cdots & 0 \\ \vdots & \ddots & \ddots & \vdots \\ 0 & \cdots & -I & I \end{bmatrix}, T_0 = \begin{bmatrix} 0 & 0 & \cdots & I \\ 0 & 0 & \cdots & 0 \\ \vdots & \ddots & \ddots & \vdots \\ 0 & 0 & \cdots & 0 \end{bmatrix},
\end{aligned}
\tag{2-29}
$$

where $\bar{\dot{u}}_{max}$ symbolizes the input rate bound $\dot{u}_{max}$ adjusted to the sampling time of the discrete system, and $\otimes$ is the Kronecker product. The term $T_0 U_{i,p,1}$ does not depend on the optimization variables and is included to account for the initial condition of the blade pitch command.

2-3-2 Quadratic programming formulation

The cost function of the reference tracking disturbance DeePC in Equation 2-26 can be rewritten as a quadratic objective, as shown in Equation 2-30. The term $r_f^{\mathrm{T}} r_f$ is discarded since it is a scalar and does not influence the solution of the optimization.

$$\min_{U_{\hat{i}_p,f,1},\hat{g}} \quad \begin{bmatrix} \hat{g}^{\mathrm{T}} & U_{\hat{i}_p,f,1}^{\mathrm{T}} \end{bmatrix} \begin{bmatrix} Z_{\bar{N}} Y_{i_p,f,\bar{N}}^{\mathrm{T}} Q Y_{i_p,f,\bar{N}} Z_{\bar{N}}^{\mathrm{T}} & 0 \\ 0 & R \end{bmatrix} \begin{bmatrix} \hat{g} \\ U_{\hat{i}_p,f,1} \end{bmatrix} + \begin{bmatrix} -2 r_f^{\mathrm{T}} Q Y_{i_p,f,\bar{N}} Z_{\bar{N}}^{\mathrm{T}} & 0 \end{bmatrix} \begin{bmatrix} \hat{g} \\ U_{\hat{i}_p,f,1} \end{bmatrix} \tag{2-30}$$

With this formulation and the linear sets of equality and inequality constraints, the optimization can be approached as a Quadratic Programming (QP) problem with the following general form:

$$\begin{aligned} \min_{x} \quad & \frac{1}{2} x^{\mathrm{T}} H x + c^{\mathrm{T}} x \\ \text{s.t.} \quad & A_{\mathrm{eq}} x = b_{\mathrm{eq}}, \\ & A_{\mathrm{ineq}} x \leq b_{\mathrm{ineq}}, \end{aligned} \tag{2-31}$$

where $x^{\mathrm{T}} = \begin{bmatrix} \hat{g}^{\mathrm{T}} & U_{\hat{i}_p,f,1}^{\mathrm{T}} \end{bmatrix}$. The equality constraints given by the DeePC characteristic equation are gathered within the pair $A_{\mathrm{eq}}, b_{\mathrm{eq}}$, while the input, input rate, and output inequality constraints are enforced by $A_{\mathrm{ineq}}, b_{\mathrm{ineq}}$. This is desired over a nonlinear optimization due to lower computation time.

An active-set method is used to find the optimal solution, considering that the QP problem has a large amount of both equality and inequality constraints. Additionally, even though Q and R might both be positive definite, the Hessian is only positive semi-definite because $Y_{i_p,f,\bar{N}}^{\mathrm{T}} Q Y_{i_p,f,\bar{N}}$ is rank deficient. However, the optimization problem has a unique solution as long as the reduced Hessian is positive semi-definite [81]. The importance of the full-row rank property of the data matrix on the left-hand side of Equation 2-18 is once again emphasized, for a rank deficiency would lead to an inconsistent set of constraints.

Finally, $\bar{N}$, p, f, Q, and R are hyperparameters that require tuning that is specific to the application. The algorithm of disturbance DeePC is listed below:

Algorithm 1 Disturbance DeePC

Require: N I/O data points $\{u_k, w_k, y_k\}_{k=0}^{N-1}$, a reference trajectory $r_f \in \mathbb{R}^{\ell f}$, past trajectories $U_{-p,p,1}, W_{-p,p,1}, Y_{-p,p,1}$, the constraint sets $\mathcal{U}$ and $\mathcal{Y}$, and the weight matrices Q and R.

1: At time t, get the disturbance preview $W_{t,f,1}$ and solve (2-26).
2: Apply the input $U_{t,f,1}^*(t)$.
3: Set $t \leftarrow t+1$ and update $U_{t-p,p,1}, W_{t-p,p,1}, Y_{t-p,p,1}$ to the most recent p I/O measurements.
4: Go back to 1.

Closed-loop robust stability of the classical DeePC scheme is approached by Bongard et al. who prove practical exponential stability relative to the noise level [75]. To this end, regularization terms are added to the objective function, which is often encountered as a method to deal with noise [68,

80]. In the presented approach, the instrumental variable $Z_{\bar{N}}$ provides a certain level of robustness to measurement and process noise in a non-deterministic setting. However, a formal stability and robustness analysis of the proposed disturbance DeePC formulation is left outside the scope of this thesis.

Chapter 3

Wind turbine linearization

3-1 Wind Turbine definition

The reference wind turbine used throughout this paper is the National Renewable Energy Laboratory (NREL) 5-MW wind turbine [1], supported by the OC3-Hywind spar-buoy concept platform [82]. This model was chosen due to its availability for simulation in OpenFAST [71], as well as QBlade [72]. Despite the increase in size and rating of wind turbines installed offshore [13], using this reference 5-MW wind turbine should not affect the controller synthesis process due to the model-free approach. The particularities of the floating wind turbine system will be captured by input-output data sets. In Table 3-I, a summary of the parameters of the reference wind turbine is given, including relevant control system properties.

Table 3-I: Specifications summary of the reference NREL 5-MW wind turbine. Adapted from [1].

Description	Value
Rating	5 MW
Rotor orientation, configuration	Upwind, 3 blades
Control	Variable speed, collective pitch
Drivetrain	High speed, multiple-stage gearbox
Rotor, hub diameter	126 m, 3 m
Cut-in, rated, cut-out wind speed	$3\,\mathrm{m\,s^{-1}}$, $11.4\,\mathrm{m\,s^{-1}}$, $25\,\mathrm{m\,s^{-1}}$
Cut-in, rated rotor speed	6.9 rpm, 12.1 rpm
Rated mechanical power	5.296 610 MW
Rated tip speed	$80\,\mathrm{m\,s^{-1}}$
Collective blade pitch angle at peak power coefficient	0°
Minimum, maximum blade pitch angle	0°, 90°
Maximum blade pitch rate	$8\,^\circ\,\mathrm{s^{-1}}$
Rated generator torque	43 093.55 N m
Maximum generator torque	47 402.91 N m
Maximum generator torque rate	$15\,000\,\mathrm{N\,m\,s^{-1}}$

3-2 Wind turbine linearization

To synthesize the data-driven controller, sets of input-output data generated by a wind turbine system are required. For this purpose, a simulator is used. OpenFAST is an open-source, dynamic response simulation tool for wind turbines developed by NREL in the United States [71]. It relies on Fatigue, Aerodynamics, Structures, and Turbulence (FAST) code and enables fully-coupled aero-hydro-servo-elastic simulation of floating and non-floating wind turbines [83]. The full wind turbine model has 22 available Degrees of Freedom (DoFs), along with another six corresponding to the floating platform. However, the resulting representation has a high degree of complexity, while a lower-fidelity model is preferred for initial control design. Therefore, a linearization of the wind turbine at an operating point in the above-rated region is obtained in Section 3-2-1 and validated in Section 3-2-2.

3-2-1 Linearization

OpenFAST has a full-system linearization functionality for Floating offshore Wind Turbines (FOWTs) [84]. The aim is to linearize the NREL 5-MW reference wind turbine with a sampling time of 0.05 s at a wind speed of $16\,\mathrm{m\,s^{-1}}$, therefore in the above-rated region. Before linearizing, an equilibrium point of the wind turbine is identified at a rotor speed $\Omega_0 = 12.1\,\mathrm{rpm}$, blade pitch angle $\theta_{c,0} = 11.79°$, a constant generator torque $\tau_{g,0} = 43.1\,\mathrm{kN\,m}$, a platform surge of 15.39 m, and platform pitch angle of 3°. The subsequent linearization will be an approximation of the nonlinear system for small perturbations, denoted by Δ, around the equilibrium $\{x_0, u_0, y_0\}$:

$$x = x_0 + \Delta x, \quad u = u_0 + \Delta u, \quad y = y_0 + \Delta y. \tag{3-1}$$

The complexity of the resulting linearization depends on the number of desired DoFs. To obtain a low complexity linearization, only four DoFs are activated. First, the generator DoF describes variable speed generator behavior. The first fore-aft tower bending-mode DoF accounts for the longitudinal fore-aft bending of the tower. Two DoFs of the platform are considered, the pitch tilt rotation and the horizontal surge translation, since they are the most sensitive DoFs of a FOWT [49].

Regarding the control system, the collective blade pitch controller is deactivated and the pitch angle remains constant at the equilibrium value of the operating point, while simple torque control is enabled to keep the generator torque at the rated value.

The wind turbine is linearized in steady wind and still water conditions. Additionally, the linearization includes wave-excitation and radiation memory-effect linear state space models that describe the transfer from wave elevation and platform translation and rotational velocities to applied point forces and moments at a reference point on the platform [84]. Only surge and pitch radiation and excitation states are included, resulting in surge force and pitch moment inputs on the wind turbine structure.

Since the wind turbine is a rotating system, the linearization process is repeated 36 times at different rotor azimuth positions across a full rotation. The linearizations are then translated to the fixed, tower-nacelle frame. However, all of the DoFs and other resulting states are non-rotating, meaning that only an averaging of the linearizations is eventually performed. The final linearization has a state space form as

$$\begin{aligned} \Delta\dot{x} &= A\Delta x + B\Delta u, \\ \Delta y &= C\Delta x + D\Delta u. \end{aligned} \tag{3-2}$$

The vector state contains 38 elements: the 4 activated DoFs and their derivatives, along with 12 wave excitation and 8 radiation states.

3-2-2 Validation

The linearization is first validated before proceeding to control design. Several sea states are considered, listed in Table 3-II. Significant wave heights H_s that are common for wind speeds close to $16\,\mathrm{m\,s^{-1}}$ were extracted from [85]. The values of the peak spectral periods T_p are common for the selected significant wave heights.

Table 3-II: Cases used for the validation of the linearized wind turbine model, where NTM stands for Normal Turbulence Model. The mean wind speed is $16\,\mathrm{m\,s^{-1}}$ in all five cases, and the first case corresponds to a turbulent wind, still water scenario.

Case	Wind type	H_s (m)	T_p (s)
1	NTM	-	-
2	Steady	3	12
3	NTM	3	12
4	Steady	4.3	10
5	NTM	4.3	10

The turbulent wind field is generated using TurbSim, a stochastic, full-field wind simulator [86]. The turbulence is normal and is based on a Kaimal turbulence model with a "B"category 15% turbulence intensity around a mean wind velocity of $16\,\mathrm{m\,s^{-1}}$.

A JONSWAP spectrum given by a significant wave height H_s and a peak-spectral wave period T_p is used to generate irregular waves [87]. The waves are considered to be unidirectional, with a heading direction of 0°. The spectrum of the waves lies in between 0.05 Hz and 0.3 Hz, and only normal sea states are considered.

The simulations for validation have a length of 1200 s. The first 500 s are discarded to avoid transient states. During the simulation, the high-fidelity model and the linearization are given the same input. Figure 3-1 presents a comparison of the wind turbine outputs for the second validation case, which entails steady wind and irregular waves. Qualitatively, the linearized model largely describes the evolution of the nonlinear model. The Root Mean Square Error (RMSE) and Variance Accounted For (VAF) are computed to quantify the validity of the wind turbine linearization. The latter is defined as

$$\mathrm{VAF}(y, y_{\mathrm{lin}}) = \max\left(0, \left(1 - \frac{\|y - y_{\mathrm{lin}}\|_2^2}{\|y\|_2^2}\right) \cdot 100\%\right), \tag{3-3}$$

where y is a high-fidelity system output vector, and y_{lin} is the corresponding linearized system output. The two metrics are shown in Table 3-III for each validation case, and confirm that the linearized model is a sufficiently accurate system description.

Introducing turbulent wind to the second validation case decreases the accuracy of the linearization, as illustrated in Figure 3-2. However, the linearized model is still deemed suitable for control design.

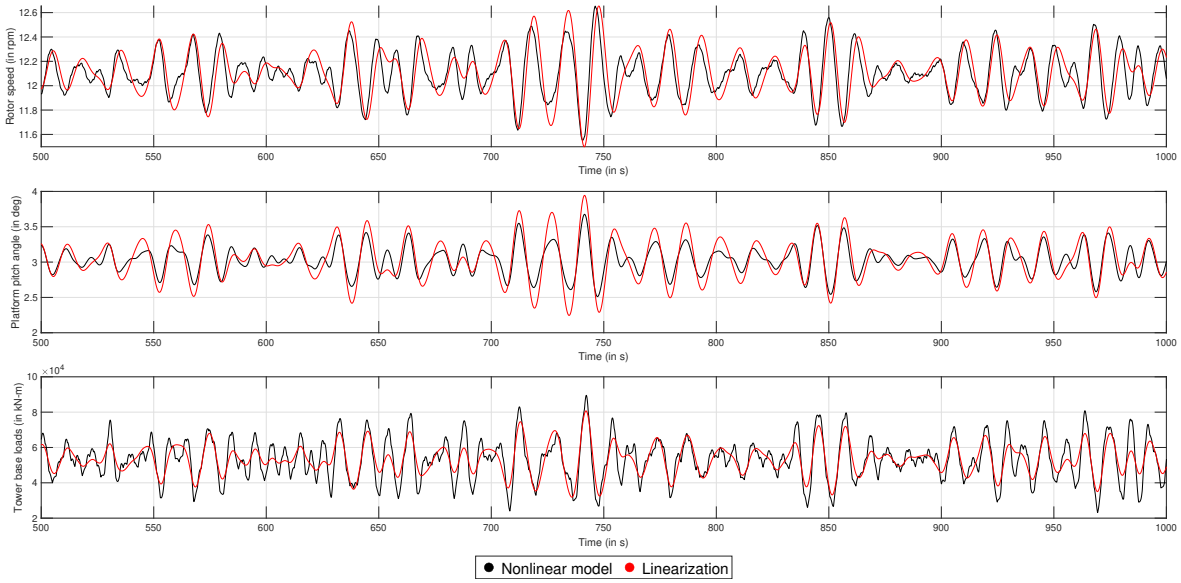

Figure 3-1: Comparison of the linearized model against the high-fidelity system, validation case 2 (nonlinear model in black, linearization in red). Up: rotor speed, middle: platform pitch angle, down: tower base loads.

Table 3-III: RMSE and VAF for each of the five validation cases, where Ω represents the rotor speed, Θ_P is the platform pitch angle, and $M_{y,T}$ denotes the tower base loads. Low RMSE and high VAF indicate a good performance of the linearization.

Case	Ω		Θ_P		$M_{y,T}$	
	RMSE (rpm)	VAF (%)	RMSE (deg)	VAF (%)	RMSE (kN-m)	VAF (%)
1	1.14	99.11	0.73	94.42	1.38×10^4	93.3
2	0.1	99.9	0.11	99.84	6.05×10^3	98.76
3	1.2	99.02	0.85	92.59	2.28×10^4	82.66
4	0.11	99.9	0.08	99.91	1.04×10^4	96.49
5	1.2	99.02	0.83	92.86	2.71×10^4	76.8

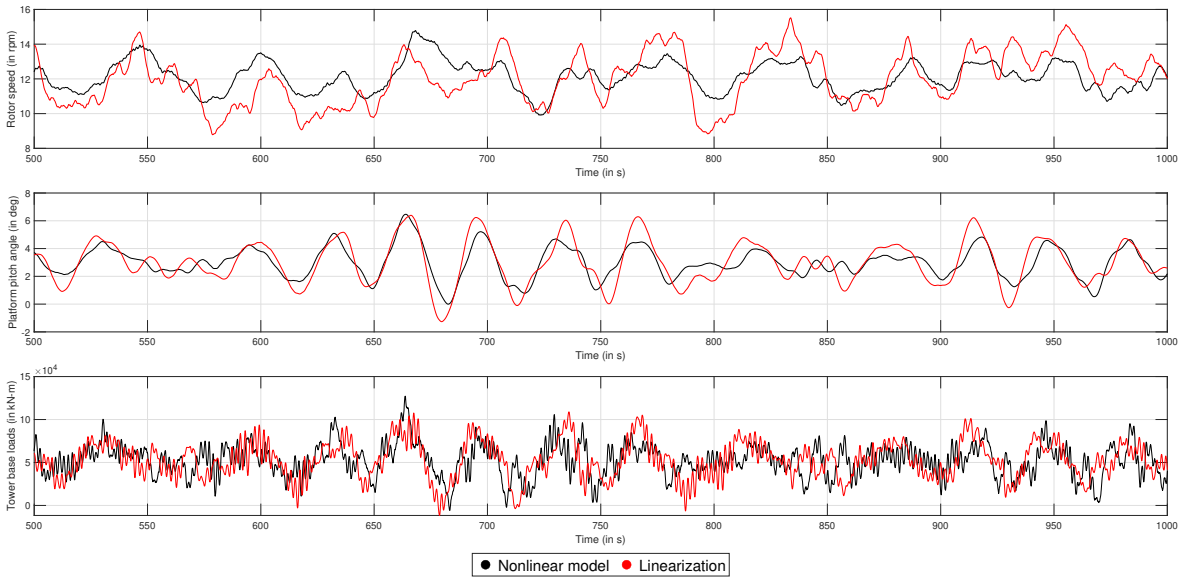

Figure 3-2: Comparison of the linearized model against the high-fidelity system, validation case 3 (nonlinear model in black, linearization in red). Up: rotor speed, middle: platform pitch angle, down: tower base loads.

Chapter 4

DeePC controller design

The wind turbine linearization obtained in Chapter 3 is used to implement a feedforward (FF) Data-enabled Predictive Control (DeePC) algorithm in a simplified configuration. The Linear Time-Invariant (LTI) system is used both during the open-loop data collection stage and inside the control loop to simulate the response of the wind turbine. This enables gaining insight into the tuning required to adapt the proposed control framework to the wind turbine system, before implementing it in a high-fidelity environment.

Firstly, the input-output behavior of the linearized wind turbine is analyzed in Section 4-1 to outline the channels of interest. Section 4-2 describes the setup of the model-free controller and describes the particularities of implementing the DeePC framework for a wind turbine system. The controller is then evaluated in several load cases in Section 4-3. Finally, Section 4-4 presents concluding remarks on implementing FF DeePC in the linear setting.

4-1 Input-output analysis

The linearized wind turbine system of Equation 3-2 can be rewritten in an input-output representation as

$$\hat{y} = \hat{G}\hat{u} + \hat{G}_d\hat{d}, \tag{4-1}$$

where $\hat{G}$ describes the transfer from the control inputs to the output, and $\hat{G}_d$ gives the relation between disturbances and outputs. The two available control inputs of the reference wind turbine are the collective blade pitch, θ_c, and the generator torque, τ_g. Although θ_c is traditionally used in the above-rated region, Lemmer et al. indicated that using both controls might result in more effective control [49]. Therefore, $\hat{u} = [\theta_c,\ \tau_\mathrm{g}]^\mathrm{T}$ will be considered as the plant input in this section. The surge force $F_{x,\mathrm{P}}$ and pitch moment $M_{y,\mathrm{P}}$ acting on the platform are available as disturbance inputs. Along with the wind speed v, they form the disturbance input $\hat{d} = [v,\ F_{x,\mathrm{P}},\ M_{y,\mathrm{P}}]^\mathrm{T}$.

Platform motions amplified by the negative damping phenomenon are the most problematic in the above-rated region, where they cause power fluctuations and large turbine loads. Therefore, restricting platform pitch angle Θ_{P} may improve the performance of the wind turbine. Although the output power quality could increase as a byproduct of platform motion reduction, it is preferred to maintain the rotor speed Ω as an explicit output of the wind turbine and control it directly. The tower base bending moment $M_{y,\mathrm{T}}$ is also of interest since tower base loads were found to be the most affected by waves [34]. The output of the plant is thus $\hat{y} = [\Omega,\, \Theta_{\mathrm{P}},\, M_{y,\mathrm{T}}]^{\mathrm{T}}$. Using this plant, an input-output analysis is carried out to determine the effectiveness of control inputs and how the disturbance signals are reflected in the outputs of interest.

4-1-1 Scaling

Several input signals, such as the wave forces and the generator torque, have a considerably larger order of magnitude compared to other variables. To ensure that every signal has the same importance, the system is first scaled to a common, dimensionless domain, as previously presented by Lemmer et al. [49]. The aim is to obtain two dimensional transfer functions G and G_d by adjusting their dimensional counterparts $\hat{G}$ and $\hat{G}_d$ through scaling matrices as

$$G = D_y^{-1}\hat{G}D_u, \quad G_d = D_y^{-1}\hat{G}_d D_d. \tag{4-2}$$

The input, disturbance, and output scaling matrices D_u, D_d, and D_y respectively, are given in Equations (4-3) and (4-4). They specify the maximum expected or allowed absolute value excursions of the signals from the operating point. For example, the first element of D_u indicates that deviations of the blade pitch angle θ_c of at most 5° around the linearization point value are anticipated.

$$D_u = \begin{bmatrix} 5\pi/180 & 0 \\ 0 & 0.1\tau_{g,0} \end{bmatrix}, \quad D_d = \begin{bmatrix} 0.1\bar{v} & 0 & 0 \\ 0 & F_{x,\mathrm{P},max} & 0 \\ 0 & 0 & M_{y,\mathrm{P},max} \end{bmatrix}, \tag{4-3}$$

$$D_y = \begin{bmatrix} 0.15\Omega_0 & 0 & 0 \\ 0 & 0.5\Theta_{\mathrm{P},0} & 0 \\ 0 & 0 & 0.5M_{y,T,0} \end{bmatrix}, \tag{4-4}$$

Above, $\tau_{g,0}$ and Ω_0 are the rated generator torque and rotor speed values. $\Theta_{P,0}$ and $M_{y,T,0}$ are the steady-state values at the linearization operating point. The wave loads are centered around zero, which also coincides with the still-water scenario in which the wind turbine was linearized. Therefore, the largest expected values $F_{x,\mathrm{P},max}$ and $M_{y,\mathrm{P},max}$ are considered to be the largest absolute value encountered, which can originate from a data set of choice.

The resulting transfer $y = Gu + G_d d$ has inputs, outputs, and disturbance signals with values in the interval $[-1, 1]$, where -1 and 1 indicate the minimum and maximum expected values respectively, while 0 corresponds to the linearization point value.

4-1-2 Open-loop frequency response

The bode plots in Figures 4-1 and 4-2 show the magnitude of the frequency response of the scaled controlled and disturbed plants G and G_d. For each plot, the first two vertical dashed lines indicate

the surge and pitch natural frequencies (0.0304 Hz and 0.0075 Hz respectively) of the Floating offshore Wind Turbine (FOWT) linearization. The wave frequency range is marked by the following two vertical dashed lines. The spectrum of the waves contains the most significant frequencies between 0.05 Hz and 0.3 Hz, while wind disturbance is mostly active in the low-frequency range.

The left column of Figure 4-1 shows the frequency response of the plant to blade pitch angle inputs, while the right column corresponds to generator torque inputs. The blade pitch angle, θ_c, is a more effective input than the generator torque τ_g for all of the considered outputs, due to the the gain being larger for the whole frequency range. However, θ_c gain decreases significantly in the wave frequency range, making it more difficult to control the plant. The blade pitch angle cannot effectively control the wind turbine around the platform pitch natural frequency, due to a magnitude dip caused by a pair of complex conjugate zeros close to the imaginary axis. Around the same frequency, the transfer of sinusoidal blade pitch commands to the platform pitch angle and tower base loads is amplified.

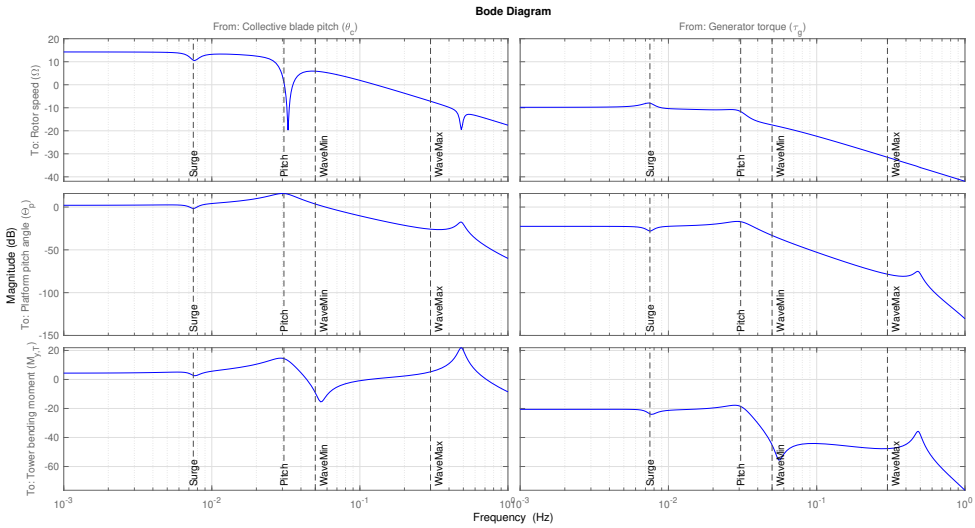

Figure 4-1: Magnitude of the frequency response of G, the scaled transfer function from control inputs to plant outputs.

In Figure 4-2, the first column depicts the frequency response magnitude to wave forces. The wave surge force and pitch moment are highly correlated and the frequency response of the respective transfer functions to output are similar, hence they are represented on the same set of plots. The right column corresponds to the horizontal wind speed. The effect of wave loads is amplified in the wave frequency range, with a significant effect on tower base loads. The wind speed disturbance has the strongest effect in the low frequency range for the rotor speed, and at the platform pitch natural frequency for the platform pitch angle and the tower bending moment. The tower bending moment is also notably excited by both wind and waves at the fore-aft eigenfrequency of the tower, which corresponds to the rightmost peak of the magnitude plots.

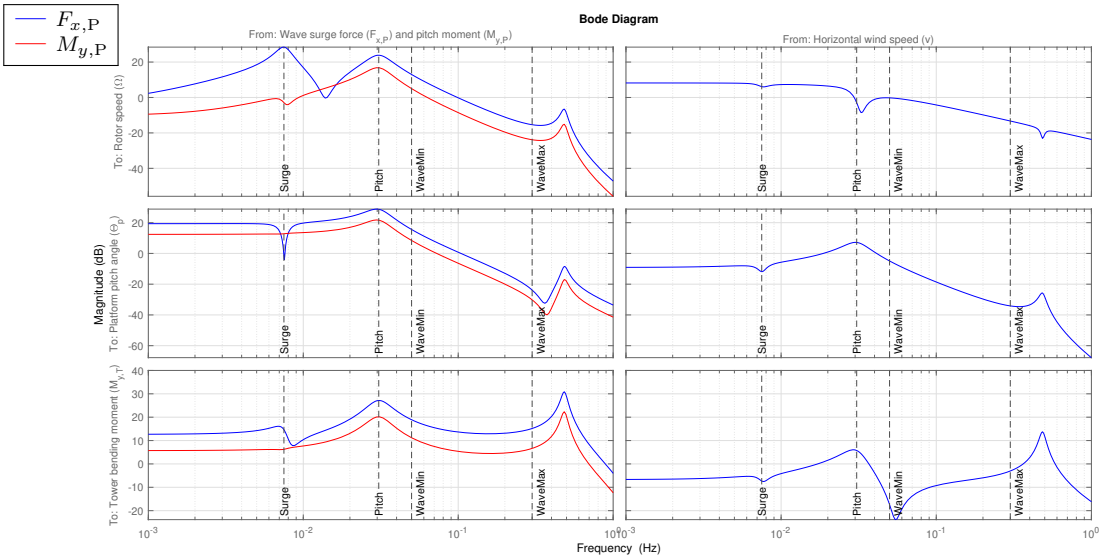

Figure 4-2: Magnitude of the frequency response of G_d, the scaled transfer function from disturbance inputs to plant outputs. The left column of plots illustrates both the surge force (in blue) and pitch moment (in red) acting on the platform.

4-2 Controller design

In the proposed framework, the feedback (FB) baseline controller of the wind turbine is completely replaced by the DeePC algorithm, as illustrated in Figure 4-3. The controller relies on output measurements to compute the input command. Simultaneously, knowledge of future perturbations is incorporated in the optimization process, meaning that the DeePC controller combines both feedback and feedforward action in one input.

The goal of the controller is to find an optimal blade pitch angle input that ensures reference tracking of the rotor speed and platform motion reduction in the presence of wave disturbance. The plant will therefore have the control input $u = \theta_c$ with output $y^{\mathrm{T}} = [\Omega,\ \Theta_{\mathrm{P}}]$. As a disturbance input, the wave pitch moment $M_{y,\mathrm{P}}$ will be considered. The surge force is not further employed because it is highly correlated with the pitch moment on the platform and the two have a similar influence on the outputs of interest in the wave frequency range. The scaling applied in the previous sections is preserved during the control design. Aside from ensuring that all signals are of the same magnitude, translating the linearization to a dimensionless domain also prevents poorly conditioned matrices during optimization.

4-2-1 Discretization of the wind turbine linearization

The DeePC algorithm works in a discrete-time setting, so the linear system must first be discretized with an adequate sampling time. Recalling Chapter 2, the length of the disturbance preview is equivalent to the prediction horizon f of the DeePC problem. Additionally, the number of decision variables and constraints of the optimization is directly proportional to the amount of samples in the past and future windows, p and f. To ensure a window length of n seconds, $n \cdot T_s$ samples are required, where T_s is the sampling time in seconds.

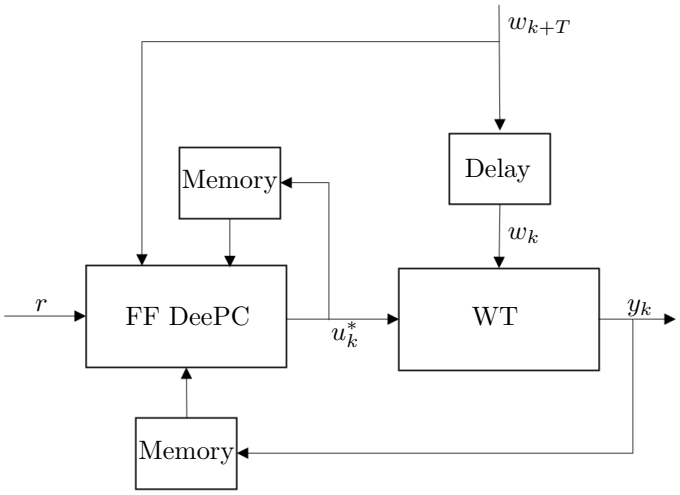

Figure 4-3: Control block scheme of the feedforward DeePC. The controller uses information of the previous input, output, and disturbance trajectories, along with a preview of future disturbances. The algorithm computes the optimal control input such that the outputs follow the prescribed reference r.

Ideally, a full period of a wave should be included in the preview. However, the slowest wave has a period of approximately 20 s. To maintain a reasonable dimension of the optimization problem while capturing enough information in the wave preview, a sampling time $T_s = 1\,\text{s}$ is used. A minimal realization of this LTI has 7 states and is controllable, thus ensuring that *Assumption 4* of Chapter 2 is fulfilled.

4-2-2 Open-loop data collection

The controller synthesis begins with the open-loop data collection stage. A pseudo-random binary sequence of blade pitch angle commands with an amplitude of 2° is generated, which ensures the input persistency of excitation of a high enough order. Even though pitch actuator dynamics are not explicitly considered, every pitch command is maintained for at least 10 s to allow a realistic interval for pitch actuators to reach the reference value. To mimic measurement noise, a zero-mean white noise disturbance e_k with $\text{var}(e_k) = (10^{-3})^2$ is added to the output.

As a disturbance input, the wave pitch moment derived from a wave elevation time series is used. To ensure full rank of the DeePC data matrices, persistency of excitation is also a required property of the disturbance signal. The pitch moment preserves the persistency of excitation of the wave elevation, which was generated as a stochastic signal. Throughout the linearization process, an LTI system that describes the transfer from wave elevation to hydrodynamic forces was obtained. This system has positive amplification throughout the whole wave frequency range, meaning that no frequency in the spectrum of the waves is attenuated.

Next, the data matrices are constructed based on the length of the data windows p, f, and N, which were selected through an iterative process. The past and future windows have a length of $p = f = 20$ samples, equivalent to 20 s. A shorter preview window proved to be insufficient for wave effect mitigation, and larger values of both window lengths do not bring a significant performance improvement. The length of the data window is chosen as $N = 500$.

4-2-3 Measurement noise level

Due to the inclusion of instrumental variables in the DeePC algorithm, the controller can handle measurement noise. However, the signal-to-noise ratio must remain high enough for the data to be relevant for controller synthesis. A simple, single-input single-output system will be considered first to explore the effect of increasing the magnitude of the measurement noise. The system uses the blade pitch angle to control the rotor speed such that it follows the rated value. Simulations with a variance of the noise ranging from $\text{var}(e_k) = (10^{-4})^2$ to $\text{var}(e_k) = (10^{-1})^2$ show that high values of the variance significantly decrease the tracking performance. The output remains unbiased, while the variance increases. This is illustrated in Figure 4-4. However, it is assumed that the rotor speed can be measured precisely enough, so the variance of the measurement noise is maintained as $\text{var}(e_k) = (10^{-3})^2$ hereafter.

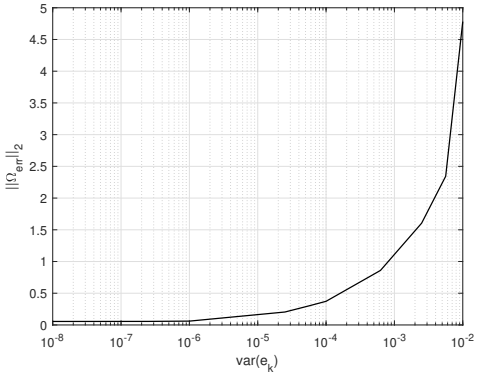

(a) Norm of the rotor speed tracking error when increasing the measurement variance.

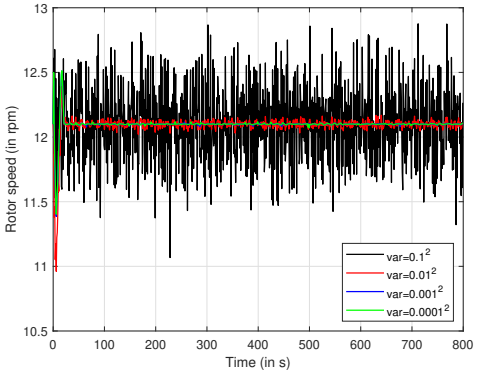

(b) Effect of increasing the measurement noise variance on the rotor speed.

Figure 4-4: Performance of the FF DeePC with varying the measurement noise level $\text{var}(e_k)$.

4-2-4 Quality of the disturbance preview

In a real scenario, the preview is obtained through prediction models based on wave elevation measurements. As a consequence, a perfect preview only occurs in a theoretical setting. Using the same Single-Input Single-Output (SISO) system, the outcome of using a non-ideal preview with FF DeePC is explored. First, a constant bias is included in the wave pitch moment preview. Alternatively, a zero mean white noise with increasing intensity is added to the perfect preview.

Constant bias

To investigate the response of the controller to a bias, a constant value ranging from 10^{-4} to 0.1 is added to the preview vector at each time step of the optimization. It is important to note that this bias is applied to the scaled system, meaning that the bias value represents a fraction of the maximum expected magnitude of the pitch moment on the platform. For example, a bias of 0.1 is physically equivalent to adding a value of 10% of the greatest wave pitch moment magnitude to the wave preview.

A constant bias can be tolerated within a restricted magnitude, as shown in Figure 4-5. Increasing the value of the bias leads to a decrease with a constant offset of the rotor speed. This is caused by an

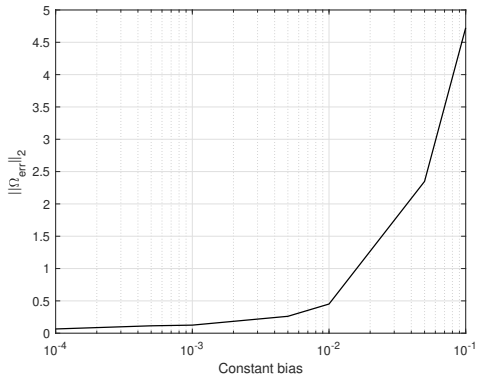

(a) Norm of the rotor speed tracking error with increasingly biased wave preview.

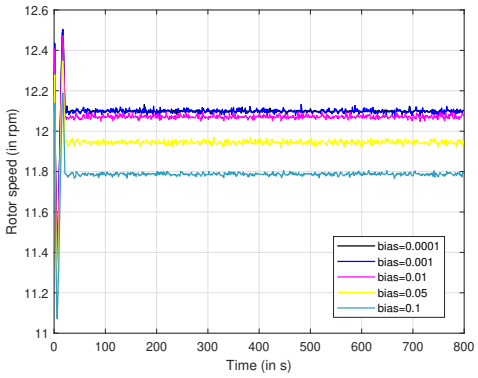

(b) Effect of increasing preview bias on the rotor speed.

Figure 4-5: Performance of the FF DeePC when a constant bias is introduced in the wave preview.

increase in the mean blade pitch command as a response to larger expected wave forces. The controller does not eventually adapt to the preview bias because it is still using unbiased data collected in open loop to generate future trajectories of the system.

Noisy preview

In the same setting, an additive white noise d_k of increasing intensity is included in the wave preview. The value of the noise variance ranges from $\text{var}(d_k) = (10^{-5})^2$ to $\text{var}(d_k) = (10^{-1})^2$. The controller can still perform reference tracking even with noisy preview data. This is explained by the inclusion of disturbance data matrices in the instrumental variables of the FF DeePC. As seen in Figure 4-6, the tracking error increases with higher preview noise intensity, the rotor speed oscillations get notably larger after a threshold of $\text{var}(d_k) = (10^{-2})^2$, when the ratio of noise increases too much. Perfect preview will be further considered.

4-3 Controller testing

In this section, the FF DeePC controller is implemented in the linear setting. Four load cases are considered. The load cases coincide with the ones used during the validation process of the wind turbine linearization and are listed in Table 4-I. The first two load cases involve steady wind conditions, with a mean horizontal wind speed of $16\,\text{m}\,\text{s}^{-1}$, along with irregular waves. The steady wind is replaced by turbulent wind conditions during the latter two cases.

A remarkable feature of the DeePC framework is that it enables multi-objective control with the possibility of specifying constraints. Therefore, the pitching motions of the platform may be explicitly limited through hard constraints simultaneously with performing rotor speed reference tracking. It is important to note that, despite the freedom of having multiple control goals, the two proposed objectives are conflicting by nature. Additionally, the rotor speed and the platform pitch angle are controlled by only one input, meaning that the system is under-actuated. Although the DeePC approach may improve both objectives, perfect performance is not possible for both channels simultaneously.

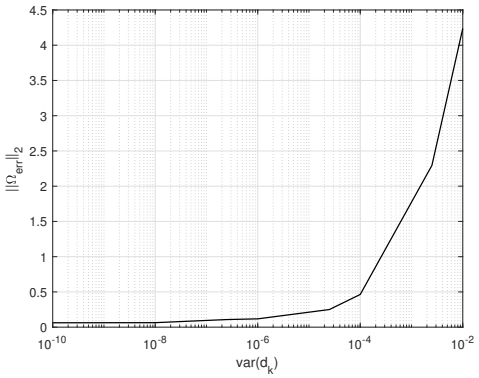

(a) Norm of the rotor speed tracking error with increasing additive noise level on the preview.

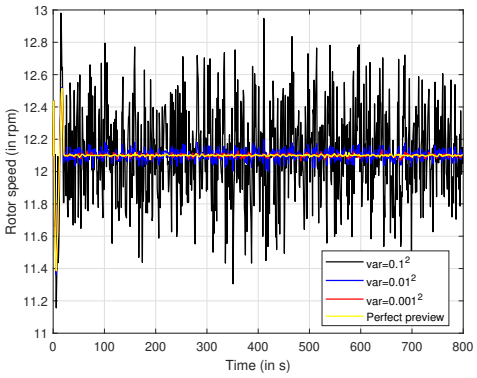

(b) Effect of increasing the noise level of the wave forces preview as seen at the rotor speed output.

Figure 4-6: Performance of the FF DeePC with increasing preview noise level $\mathrm{var}(d_k)$.

Table 4-I: Load cases used for controller testing, where NTM stands for Normal Turbulence Model. The load cases coincide with the ones used for the linearization validation in Table 3-II.

Case	Wind type	H_s (m)	T_p (s)
1	Steady	3	12
2	Steady	4.3	10
3	NTM	3	12
4	NTM	4.3	10

In subsections 4-3-1 and 4-3-2, a controller that balances rotor speed tracking and platform pitching reduction is implemented. The compromise is pursued because, aside from stabilization, it is expected that a reduction in platform movement also leads to a reduction in wind turbine loading. The first subsection is concerned with the steady wind scenario, while the turbulent wind conditions are approached in the latter. A quantitative evaluation of the controllers through performance metrics is then presented in Section 4-3-3 for all four load cases. Section 4-3-4 investigates the effect of focusing the controller on either rotor speed tracking or platform motion reduction.

4-3-1 Steady wind and irregular waves conditions

The constraints and tuned performance weights used in this scenario are listed in Table 4-II. The rotor speed is allowed to vary at most 15% around the rated value to ensure no emergency shutdown occurs. The input performance weight R is constructed as $R = I \otimes R_k$, with $I \in \mathbb{R}^f$ being the identity matrix. The output weight Q has a similar structure. The output weight enforces reference tracking for the rotor speed. The platform pitch angle is not included in the cost function because the aim is not to force the wind turbine to be completely still, but rather to limit the rocking motions. The reference signal for the rotor speed output remains constant at the rated value of 12.1 rpm.

For each load case, three controllers are compared: the baseline gain-scheduled PI controller, a DeePC controller with no preview included, and the FF DeePC controller presented in Chapter 2. However, the qualitative behavior of the wind turbine is very similar for the two steady wind load cases, therefore only the first load case will be illustrated.

Table 4-II: Tuning parameters used for the FF DeePC in the steady wind case. The intervals indicate within what bounds the respective input or output is allowed to vary around the linearization point value.

Parameter	θ_c (°)	$\dot{\theta}_{c,\max}$ (°/s)	Ω (rpm)	Θ_{P} (°)	Q_k	R_k
Interval or value	[-5,5]	8	[-1.8, 1.8]	[-0.45, 0.45]	diag(100, 0)	1

The left column of Figure 4-7 presents a part of a time series obtained by simulating the three controllers in a closed loop with the wind turbine linearization. The baseline controller has been activated since the beginning of the simulation. For both DeePC controllers, the first 800 s correspond to the open-loop data collection stage. The same input-output data set is used in both cases, but the FF DeePC also collects a disturbance trajectory. After 800 s, the controller is activated. The two DeePC controllers are still adjusting during the first approximately 50 s, which may be explained by the controllers still adapting to closed-loop operation.

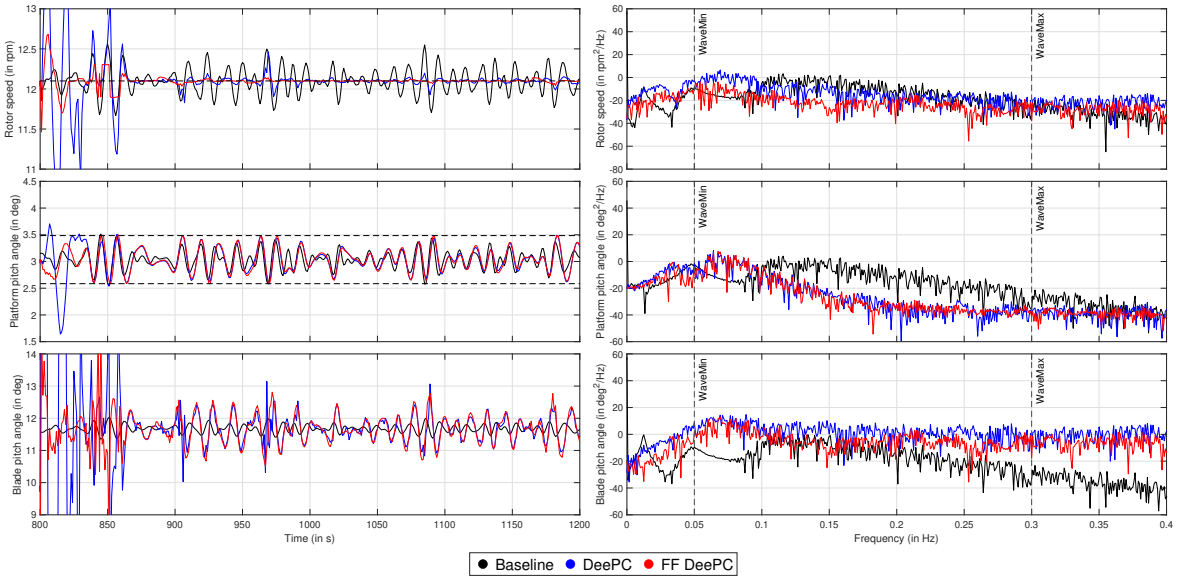

Figure 4-7: Simulation of a steady wind, irregular waves scenario, with $H_s = 3\,\mathrm{m}$ and $T_p = 12\,\mathrm{s}$. The baseline controller is represented in black, a DeePC controller with no disturbance preview in blue, and the FF DeePC controller in red. **Left column**: extract of a time series of the rotor speed, platform pitch angle, and blade pitch angle input. The two DeePC controllers are activated at 800 s. The dashed horizontal lines represent constraints used during the optimization. The bounds on blade pitch angle are enabled, but not visible. **Right column**: Power Spectral Density (PSD) of the respective signals on the left. The two vertical dashed lines delimit the frequency range of the wave disturbance.

The two DeePC controllers perform similarly well and bring an improvement to the baseline controller in terms of rotor speed reference tracking. The platform pitch angle remains within the specified bounds and has a similar profile to the baseline case. No improvement is visible because the platform pitch angle is already within the imposed limits in the baseline case. The blade pitching activity of both DeePC controllers is notably increased relative to the baseline.

Specifying tight constraints on the rotor speed leads to constraint violations or infeasible problems for the DeePC without preview. Including wave preview in the DeePC controller results in improved reference tracking and the possibility of specifying tighter bounds on both outputs with fewer infeasibility

issues.

The right column of Figure 4-7 shows the PSD of the signals. The following analysis focuses on the effect of the controllers in the frequency range between 0.05 Hz and 0.3 Hz, where waves are active. Illustrated in the top-right plot, the FF DeePC decreases the power carried by the rotor speed signal compared to both the baseline controller and the DeePC without preview. This indicates that including feedforward information in DeePC results in less energy being concentrated from the wave disturbance to the rotor speed. Regarding the platform motions, both DeePC controllers similarly decrease the energy transferred from high-frequency waves to platform pitching while visibly accentuating the energy content of a range excited by low-frequency waves compared to the baseline. In this case, including wave preview does not bring a visible improvement. More energy is condensed in the blade pitch input command of the DeePC controllers in the wave frequency range, indicating that the pitch controller is actively attempting to counteract wave disturbances. Additionally, the FF DeePC is attenuating the resonance peak present in the blade pitch input of the baseline controller at the platform's natural surge frequency.

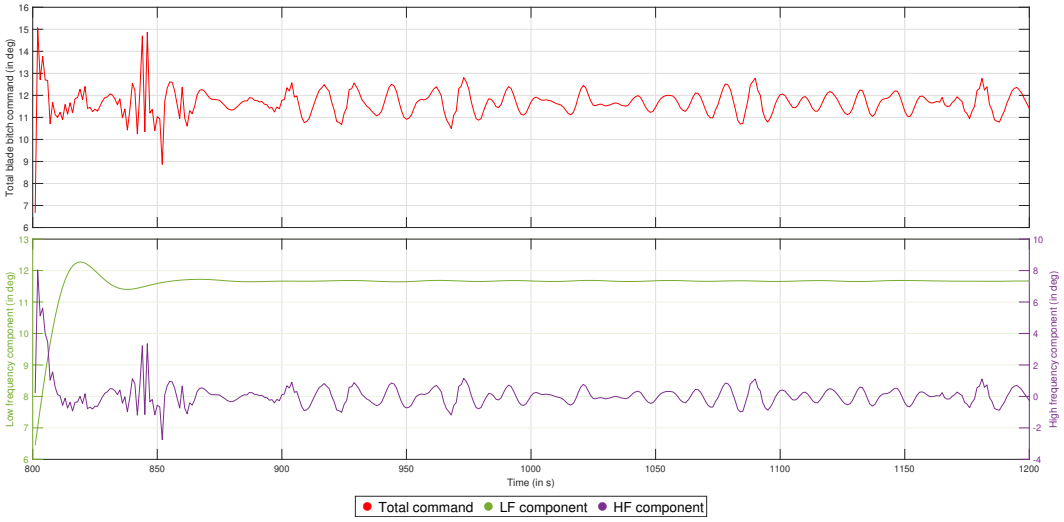

Figure 4-8: Filtered control input provided by the FF DeePC in a steady wind scenario. LF stands for low frequency, HF for high frequency.

Since the FF DeePC controller computes a command based on both measured and future signals, the control action cannot be explicitly separated into feedforward and feedback components. However, considering that the wind disturbance is mostly active at low frequencies below the wave range, the blade pitch command can be roughly separated to illustrate the component that compensates for each of the two disturbance types. In Figure 4-8, the FF DeePC input is filtered into a low-frequency and a high-frequency component. The low-frequency part of the signal remains constant at the operating point value due to a lack of change in wind speed. The controller adds a higher frequency component that addresses the wave disturbance.

4-3-2 Turbulent wind and irregular waves conditions

In this scenario, turbulent wind is considered along with the two sea states of the previous section. As observed by Hegazy et al., wind turbulence has more dominance on the dynamical response of floating

wind turbines than waves, diminishing the effect of wave FF control. The DeePC that includes wave feedforward information used in the previous subsection was found to perform similarly or slightly worse than the DeePC with no preview in the two turbulent wind load cases. Compared to the baseline, an improvement is observed in terms of platform pitch variance and tower base loads, but a degradation in performance occurs for every other considered aspect. These results can be found in Appendix A.

To this end, a modification is first brought to the controller. The DeePC framework is not limited to one-dimensional disturbance inputs, and including more information on incoming conditions improves the prediction over the future horizon. Obtaining wind preview is possible due to the existence of LIght Detection And Ranging (LIDAR) sensors, therefore knowledge of the incoming wind speed was incorporated in the FF DeePC controller along with the platform pitching moment. During open-loop data collection, a white noise v_k with a mean of $16\,\mathrm{m\,s^{-1}}$ and $\mathrm{var}(v_k) = 0.5^2$ was fed on the horizontal wind speed input channel of the linearization. Although a turbulent wind time series generated with TurbSim has enough persistency of excitation, this wind profile has a high destabilizing potential during open-loop operation, so it is not used at this stage. Data from both disturbance channels is further used to construct the DeePC data matrices.

The constraints and tuned performance weights used are listed in Table 4-III. The blade pitch angle is allowed to vary more around the linearization point compared to the steady wind case because the turbine is expected to need ampler pitching to handle wind turbulence.

Table 4-III: Tuning parameters used for the FF DeePC in the turbulent wind load cases. The intervals indicate within what bounds the respective input or output is allowed to vary around the linearization point value.

Parameter	θ_c (°)	$\dot{\theta}_{c,\max}$ (°/s)	Ω (rpm)	Θ_P (°)	Q_k	R_k
Interval or value	[-8,8]	8	[-1.8, 1.8]	[-1, 1]	$\mathrm{diag}(500, 0)$	1

Figure 4-9 compares the outcome of the baseline, DeePC, and FF DeePC controllers simulated in identical conditions. The DeePC leads to high rotor speed oscillations and constraint violations for both outputs. The DeePC with wave and wind preview manages to track the rotor speed reference with lower amplitude oscillations than both the baseline and the classical DeePC controllers, while adhering to the platform motion restrictions. The blade pitching activity of the DeePC controllers is significantly higher compared to the baseline, both in magnitude and rate. The PSDs in Figure 4-9 confirm that the FF controller reduces the energy in rotor speed oscillations caused by the waves, while also compensating for the effect of wind perturbation in the low-frequency range. This is due to both previews being included in the optimization process. A similar amount of energy is concentrated in the blade pitch input in the low-frequency range, indicating that all three controllers are actively counteracting wind turbulence. However, the FF control input maintains a high energy content in the wave frequency as well.

The control input of the FF DeePC follows the continuous profile of the baseline sequence, while also displaying superimposed higher frequency oscillations. This is outlined in Figure 4-10, which was obtained by filtering the input sequence similarly to the steady wind case. It can be observed that the low-frequency component of the feedforward command is shifted forward in time relative to the baseline command, indicating that the controller is preemptively pitching the blades based on the preview knowledge to compensate for the incoming wind turbulence. The wave disturbance is mitigated through the higher frequency component.

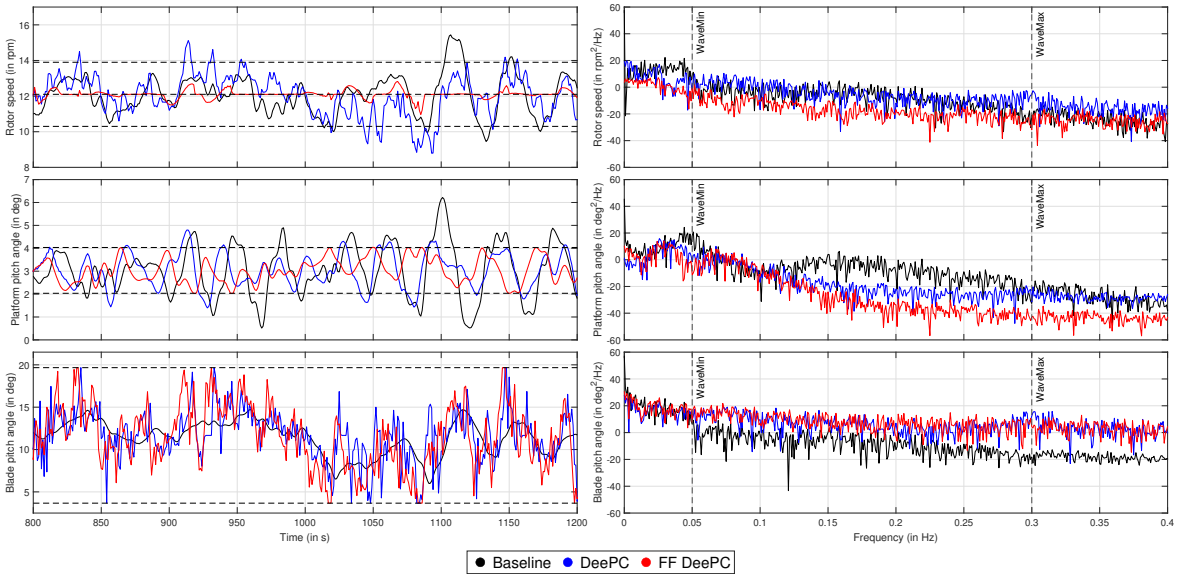

Figure 4-9: Simulation of a turbulent wind, irregular waves scenario. The turbulent wind has a mean speed of $16\,\mathrm{m\,s^{-1}}$ and a turbulence intensity of 15%. The wave profile has $H_s = 3\,\mathrm{m}$ and $T_p = 12\,\mathrm{s}$. The baseline controller is represented in black, a DeePC controller with no disturbance preview in blue, and the FF DeePC controller in red. **Left column**: time series of the rotor speed, platform pitch angle, and blade pitch angle input. The dashed horizontal lines represent constraints used during the optimization. **Right column**: PSD of the signals on the left.

4-3-3 Performance evaluation

The performance of the FF DeePC is further compared to the baseline controller in the four load cases defined by Table 4-I. The mean power production is similar for both controllers since, although the baseline controller leads to higher oscillations around the reference rotor speed, the signal is primarily centered around the rated value. As a measure of power quality, the power variance is considered. Rotor speed variance and Root Mean Square Error (RMSE) are used to assess the quality of rotor speed tracking. The extent of platform motions is evaluated by computing the variance of the platform pitch angle. Blade pitch actuation is evaluated through the variance of the collective pitch input, and the actuator duty cycle (ADC) metric given as

$$\mathrm{ADC} = \frac{1}{T}\sum_{k=1}^{n} \frac{|\dot{\theta}_{c,k}|}{\dot{\theta}_{c,max}} T_s, \tag{4-5}$$

where T is the length of the time frame over which the ADC is evaluated, n represents the number of samples of the blade pitching rate series, $\dot{\theta}_{c,\max}$ is the maximum pitching rate, and T_s is the sampling time in seconds. The relative performance is evaluated using

$$P_{\mathrm{rel}} = \left(\frac{P_{\mathrm{FF}}}{P_{\mathrm{baseline}}} - 1\right) \cdot 100\%, \tag{4-6}$$

where P_{FF} and P_{baseline} represent the performance of the FF DeePC and the baseline controller respectively.

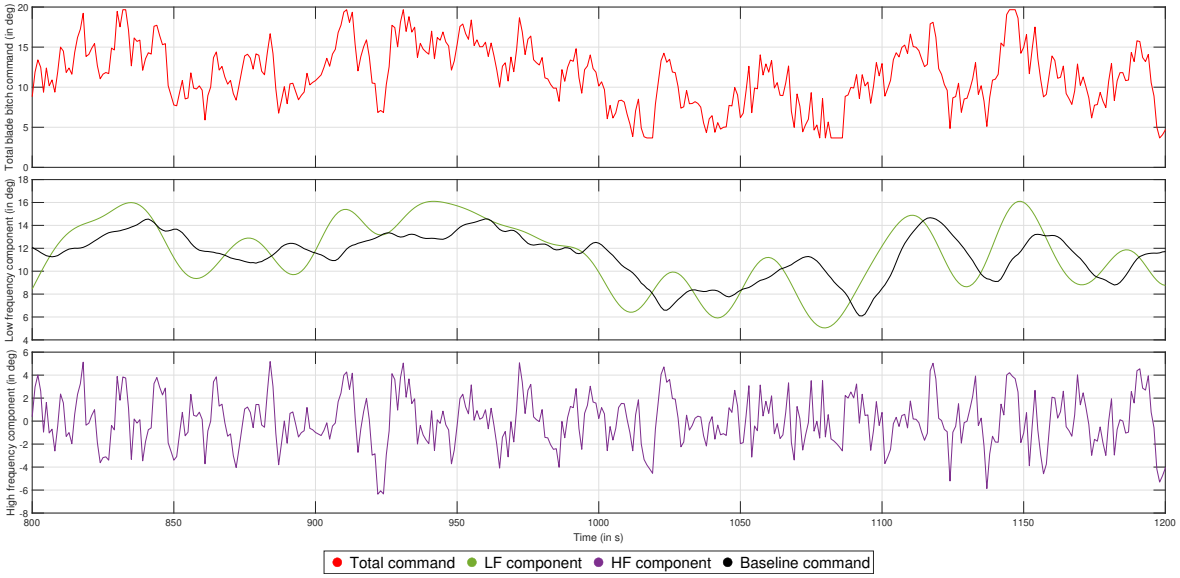

Figure 4-10: Filtered control input provided by the FF DeePC in turbulent wind conditions. LF stands for low frequency, HF for high frequency. The baseline command is included in the plot of the LF component to outline the effect of including feedforward action in the DeePC controller. The continuous component of the DeePC without preview is highly similar to the baseline and is thus left out of the figure.

Table 4-IV: Average of the performance metrics of the three controllers in Load cases 1 and 2, linear simulation.

	P_{var} (kW)	$\Omega_{\text{var}}(\text{rpm}^2)$	Ω_{RMSE} (rpm)	$\theta_{c,\text{var}}(\text{deg}^2)$	$\theta_{c,\text{ADC}}$ (%)	$\Theta_{\text{P,var}}(\text{deg}^2)$
Baseline	5.95×10^3	0.034	0.19	0.021	0.8	0.046
DeePC	9.9×10^3	0.058	0.239	0.58	5.9	0.055
FF DeePC	0.85×10^3	0.05	0.068	0.306	3.9	0.048

Figure 4-11 outlines the same trend in all four load cases: rotor speed oscillations are lowered and the rotor speed tracking error is improved, which is directly reflected in the quality of the generator power since the torque controller maintains the generator torque constant. This comes at the cost of a significantly larger actuation effort relative to the baseline. Except for the first load case, the variance of the platform pitch angle decreases compared to the baseline controller. For the first load case, the platform pitch angle could be further restricted, but the platform pitch angle of the baseline controller already remains within a quite reduced interval.

Using the FF DeePC in steady wind leads to a rotor speed variance decrease of on average 80%, and the RMSE is reduced by 68%. To achieve this, three times more actuation effort is necessary. The considerable increase in blade pitch variance can be explained by the baseline controller being only slightly reactive to this disturbance scenario. The absolute numerical values of the considered metrics are listed in Table 4-IV for steady wind conditions.

In turbulent wind conditions, the baseline controller increases the pitching activity, leading to a less pronounced relative increase in the variance of the input command. However, the actuation effort is even higher, with a 10-fold increase indicated by Figure 4-11. The rotor speed variance is, however, decreased by an average of 95%, and the RMSE by 82%. A significant improvement is observed in the

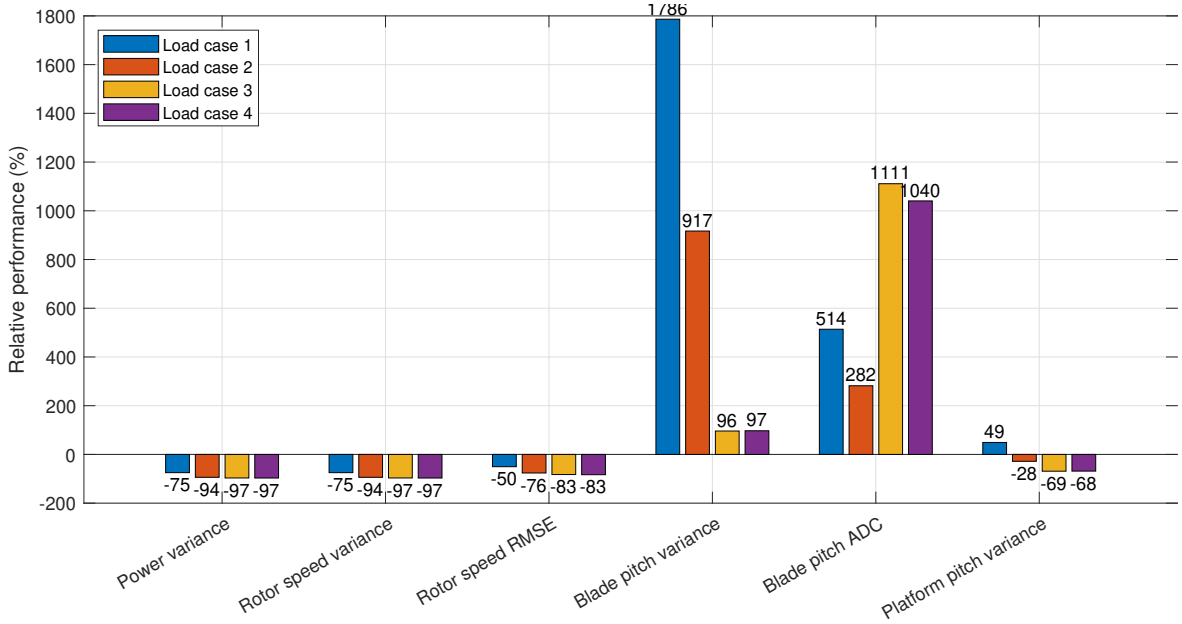

Figure 4-11: Performance statistics of the FF DeePC controller relative to the baseline controller for each load case. A positive value indicates an increase and, therefore, a degradation. A negative value indicates a decrease, equivalent to an improvement. The change in performance of the FF controller is given as a percentage of the baseline metric.

Table 4-V: Average of the performance metrics of the three controllers in Load cases 3 and 4, linear simulation.

	P_{var} (kW)	$\Omega_{\text{var}}(\text{rpm}^2)$	Ω_{RMSE} (rpm)	$\theta_{c,\text{var}}(\text{deg}^2)$	$\theta_{c,\text{ADC}}$ (%)	$\Theta_{\text{P,var}}(\text{deg}^2)$
Baseline	1.65×10^5	0.969	1.01	5.91	1.8	0.98
DeePC	1.88×10^5	1.104	1.06	6.38	19	0.44
FF DeePC	1.78×10^4	0.104	0.324	11.01	21	0.29

platform pitch angle variance, which is lowered by 68%. Absolute values of these metrics for turbulent wind conditions are presented in Table 4-V.

It is also expected that the wind turbine structural loads will be affected. The effect of the FF DeePC controller on the tower base bending loads, the low-speed shaft torsion, and the blade out-of-plane root bending moment is therefore investigated. The relative damage equivalent loads (DELs) were computed using the same relative relation to the baseline controller, and are illustrated in Figure 4-12. As a general trend, the low-speed shaft torsion is decreased in all simulation scenarios due to the reduction in rotor speed oscillations. In steady wind conditions, the FF controller increased the tower base loads by approximately 50%. An increase in the blade out-of-plane bending moment is also observed, while the shaft torsion decreased on average by 35%. A significant alleviation of tower base loads of 60% is encountered in turbulent wind conditions, along with a decrease in low-speed shaft torsion of 85%, and 50% for the blade out-of-plane bending moment.

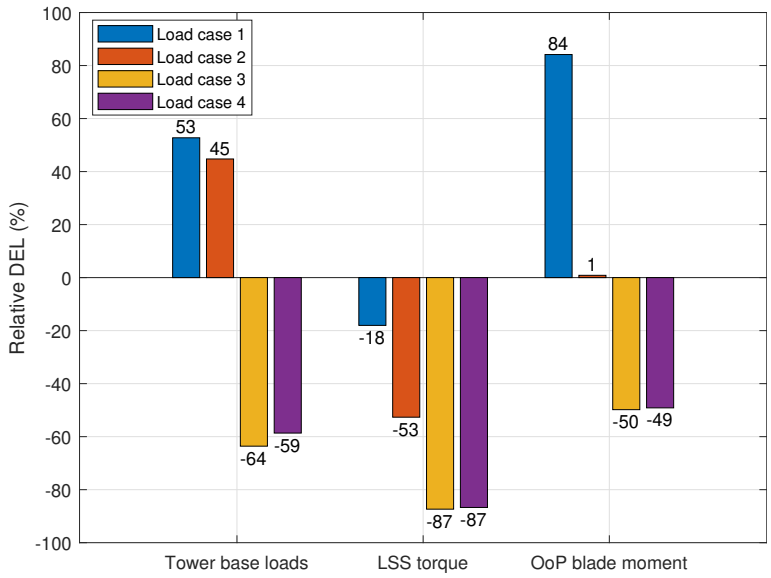

Figure 4-12: Damage equivalent loads of the tower bending moment, low-speed shaft torsion, and out-of-plane blade bending moment of the FF controller relative to the baseline. A positive value indicates an increase, while a negative value suggests a decrease.

4-3-4 Balance of the control objectives

The FF DeePC employed in the previous subsection was tuned for a compromise between good reference regulation and reduced fore-aft motions of the wind turbine platform. This subsection aims to analyze whether giving more weight to either of the two control objectives brings any advantage. Additionally, the consequences of focusing the FF DeePC on only one of the two objectives are outlined. To this end, the balanced controller previously employed is compared to a controller that focuses on rotor speed tracking (FF DeePC $-\ \Omega$) and a controller that solely aims for platform motion minimization (FF DeePC $-\ \Theta_P$). The rotor speed-focused DeePC does not constrain the platform pitch angle, while the platform pitch-focused controller does not aim to perform rotor reference tracking. However, no plant output is discarded in any of the scenarios.

Steady wind

For this analysis, only Load case 1 of Table 4-I is considered. The outcome of the simulation is illustrated in Figure 4-13. It can be observed that FF DeePC$-\Omega$ leads to excellent rotor speed tracking, with a slight increase in platform pitching and similar control input to the balanced FF DeePC. This also outlines that the implemented balanced controller inclines toward a focus on reference tracking. The energy concentrated from waves to rotor speed is decreased, but an amplification peak becomes visible at the platform pitch natural frequency in the power spectral density of the platform pitch and blade input, which suggests that disregarding platform motions may lead to resonance issues.

The FF DeePC $-\ \Theta_P$ achieves a significant reduction in platform movements, at the cost of notably larger rotor speed oscillations and blade pitching. While no resonance peaks are visible in the PSDs of the signals, this controller leads to a significant increase of condensed energy in the rotor speed signal

frequencies excited by the waves. The blade pitch signal focuses energy in this frequency range as well, which results in less energy being transferred from wave disturbance to the platform pitch angle.

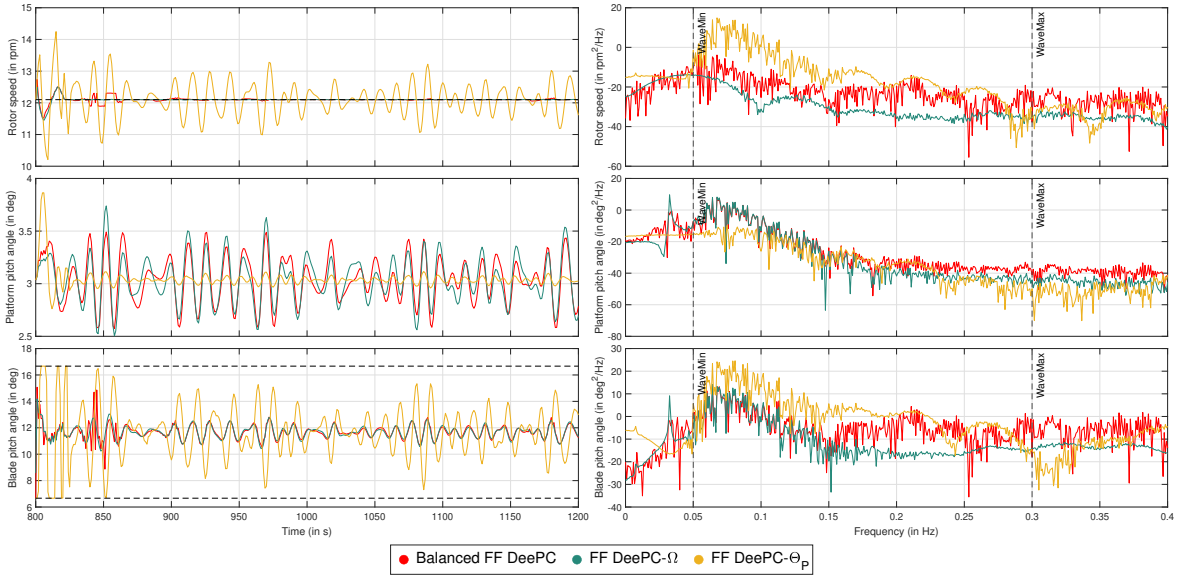

Figure 4-13: Response of the three FF DeePC controllers with different control objectives in Load case 1. **Left column:** extract of a time series. **Right column:** PSD of the signals on the left.

The performance of all three controllers relative to the baseline is presented in Figure 4-14. Except for a reduction in platform movements, the FF DeePC $-\Theta_P$ controller leads to a substantial degradation of all performance metrics. Simultaneously, focusing the controller on rotor speed tracking results in an improvement of the metrics compared to the baseline and the balanced controller, at the cost of slightly larger platform motions.

Regarding turbine loads, FF DeePC $-\Omega$ reduces the low-speed shaft torsion due to the decrease in rotor speed oscillations. However, the FF DeePC $-\Theta_P$ largely increases this load along with the blade out-of-plane moment. The tower loads are also increased, which may be due to the controller inducing lower amplitude but higher frequency movements of the platform that result in higher loads.

Overall, no significant advantage of emphasizing rotor tracking more than already done in the balanced controller is observed, while the improvement brought by FF DeePC $-\Theta_P$ in terms of platform motion reduction is considered unreasonable relative to the consequent performance degradation. Therefore, a balanced approach is considered the most suitable in steady wind conditions.

Turbulent wind

Only Load case 3 of Table 4-I is considered in this part. Figure 4-16 shows the response of the system. FF DeePC $-\Omega$ displays large oscillations of the floating platform compared to the other two controllers. Similarly to the steady wind case, the platform pitching eigenfrequency is also amplified by the rotor speed-focused controller. The FF DeePC $-\Theta_P$ controller attenuates the energy of this frequency. However, a significant amount of energy is added to the rotor speed signal in the wave frequency.

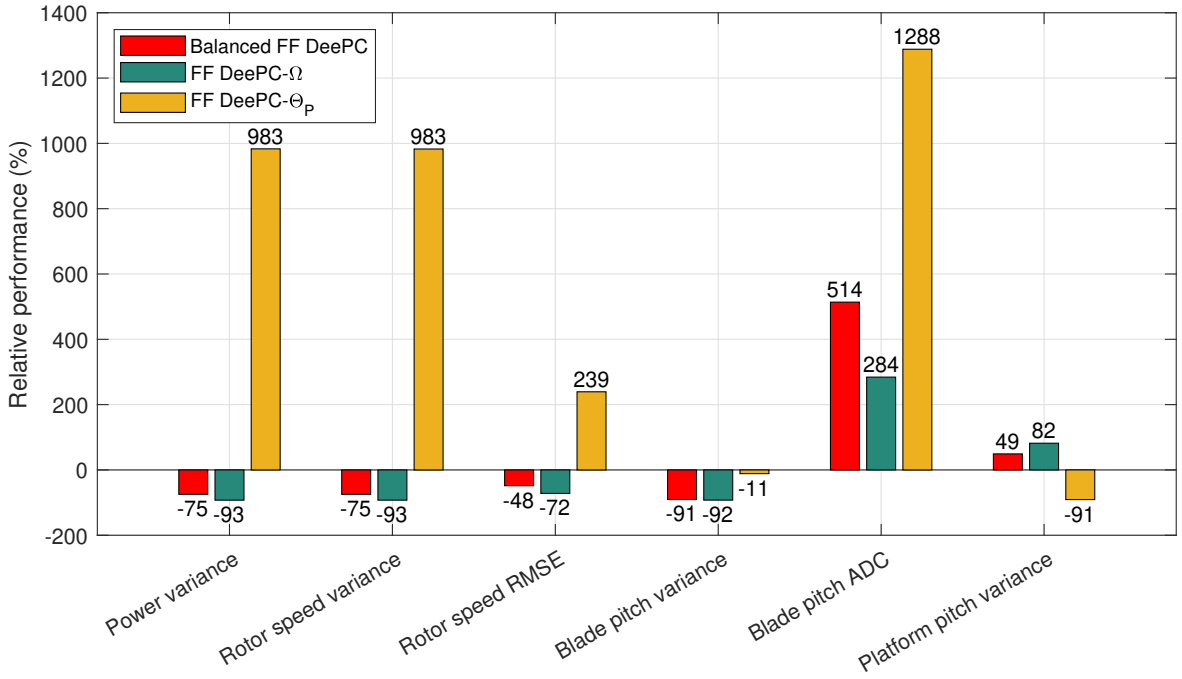

Figure 4-14: Relative performance of the FF DeePC controllers with different control objectives in Load case 1 compared to the baseline. A negative value indicates an improvement, while a positive one suggests a degradation.

The relative performance and DELs to the baseline controller can be observed in Figures 4-17 and 4-18, respectively. Biasing the controller toward rotor speed tracking largely increases platform motions and tower base loads without displaying any improvement in other performance indicators. FF DeePC$-\Theta_P$ generally leads to a decrease in performance compared to its balanced counterpart. Despite achieving a reduction in platform pitching, the tower base loads are similar to the balanced FF DeePC. Hence, reducing the amplitude of the platform pitching motions is not necessarily equivalent to a reduction in tower base loads.

Therefore, in turbulent wind conditions, disregarding the platform pitch control objective leads to large tower base loads and potential negative damping issues without gaining significant rotor speed tracking quality. On the other hand, solely focusing on platform motion reduction does not bring any major improvement, and a balanced controller performs better than both extremes.

4-4 Concluding remarks on the linear simulation

In this chapter, the FF DeePC framework was adapted to a wind turbine system and tested in a linear setting using a linearization of the FOWT. As a preview signal, the pitch moment acting on the platform was used. It was found that at least one period of a wave disturbance must be included in the preview. To maintain a reasonable dimension of the optimization problem, a sampling time of 1 s was used. A scaling of the linearization was adopted to ensure numerical stability during the optimization process and uniform priority of the signals during control.

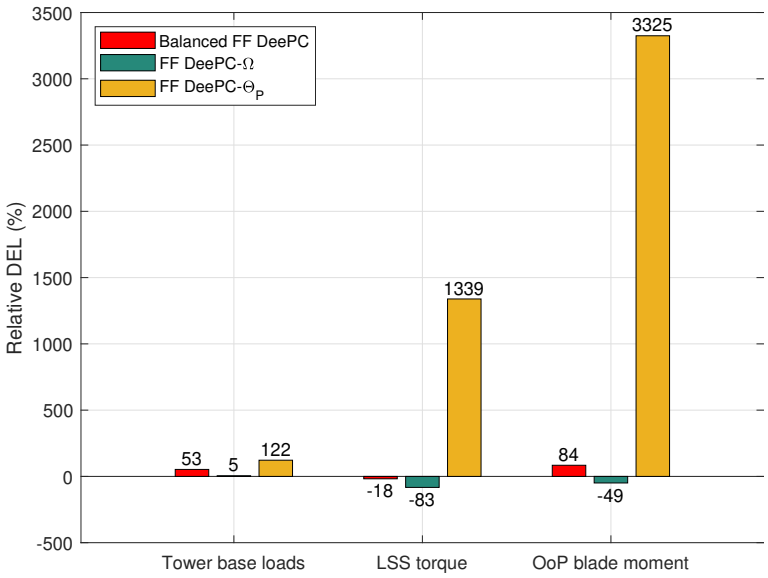

Figure 4-15: Relative DELs of the FF DeePC controllers with different control objectives in Load case 1 compared to the baseline.

A FF DeePC controller that balances the two control objectives, namely rotor speed tracking and platform motion minimization, was tested in both steady and turbulent wind conditions, and compared with a DeePC controller with no preview and the baseline controller of the reference wind turbine. The steady wind simulations outlined that the proposed controller can simultaneously adhere to the reference tracking objective while maintaining the platform pitch angle within the specified bounds, and including wave preview leads to better performance and fewer constraint violations. Additionally, an improvement of these objectives over the baseline controller was obtained. However, the pitching activity of the data-driven controllers is significantly increased.

In turbulent conditions, the wind disturbance dominates the response of the wind turbine, and feedforward control that solely relies on wave preview data does not bring a visible improvement compared to the classical DeePC. However, including LIDAR wind speed data in the FF controller along with wave information leads to an enhancement in both the quality of the rotor speed output and the platform pitching motions, along with a reduction in turbine loads.

Finally, the compromises in performance entailed by focusing the FF DeePC exclusively on either of the two control goals were outlined. It was observed that a controller that simultaneously considers both objectives in an appropriate proportion is preferred and generally performs better than a single-objective controller.

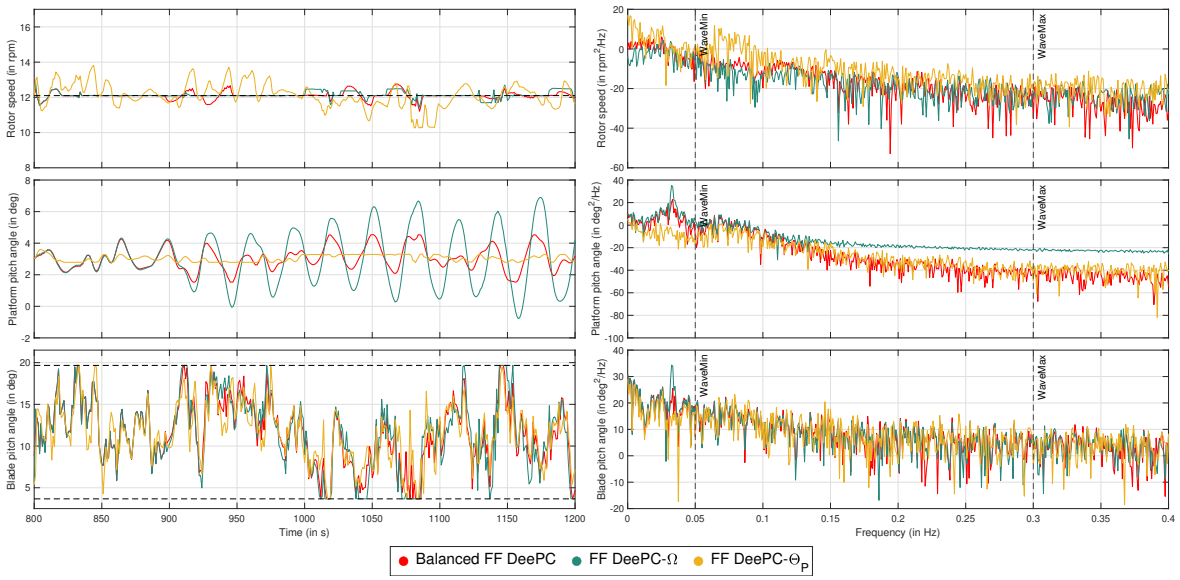

Figure 4-16: Response of the three FF DeePC controllers with different control objectives in Load case 3. **Left column:** extract of a time series. **Right column:** PSD of the signals on the left.

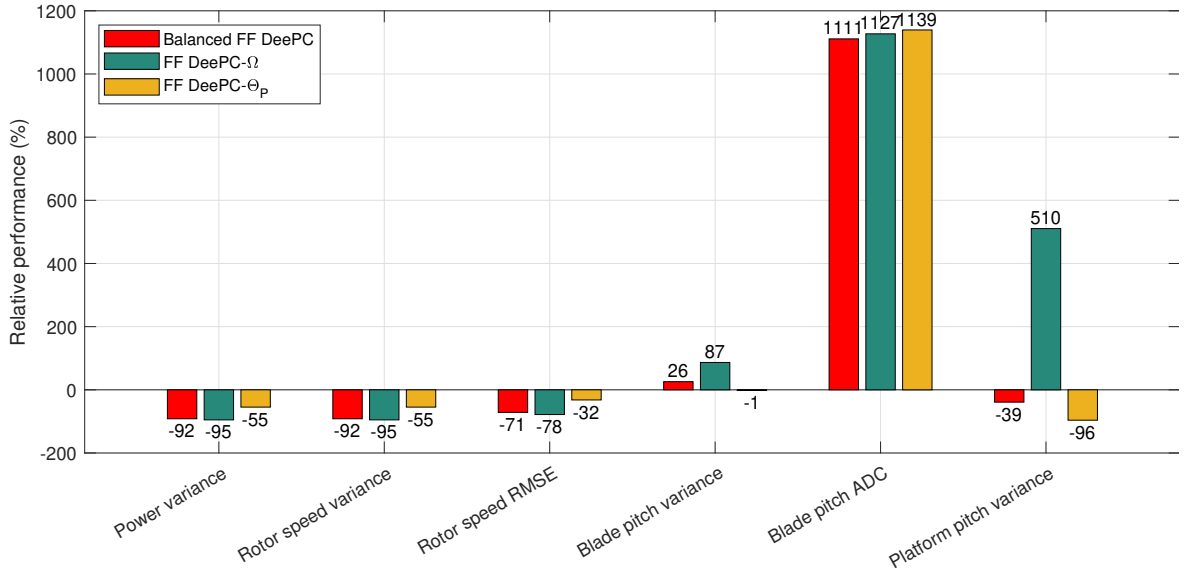

Figure 4-17: Relative performance of the FF DeePC controllers with different control objectives in Load case 3 compared to the baseline.

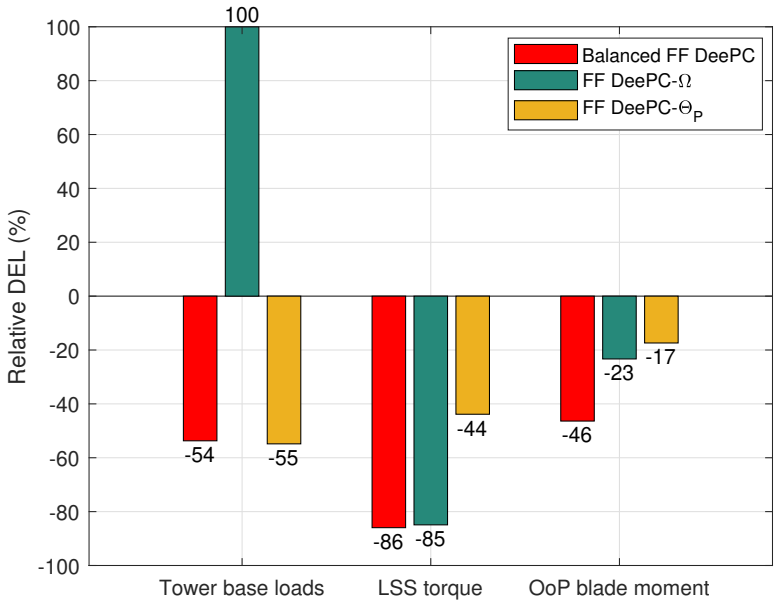

Figure 4-18: Relative DELs of the FF DeePC controllers with different control objectives in Load case 3 compared to the baseline.

Chapter 5

QBlade high fidelity simulation

The objective of this chapter is to test the wave feedforward Data-enabled Predictive Control (DeePC) algorithm in a more realistic configuration. For this purpose, the proposed model-free controller is subjected to high-fidelity simulations using QBlade. QBlade is a modular implementation of highly efficient multi-fidelity aerodynamic, structural dynamic, and hydrodynamic solvers [72]. With a software-in-loop interface, QBlade enables controlling the simulation loop while co-simulating from MATLAB. The same configuration of an NREL 5-MW reference wind turbine mounted on an OC3-SPAR floating platform is used throughout this chapter, illustrated in Figure 5-1. Similarly to the previous chapters, steady and turbulent wind inflow conditions are investigated, and simulations for the same load cases as in Table 4-I are carried out. The performance metrics and damage equivalent loads (DELs) used for the linear simulation are computed for the nonlinear configuration as well.

5-1 DeePC adaptation for high-fidelity simulations

A preview of wave hydrodynamic forces can be provided by QBlade at a requested time interval ahead of the current simulation time step. However, the preview is not perfect, and the error between the predicted value and the measured wave pitch force increases with larger wind preview windows. The error is non-constant, with a Root Mean Square Error (RMSE) of 4.5×10^7 N m found during a simulation time of 100 s and a preview length of 20 s.

Due to the large wave pitch moment prediction errors, the equality constraints of the optimization problem lead to infeasibility. The infeasibility issues persist even when a perfect preview is provided due to the accentuated nonlinearity of the plant. As presented by Coulson et al., regularization terms may be included to relax the equality constraints such that an optimum may be found even if the equalities are not strictly satisfied [79]. Regularization terms were therefore added for the disturbance input and output trajectories. The objective function and constraints of Equation 2-26 are updated to

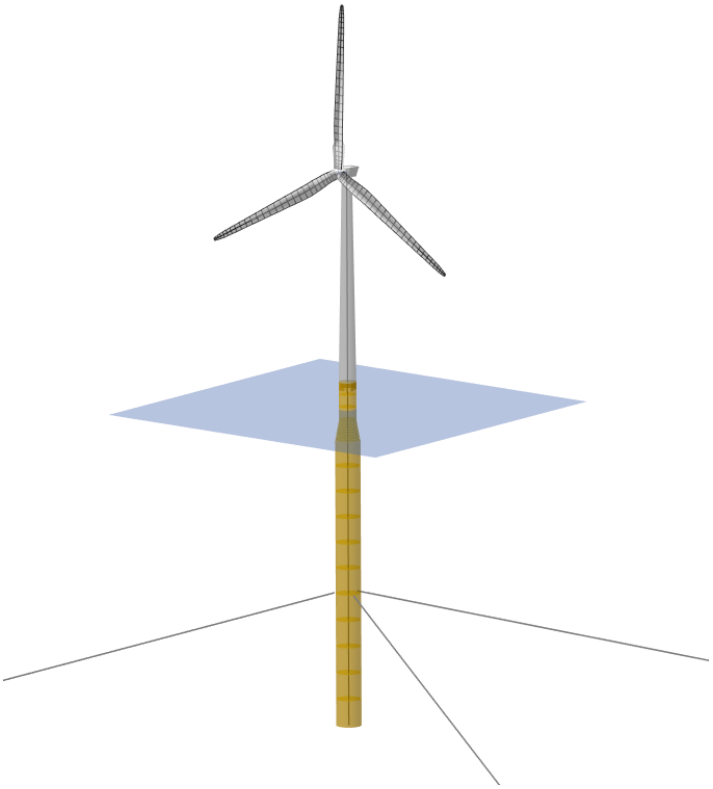

Figure 5-1: NREL 5-MW reference wind turbine installed on an OC3-SPAR floating structure, visualization of the model extracted from QBlade.

$$
\begin{aligned}
\min_{U_{\hat{i}_p,f,1},\hat{g},\sigma_y,\sigma_w} \quad & \left(Y_{i_p,f,\bar{N}} Z_{\bar{N}}^{\mathrm{T}} \hat{g} - r_f\right)^{\mathrm{T}} Q \left(Y_{i_p,f,\bar{N}} Z_{\bar{N}}^{\mathrm{T}} \hat{g} - r_f\right) + U_{\hat{i}_p,f,1}^{\mathrm{T}} R U_{\hat{i}_p,f,1} + \lambda_y \|\sigma_y\|_2 + \lambda_w \|\sigma_w\|_2 \\
\text{s.t.} \quad & \begin{bmatrix} U_{i,p,\bar{N}} \\ W_{i,p,\bar{N}} \\ Y_{i,p,\bar{N}} \\ U_{i_p,f,\bar{N}} \\ W_{i_p,f,\bar{N}} \end{bmatrix} Z_{\bar{N}}^{\mathrm{T}} \hat{g} = \begin{bmatrix} U_{\hat{i},p,1} \\ W_{\hat{i},p,1} \\ Y_{\hat{i},p,1} \\ U_{\hat{i}_p,f,1} \\ W_{\hat{i}_p,f,1} \end{bmatrix} + \begin{bmatrix} o \\ \sigma_w \\ \sigma_y \\ o \\ o \end{bmatrix}, \\
& Y_{i_p,f,\bar{N}} Z_{\bar{N}}^{\mathrm{T}} \hat{g} = Y_{\hat{i}_p,f,1}, \\
& u_k \in \mathcal{U}, \forall k \in \{0, \cdots, f-1\}, \\
& y_k \in \mathcal{Y}, \forall k \in \{0, \cdots, f-1\},
\end{aligned}
\tag{5-1}
$$

where $\lambda_y, \lambda_w \in \mathbb{R}_{>0}$ are regularization weights, and $\sigma_y \in \mathbb{R}^{\ell p}$, $\sigma_w \in \mathbb{R}^{qp}$ are auxiliary slack variables. The values of the regularization weights are chosen to be high enough such that the slack variables are non-zero only if the problem is infeasible. A 2-norm of the slack variable vectors is used to preserve the convexity of the optimization problem.

5-2 Simulation results

The high-fidelity experiment is set up similarly to the linear case. The lengths of the data sets are maintained at $p = f = 20$, and $N = 500$, and the persistently exciting control input is generated in the same manner. During the open-loop data collection, no controller is activated. Before starting the data collection experiment, the wind turbine is simulated for 100 s to ensure it has reached a steady state. The signals are detrended and scaled before being provided to the controller.

In Chapter 4, a sampling time of 1 s was used both to simulate the wind turbine linearization and for control purposes. However, this value is too large for the multi-physics solvers of QBlade. Therefore, the simulations are carried out on a sampling time of 0.05 s, while the feedforward (FF) DeePC uses subsampled versions of the input-output signals to maintain the sampling time of 1 s. Thus, the optimal control input is computed only once every second and then maintained constant until a new command is computed. The load cases used in the previous chapter and listed in Table 4-I are used. The FF DeePC controller is compared to a DeePC controller without preview and a baseline controller of the reference Floating offshore Wind Turbine (FOWT).

5-2-1 Steady wind inflow

The results of simulations in steady wind conditions are illustrated in Figure 5-2. Both data-driven controllers generally limit the platform pitch angle, but the DeePC with no preview accentuates the oscillations of the rotor speed and leads to a large actuation effort. Including feedforward information in the DeePC controller decreases the oscillations and reduces the blade pitching. Still, the required amount of actuation is quite large compared to the baseline. The peaks below the wave frequency range that can be observed in the Power Spectral Density (PSD) plots of the baseline controller correspond to the platform pitching natural frequency. The FF DeePC controller has a significant attenuating effect. Compared to the baseline controller, the blade pitching does not excite this eigenfrequency, indicating that the model-free feedforward controller eliminates the resonance issue caused by the baseline controller.

5-2-2 Turbulent wind inflow

Figure 5-3 shows the results of the high-fidelity simulation in turbulent wind conditions. Only wave preview is included in the FF controller. Although incorporating wind preview improves the performance of the controller as observed in Chapter 4, combining wind and wave preview led to infeasibilities that were not resolved. Using feedforward information on incoming waves leads to a slight improvement in constraining the platform motions. Numerous constraint violations of the platform pitch angle occur due to the intensity of the wind turbulence and are particularly visible after 300 s. These might also be caused by the lower bound imposed on the blade pitch angle command. As well as in the steady wind scenario, the DeePC controllers appear to attenuate the platform pitching natural frequency excitation observed with the baseline controller, which is visible in the PSD of the platform pitch angle signal.

5-2-3 Performance

The relative performance and DELs to the baseline controller are plotted in Figure 5-4 and Figure 5-5 respectively. The FF DeePC lead to a decrease in rotor speed variance of approximately 70% in all

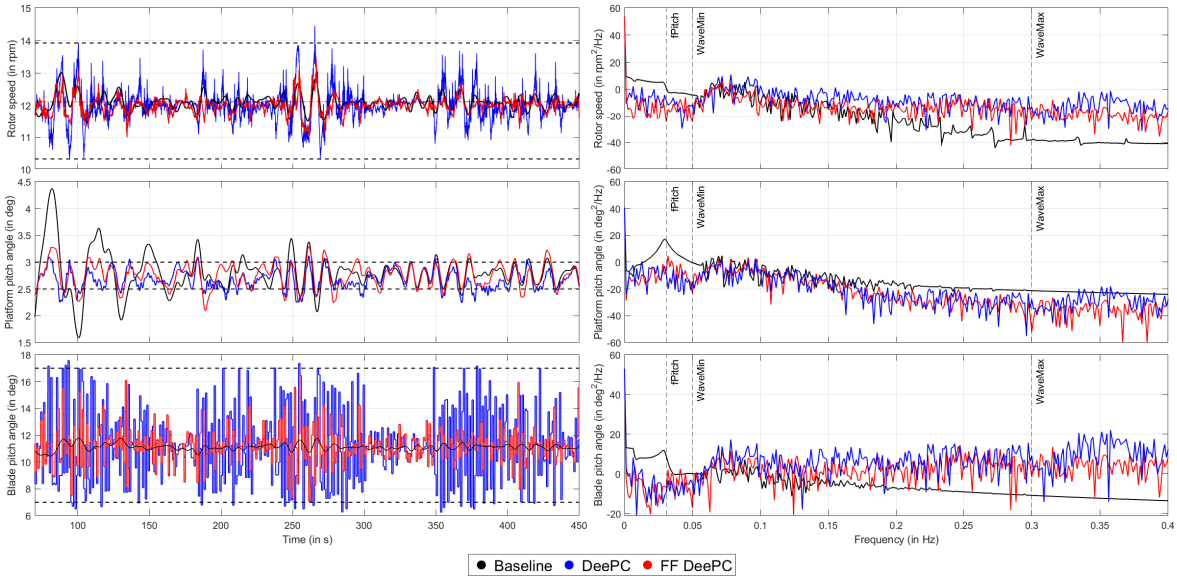

Figure 5-2: Part of a high-fidelity simulation of Load case 1 (steady wind, irregular waves). The baseline controller is represented in black, and the FF DeePC controller is in red. **Left column:** time series of the rotor speed, platform pitch angle, and blade pitch angle input. The rated reference rotor speed is represented as a dash-dotted line in the left-upper plot. The dashed horizontal lines represent constraints used during the optimization. **Right column:** PSD of the respective signals on the left. The first vertical dashed line indicates the platform pitching natural frequency, while the next two vertical lines mark the frequency range across which the wave disturbance is usually active.

Table 5-I: Performance metrics of the three controllers in Load case 1, high-fidelity simulation.

	P_{var} (kW)	$\Omega_{\text{var}}(\text{rpm}^2)$	Ω_{RMSE} (rpm)	$\theta_{c,\text{var}}(\text{deg}^2)$	$\theta_{c,\text{ADC}}$ (%)	$\Theta_{\text{P,var}}(\text{deg}^2)$
Baseline	4.08×10^4	0.206	0.457	0.505	1.07	0.419
DeePC	4×10^4	0.208	0.468	7.969	49.8	0.032
FF DeePC	1.11×10^4	0.058	0.273	1.534	17.5	0.043

four load cases. The rotor speed RMSE was lowered by 40% in steady wind and 35% in turbulent wind conditions. The platform pitch variance decreased by 85% with steady wind and by 71% with turbulent wind inflow. However, in the same conditions, the blade pitch actuator duty cycle (ADC) was 15 and 7 times higher, respectively. The accentuated oscillations of the rotor speed led to an increase in the low-speed shaft torsion, as opposed to the findings of the linear simulations. Larger values of tower base loads and blade out-of-plane bending moment are also observed in the high-fidelity setting. The absolute values of the performance indicators are listed in Table 5-I for steady wind inflow, and Table 5-II for turbulent wind conditions.

5-3 Concluding remarks on high-fidelity simulation

In this chapter, a high-order model of National Renewable Energy Laboratory (NREL) 5-MW reference wind turbine mounted on an OC3-Hywind spar-buoy floating platform was simulated in a closed-loop with the proposed DeePC controller including wave forces feedforward information. The instrumental

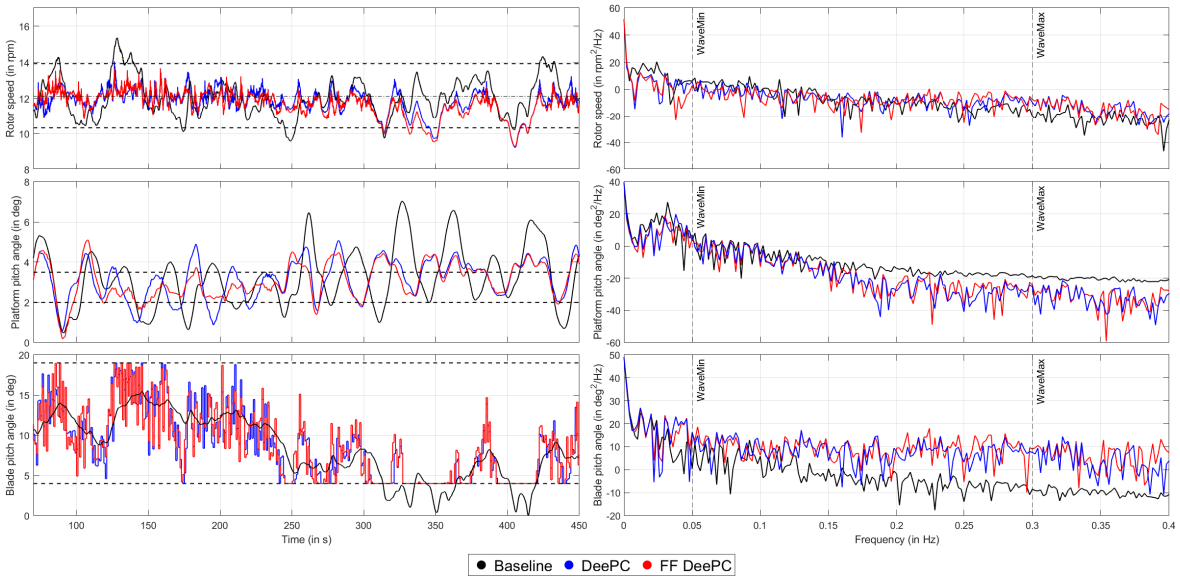

Figure 5-3: Part of a high-fidelity simulation of Load case 3 (turbulent wind, irregular waves). The baseline controller is represented in black, and the FF DeePC controller is in red. **Left column:** time series of the rotor speed, platform pitch angle, and blade pitch angle input. The rated reference rotor speed is represented as a dash-dotted line in the left-upper plot, and the dashed horizontal lines represent constraints used during the optimization. **Right column:** PSD of the respective signals on the left.

Table 5-II: Performance metrics of the three controllers in Load case 3, high fidelity simulation.

	P_{var} (kW)	$\Omega_{\text{var}}(\text{rpm}^2)$	Ω_{RMSE} (rpm)	$\theta_{c,\text{var}}(\text{deg}^2)$	$\theta_{c,\text{ADC}}$ (%)	$\Theta_{\text{P,var}}(\text{deg}^2)$
Baseline	2.89×10^5	1.466	1.214	14.155	3.56	2.602
DeePC	8.87×10^4	0.463	0.775	16.630	23.4	0.883
FF DeePC	9.02×10^4	0.469	0.721	16.479	29.4	0.686

variable introduced in the DeePC proved to be insufficient in dealing with the nonlinearities of the system and the wave forces preview prediction error. This problem was lessened by introducing quadratic regularization terms in the optimization problem.

Multi-objective control was successfully implemented on the wind turbine system using the proposed model-free, direct data-driven approach in all of the proposed load cases. When waves are the only disturbance acting on the wind turbine, including feedforward action in the DeePC controller improved both control goals and led to fewer infeasibility issues of the optimization problem. In turbulent wind, DeePC performs rotor speed tracking and limits the pitching of the platform, but including wave preview does not bring an improvement. In all load cases, it was observed that the DeePC controllers lower the energy contained in the platform pitch angle signal at the platform pitch natural frequency.

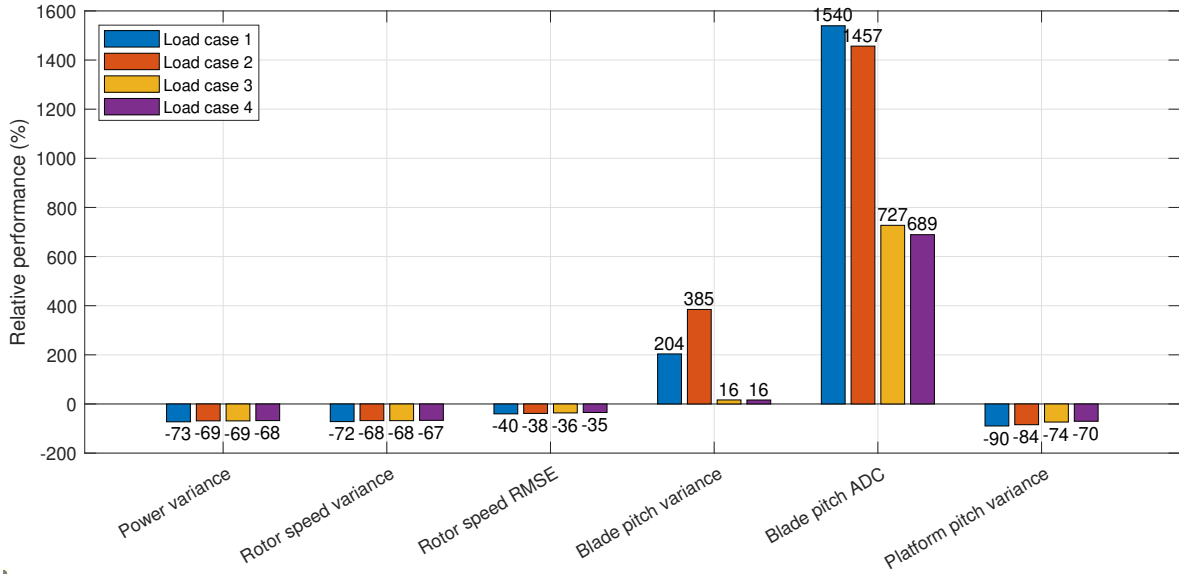

Figure 5-4: Performance metrics of the FF DeePC controller relative to the baseline controller in steady wind conditions and irregular waves.

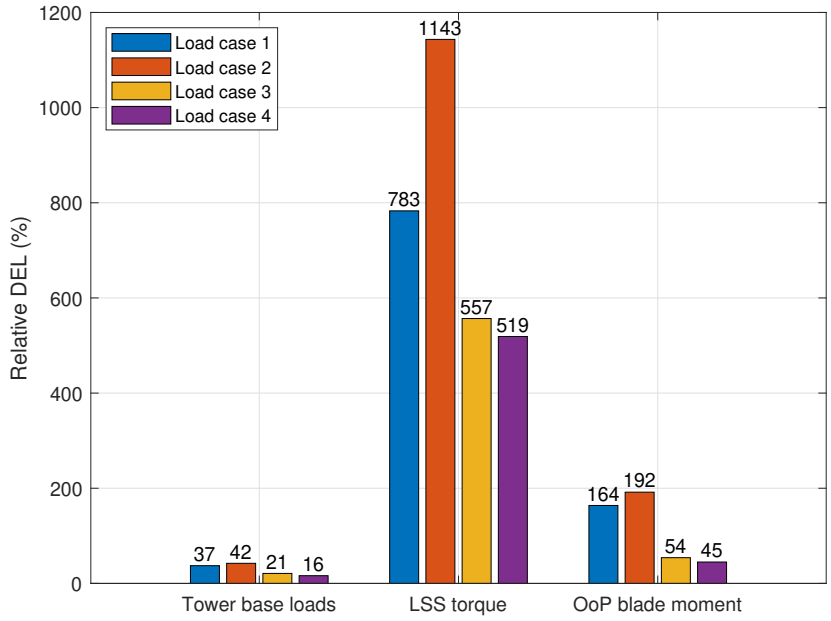

Figure 5-5: Damage equivalent loads of the FF DeePC controller relative to the baseline controller in steady wind conditions and irregular waves.

Chapter 6

Conclusion

6-1 General conclusion

Existing control strategies of Floating offshore Wind Turbines (FOWTs) have to face the negative damping issue, accentuated environmental disturbances, and enhanced model complexity due to both the floating structure and the increase in wind turbine size. This thesis aimed to implement a model-free, multiple-objective, feedforward controller for the above-rated region of a FOWT to tackle these challenges. As a model-free control method, the Data-enabled Predictive Control (DeePC) framework was explored partly due to the open opportunity of including disturbance measurements and preview in the already existing formulation. Thus, the main research question was formulated as:

Can a data-driven, feedforward, predictive controller that includes wave disturbance preview be synthesized for a floating offshore wind turbine?

To systematically answer this question, a set of sub-questions was followed, which will be reiterated to highlight the outcome of each stage.

1. *How may the DeePC algorithm be extended to include knowledge about incoming disturbances?* As initially presented by Coulson et al., DeePC relies on the assumption that the input-output trajectories are generated by a deterministic Linear Time-Invariant (LTI) system [73]. To explicitly specify the effect of measurable disturbances, a non-controllable input was included in the state-space description, along with corresponding input and direct feed-through matrices. Additionally, zero-mean white measurement noise was considered. With this formulation, disturbance data has to be collected aside from input-output trajectories to construct data matrices corresponding to the disturbance input. An assumption on the persistency of excitation of the disturbance trajectory is necessary, but not limiting since environmental perturbations are generally stochastic. The obtained disturbance data matrices eventually extend the set of equality constraints that encapsulate the system behavior. Measurement noise is rejected by implementing an instrumental variable, as presented by van Wingerden et al. [4]. To prepare for

the implementation on a wind turbine system with physical operational limits, linear inequality constraints of the input, input rate, and output are considered. The final optimization problem consists of a quadratic objective function with linear constraints, which can be solved efficiently.

2. *What adaptations are necessary to implement this algorithm on a FOWT using wave preview?*
The control design stage was initially carried out in a simplified setting, using a linearization of the reference wind turbine around an operating point in the above-rated region. Two control goals that target challenges commonly encountered in this operational region were established: reference rotor tracking and platform motion reduction. As a wave preview signal, the pitching moment acting on the platform was used. It was found that the future data window should include a preview of a full period of a wave and, to avoid excessively increasing the dimension of the optimization problem, a large sampling time was selected. A scaling was applied to bring all signals in the same order of magnitude and subsequently ensure good numerical properties of the optimization problem. Additionally, Chapter 4 outlined that a balance between the two control objectives is preferable.

3. *Can this data-driven control method be integrated with a high-fidelity wind turbine simulator?*
In Chapter 4 it was confirmed that the feedforward (FF) DeePC with instrumental variables can tolerate a certain level of noise on both the measured output and the disturbance preview. Nevertheless, in a high-fidelity setting, the instrumental variable was not sufficient to ensure the robustness of the control scheme. To this end, regularization terms were introduced in the optimization problem [73]. Aside from scaling, the input-output signals required detrending as well. Simulations of several load cases at a mean wind speed of $16\,\mathrm{m\,s^{-1}}$ were conducted. Simultaneous good rotor speed tracking and a reduction in platform motions were successfully achieved in a nonlinear environment using the proposed model-free controller.

4. *How does the developed control strategy perform compared to a conventional controller?*
Comparing the FF DeePC with the baseline controller in several load cases both in linear and high-fidelity environments outlined an overall improvement in both considered control objectives. The decrease in rotor speed tracking error, variance, and platform motions was achieved through considerably higher blade pitching effort. Furthermore, the data-driven controller attenuated the resonance peak present at the natural platform pitch frequency, indicating an alleviation of the negative damping issue. In steady wind load cases, including wave preview significantly improved the performance of the controller. This was not observed in turbulent wind conditions, where the wind disturbance proved to be the main driving perturbation. Using a preview of the horizontal wind speed along with the wave pitch moment led to excellent results during linear simulations. Regarding wind turbine loading, the linear and high-fidelity simulations disagreed, with the latter indicating an increase in all considered loads.

Following the answer to the sub-questions, it is concluded that the DeePC framework can be extended with feedforward action. Furthermore, this algorithm can be adapted for model-free control in the above-rated region of a floating offshore wind turbine using a preview of the incoming wave disturbance. No other extension of the DeePC approach was found in the considered literature, and data-driven control of floating wind turbines is still a developing area of research. For these reasons, additional effort is required to test, validate, and refine the proposed control method.

6-2 Future work and recommendations

This thesis presented an implementation of a feedforward, model-free method in a controlled, simulation-based environment. More steps need to be carried out to adapt this control strategy to a real-life application. The following recommendations indicate a few of these aspects that stem directly from this work:

1. *Study the potential of the FF DeePC controller in various environmental conditions across the entirety of the above-rated region.*
   This thesis investigated the effectiveness of the model-free controller around a single mean wind speed in the above-rated region during both linear and high-fidelity simulations. It is expected that the controller can learn the behavior of the wind turbine irrespective of the operating point, but testing should nonetheless be carried out. Additionally, the simulations should also consider multi-directional incoming waves.

2. *Identify an alternative approach to open-loop data collection.*
   Wind turbines are rarely operated in open-loop conditions for safety reasons and collecting data for controller synthesis in a closed-loop configuration would be preferable. When closed-loop data is used without any adaptation, the control input becomes correlated to the noise, breaking one of the assumptions on which DeePC is based. Hence, developing and using a closed-loop DeePC method is recommended for wind turbine control.

3. *Adapt the controller to consider changes in the operating point.*
   Although the control design process does not depend on the operating point of the wind turbine, the trajectories stored in the data matrices describe the behavior of the system in a specific operational region. If the dynamic response of the wind turbine is modified due to a change in the mean wind speed, the trajectories in the data matrices are no longer representative. To handle this, an adaptive strategy aimed at updating the data matrices is suggested. This recommendation is closely related to the previous one because it also calls for a closed-loop adaptation since it was observed that using closed-loop data may lead to a biased output prediction and potential instability [89].

4. *Investigate the inclusion of the generator torque as a control input.*
   Since only the blade pitch input is employed to control both the rotor speed and the platform pitch angle, the system is under-actuated. Hence, including a second control input may improve the performance if the transfer functions are sufficiently decoupled.

5. *Pursue further tuning and validation of the method in the high-fidelity setting.*
   The parameters of the controller used in the linear setting were transferred with minimal adaptations to the nonlinear case. Modifying the data window sizes might improve the performance of the controller. Including LIght Detection And Ranging (LIDAR) wind preview beside wave knowledge is encouraged and is expected to have the beneficial effect observed in the linear case.

Appendix A

Wave preview in turbulent wind

Including only wave preview in the Data-enabled Predictive Control (DeePC) controller in turbulent wind conditions does not bring an improvement to the simple DeePC controller, as illustrated in Figure A-1. Except for a reduction in the platform pitch variance, the feedforward (FF) DeePC relying only on wave preview leads to a performance degradation relative to the baseline controller and the DeePC with no preview, as outlined by Figure A-2. Moreover, the addition of wave preview results in an even larger pitch actuating effort.

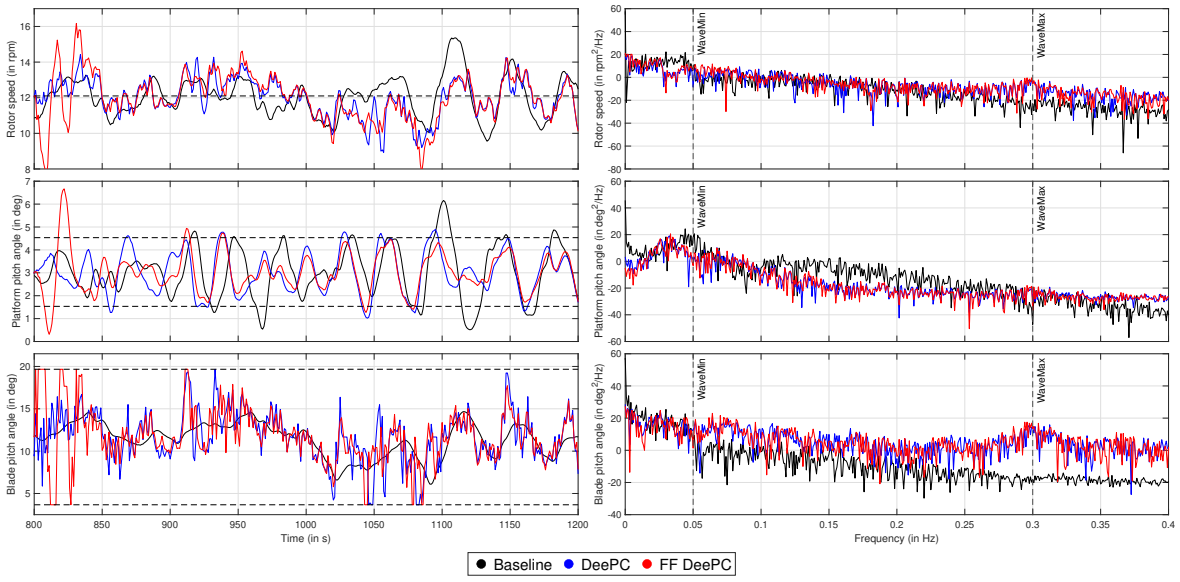

Figure A-1: Simulation of a turbulent wind, irregular waves scenario, with $H_s = 3\,\mathrm{m}$ and $T_p = 12\,\mathrm{s}$. **Left column**: extract of a time series of the rotor speed, platform pitch angle, and blade pitch angle input. **Right column**: Power Spectral Density (PSD) of the respective signals on the left. The two vertical dashed lines delimit the frequency range of the wave disturbance.

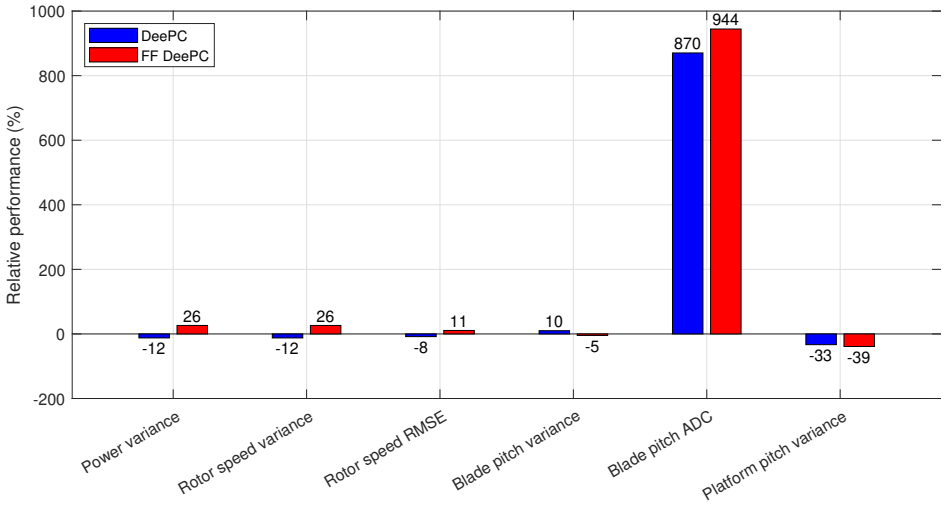

Figure A-2: The performance of the DeePC and FF DeePC relative to the baseline controller in Load case 3.

Due to the reduction in platform pitching motions, the FF DeePC achieves 30% less tower base loads compared to the baseline, but the low-speed shaft torque and out-of-plane blade root bending moment increase by 60% and 50% respectively. In terms of turbine loads, the DeePC without preview also outperforms its feedforward counterpart.

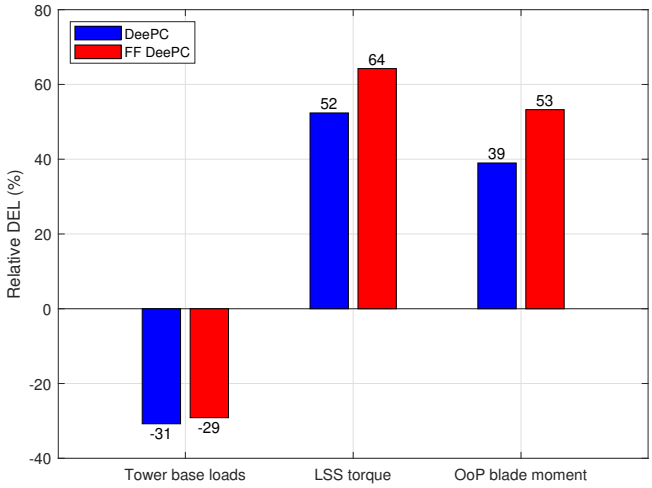

Figure A-3: DELs of the DeePC and FF DeePC relative to the baseline controller in Load case 3.

Bibliography

[1] J. Jonkman, S. Butterfield, W. Musial, and G. Scott, "Definition of a 5-MW reference wind turbine for offshore system development,"National Renewable Energy Lab.(NREL), Golden, CO (United States), Tech. Rep., 2009.

[2] L. Y. Pao and K. E. Johnson, "A tutorial on the dynamics and control of wind turbines and wind farms,"in *2009 American Control Conference*. IEEE, 2009, pp. 2076–2089.

[3] T. J. Larsen and T. D. Hanson, "A method to avoid negative damped low frequent tower vibrations for a floating, pitch controlled wind turbine,"in *Journal of Physics: Conference Series*, vol. 75, no. 1. IOP Publishing, 2007.

[4] J.-W. van Wingerden, S. P. Mulders, R. Dinkla, T. Oomen, and M. Verhaegen, "Data-enabled predictive control with instrumental variables: the direct equivalence with subspace predictive control,"in *2022 IEEE 61st Conference on Decision and Control (CDC)*. IEEE, 2022, pp. 2111–2116.

[5] J. L. Holechek, H. M. Geli, M. N. Sawalhah, and R. Valdez, "A global assessment: can renewable energy replace fossil fuels by 2050?"*Sustainability*, vol. 14, no. 8, p. 4792, 2022.

[6] N. Abas, A. Kalair, and N. Khan, "Review of fossil fuels and future energy technologies,"*Futures*, vol. 69, pp. 31–49, 2015.

[7] K. R. Smith, M. Jerrett, H. R. Anderson, R. T. Burnett, V. Stone, R. Derwent, R. W. Atkinson, A. Cohen, S. B. Shonkoff, D. Krewski *et al.*, "Public health benefits of strategies to reduce greenhouse-gas emissions: health implications of short-lived greenhouse pollutants,"*The Lancet*, vol. 374, no. 9707, pp. 2091–2103, 2009.

[8] V. Masson-Delmotte, P. Zhai, H.-O. Pörtner, D. Roberts, J. Skea, P. R. Shukla *et al.*, "Global warming of 1.5° C: IPCC special report on impacts of global warming of 1.5° C above pre-industrial levels in context of strengthening response to climate change, sustainable development, and efforts to eradicate poverty,"Intergovernmental Panel on Climate Change, Tech. Rep., 2022.

[9] World Meteorological Organization (WMO). (2021) State of the climate 2020: Impacting indicators. [Accessed: 03/05/2023]. [Online]. Available: https://library.wmo.int/doc_num.php?explnum_id=10618

[10] Y. Yang, K. Javanroodi, and V. M. Nik, "Climate change and renewable energy generation in europe—long-term impact assessment on solar and wind energy using high-resolution future climate data and considering climate uncertainties,"*Energies*, vol. 15, no. 1, p. 302, 2022.

[11] L. Sens, U. Neuling, and M. Kaltschmitt, "Capital expenditure and levelized cost of electricity of photovoltaic plants and wind turbines–development by 2050,"*Renewable Energy*, vol. 185, pp. 525–537, 2022.

[12] C. Maienza, A. M. Avossa, V. Picozzi, and F. Ricciardelli, "Feasibility analysis for floating offshore wind energy,"*The International Journal of Life Cycle Assessment*, vol. 27, no. 6, pp. 796–812, 2022.

[13] G. Costanzo, G. Brindley, and P. Cole, "Wind energy in europe: 2022 statistics and the outlook for 2023-2027,"WindEurope, Tech. Rep., 2023.

[14] I. Piasecka, A. Tomporowski, J. Flizikowski, W. Kruszelnicka, R. Kasner, and A. Mroziński, "Life cycle analysis of ecological impacts of an offshore and a land-based wind power plant,"*Applied Sciences*, vol. 9, no. 2, p. 231, 2019.

[15] W. Musial, S. Butterfield, and B. Ram, "Energy from offshore wind,"in *Offshore technology conference*. OnePetro, 2006.

[16] A. Martinez and G. Iglesias, "Mapping of the levelised cost of energy for floating offshore wind in the european atlantic,"*Renewable and Sustainable Energy Reviews*, vol. 154, 2022.

[17] M. Ram, M. Child, A. Aghahosseini, D. Bogdanov, A. Lohrmann, and C. Breyer, "A comparative analysis of electricity generation costs from renewable, fossil fuel and nuclear sources in g20 countries for the period 2015-2030,"*Journal of Cleaner Production*, vol. 199, pp. 687–704, 2018.

[18] H. Díaz, J. Serna, J. Nieto, and C. Guedes Soares, "Market needs, opportunities and barriers for the floating wind industry,"*Journal of Marine Science and Engineering*, vol. 10, no. 7, p. 934, 2022.

[19] J. Jonkman and D. Matha, "Dynamics of offshore floating wind turbines—analysis of three concepts,"*Wind Energy*, vol. 14, no. 4, pp. 557–569, 2011.

[20] S. Butterfield, W. Musial, J. Jonkman, and P. Sclavounos, "Engineering challenges for floating offshore wind turbines,"National Renewable Energy Lab.(NREL), Golden, CO (United States), Tech. Rep., 2007.

[21] T. Salic, J. F. Charpentier, M. Benbouzid, and M. Le Boulluec, "Control strategies for floating offshore wind turbine: challenges and trends,"*Electronics*, vol. 8, no. 10, p. 1185, 2019.

[22] K. E. Johnson, L. Y. Pao, M. J. Balas, and L. J. Fingersh, "Control of variable-speed wind turbines: standard and adaptive techniques for maximizing energy capture,"*IEEE Control Systems Magazine*, vol. 26, no. 3, pp. 70–81, 2006.

[23] E. A. Bossanyi, "Wind turbine control for load reduction,"*Wind Energy: An International Journal for Progress and Applications in Wind Power Conversion Technology*, vol. 6, no. 3, pp. 229–244, 2003.

[24] ——, "The design of closed loop controllers for wind turbines,"*Wind energy: An International Journal for Progress and Applications in Wind Power Conversion Technology*, vol. 3, no. 3, pp. 149–163, 2000.

[25] F. Lemmer, "Low-Order Modeling, Controller Design and Optimization of Floating Offshore Wind Turbines,"Ph.D. dissertation, University of Stuttgart, 2018.

[26] D. Micallef and A. Rezaeiha, "Floating offshore wind turbine aerodynamics: Trends and future challenges,"*Renewable and Sustainable Energy Reviews*, vol. 152, p. 111696, 2021.

[27] G. Van Kuik, J. Peinke, R. Nijssen, D. Lekou, J. Mann, J. N. Sørensen, C. Ferreira, J.-W. van Wingerden, D. Schlipf, P. Gebraad *et al.*, "Long-term research challenges in wind energy - a research agenda by the european academy of wind energy," *Wind energy science*, vol. 1, no. 1, pp. 1–39, 2016.

[28] S. Skogestad and I. Postlethwaite, *Multivariable feedback control: analysis and design*. John Wiley & Sons, 2005.

[29] G. J. Van der Veen, I. J. Couchman, and R. Bowyer, "Control of floating wind turbines,"in *2012 American Control Conference (ACC)*. IEEE, 2012, pp. 3148–3153.

[30] J. Jonkman, "Influence of control on the pitch damping of a floating wind turbine,"in *46th AIAA aerospace sciences meeting and exhibit*, 2008, p. 1306.

[31] W. Yu, F. Lemmer, D. Schlipf, P. W. Cheng, B. Visser, H. Links, N. Gupta, S. Dankemann, B. Counago, and J. Serna, "Evaluation of control methods for floating offshore wind turbines,"in *Journal of Physics: Conference Series*, vol. 1104, no. 1. IOP Publishing, 2018.

[32] H. Namik and K. Stol, "A review of floating wind turbine controllers,"*Handbook of Wind Power Systems*, pp. 415–441, 2013.

[33] J. López-Queija, E. Robles, J. Jugo, and S. Alonso-Quesada, "Review of control technologies for floating offshore wind turbines,"*Renewable and Sustainable Energy Reviews*, vol. 167, 2022.

[34] M. Al, "Feedforward control for wave disturbance rejection on floating offshore wind turbines,"Master's thesis, Delft University of Technology, the Netherlands, 2020.

[35] K. A. Shah, F. Meng, Y. Li, R. Nagamune, Y. Zhou, Z. Ren, and Z. Jiang, "A synthesis of feasible control methods for floating offshore wind turbine system dynamics,"*Renewable and Sustainable Energy Reviews*, vol. 151, 2021.

[36] Y. Ma, P. D. Sclavounos, J. Cross-Whiter, and D. Arora, "Wave forecast and its application to the optimal control of offshore floating wind turbine for load mitigation,"*Renewable Energy*, vol. 128, pp. 163–176, 2018.

[37] F. Lemmer, S. Raach, D. Schlipf, and P. W. Cheng, "Parametric wave excitation model for floating wind turbines,"*Energy Procedia*, vol. 94, pp. 290–305, 2016.

[38] M. A. Lackner, "Controlling platform motions and reducing blade loads for floating wind turbines," *Wind Engineering*, vol. 33, no. 6, pp. 541–553, 2009.

[39] H. Namik, K. Stol, and J. Jonkman, "State-space control of tower motion for deepwater floating offshore wind turbines,"in *46th AIAA aerospace sciences meeting and exhibit*, 2008, p. 1307.

[40] S. Sarkar, B. Fitzgerald, and B. Basu, "Individual blade pitch control of floating offshore wind turbines for load mitigation and power regulation,"*IEEE Transactions on Control Systems Technology*, vol. 29, no. 1, pp. 305–315, 2020.

[41] P. A. Fleming, A. Peiffer, and D. Schlipf, "Wind turbine controller to mitigate structural loads on a floating wind turbine platform,"*Journal of Offshore Mechanics and Arctic Engineering*, vol. 141, no. 6, 2019.

[42] F. Sandner, D. Schlipf, D. Matha, and P. W. Cheng, "Integrated optimization of floating wind turbine systems,"in *International Conference on Offshore Mechanics and Arctic Engineering*, vol. 45547. American Society of Mechanical Engineers, 2014.

[43] P. A. Fleming, I. Pineda, M. Rossetti, A. D. Wright, and D. Arora, "Evaluating methods for control of an offshore floating turbine,"in *International Conference on Offshore Mechanics and Arctic Engineering*, vol. 45547. American Society of Mechanical Engineers, 2014.

[44] F. Lemmer, W. Yu, D. Schlipf, and P. W. Cheng, "Robust gain scheduling baseline controller for floating offshore wind turbines,"*Wind Energy*, vol. 23, no. 1, pp. 17–30, 2020.

[45] K. Takaba, "A tutorial on preview control systems,"in *SICE 2003 annual conference (IEEE Cat. No. 03TH8734)*, vol. 2. IEEE, 2003, pp. 1388–1393.

[46] D. Schlipf, E. Simley, F. Lemmer, L. Pao, and P. W. Cheng, "Collective pitch feedforward control of floating wind turbines using lidar,"in *The Twenty-fifth International Ocean and Polar Engineering Conference*. OnePetro, 2015.

[47] T. Wakui, K. Tanaka, and R. Yokoyama, "Reduction in platform motion and dynamic loads of a floating offshore wind turbine-generator system by feedforward control using wind speed preview,"*Mechanical Engineering Journal*, vol. 9, no. 4, pp. 22–00 066, 2022.

[48] A. Fontanella, M. Al, J.-W. van Wingerden, and M. Belloli, "Model-based design of a wave-feedforward control strategy in floating wind turbines,"*Wind Energy Science*, vol. 6, no. 3, pp. 885–901, 2021.

[49] F. Lemmer, D. Schlipf, and P. W. Cheng, "Control design methods for floating wind turbines for optimal disturbance rejection,"in *Journal of Physics: Conference Series*, vol. 753, no. 9. IOP Publishing, 2016.

[50] S. Christiansen, T. Knudsen, and T. Bak, "Optimal control of a ballast-stabilized floating wind turbine,"in *2011 IEEE international symposium on computer-aided control system design (CACSD)*. IEEE, 2011, pp. 1214–1219.

[51] O. Bagherieh and R. Nagamune, "Gain-scheduling control of a floating offshore wind turbine above rated wind speed,"*Control Theory and Technology*, vol. 13, no. 2, pp. 160–172, 2015.

[52] G. Betti, M. Farina, A. Marzorati, R. Scattolini, and G. Guagliardi, "Modeling and control of a floating wind turbine with spar buoy platform,"in *2012 IEEE international energy conference and exhibition (ENERGYCON)*. IEEE, 2012, pp. 189–194.

[53] T. Bakka and H. R. Karimi, "Robust dynamic output feedback control synthesis with pole placement constraints for offshore wind turbine systems,"*Mathematical Problems in Engineering*, vol. 2012, 2012.

[54] S. T. Navalkar, J.-W. van Wingerden, P. A. Fleming, and G. Van Kuik, "Integrating robust lidar-based feedforward with feedback control to enhance speed regulation of floating wind turbines,"in *2015 American Control Conference (ACC)*. IEEE, 2015, pp. 3070–3075.

[55] T. Bakka and H. R. Karimi, "Mixed H_2/H_∞ control design for wind turbine system with pole placement constraints,"in *Proceedings of the 31st Chinese Control Conference*. IEEE, 2012, pp. 4775–4780.

[56] H. Namik and K. Stol, "Disturbance accommodating control of floating offshore wind turbines,"in *47th AIAA aerospace sciences meeting including the new horizons forum and aerospace exposition*, 2009, p. 483.

[57] T. Bakka, H.-R. Karimi, and S. Christiansen, "Linear parameter-varying modelling and control of an offshore wind turbine with constrained information,"*IET Control Theory & Applications*, vol. 8, no. 1, pp. 22–29, 2014.

[58] J. Laks, L. Pao, A. Wright, N. Kelley, and B. Jonkman, "The use of preview wind measurements for blade pitch control,"*Mechatronics*, vol. 21, no. 4, pp. 668–681, 2011.

[59] D. Schlipf, F. Lemmer, and S. Raach, "Multi-variable feedforward control for floating wind turbines using lidar,"in *The 30th International Ocean and Polar Engineering Conference*. OnePetro, 2020.

[60] A. Hegazy, P. Naaijen, and J.-W. van Wingerden, "Wave feedforward control for large floating wind turbines,"in *2023 IEEE Conference on Control Technology and Applications (CCTA)*. IEEE, 2023, pp. 593–598.

[61] K. A. Shah, Y. Li, R. Nagamune, Y. Zhou, and W. U. Rehman, "Platform motion minimization using model predictive control of a floating offshore wind turbine,"*Theoretical and Applied Mechanics Letters*, vol. 11, no. 5, 2021.

[62] F. Lemmer, S. Raach, D. Schlipf, and P. W. Cheng, "Prospects of linear model predictive control on a 10 mw floating wind turbine,"in *International Conference on Offshore Mechanics and Arctic Engineering*, vol. 56574. American Society of Mechanical Engineers, 2015, p. V009T09A071.

[63] S. Christiansen, S. M. Tabatabaeipour, T. Bak, and T. Knudsen, "Wave disturbance reduction of a floating wind turbine using a reference model-based predictive control,"in *2013 American Control Conference*. IEEE, 2013, pp. 2214–2219.

[64] T. Wakui, A. Nagamura, and R. Yokoyama, "Stabilization of power output and platform motion of a floating offshore wind turbine-generator system using model predictive control based on previewed disturbances,"*Renewable Energy*, vol. 173, pp. 105–127, 2021.

[65] F. Sandner, D. Schlipf, D. Matha, R. Seifried, and P. W. Cheng, "Reduced nonlinear model of a spar-mounted floating wind turbine,"2012.

[66] D. Schlipf, F. Sandner, S. Raach, D. Matha, and P. W. Cheng, "Nonlinear model predictive control of floating wind turbines,"in *The Twenty-third International Offshore and Polar Engineering Conference*. OnePetro, 2013.

[67] Z.-S. Hou and Z. Wang, "From model-based control to data-driven control: Survey, classification and perspective,"*Information Sciences*, vol. 235, pp. 3–35, 2013.

[68] F. Dörfler, J. Coulson, and I. Markovsky, "Bridging direct and indirect data-driven control formulations via regularizations and relaxations,"*IEEE Transactions on Automatic Control*, vol. 68, no. 2, pp. 883–897, 2022.

[69] Y. Liu, R. M. Ferrari, and J.-W. van Wingerden, "Periodic Load Rejection for Floating Offshore Wind Turbines via Constrained Subspace Predictive Repetitive Control,"in *2021 American Control Conference (ACC)*. IEEE, 2021, pp. 539–544.

[70] R. Dinkla, T. Oomen, J.-W. van Wingerden, and S. P. Mulders, "Data-driven lidar feedforward predictive wind turbine control,"in *2023 IEEE Conference on Control Technology and Applications (CCTA)*. IEEE, 2023, pp. 559–565.

[71] OpenFAST Documentation. [Accessed: 03/05/2023]. [Online]. Available: https://openfast.readthedocs.io/en/main/index.html

[72] D. Marten, "Qblade: a modern tool for the aeroelastic simulation of wind turbines,"2020. [Online]. Available: https://depositonce.tu-berlin.de/handle/11303/11758

[73] J. Coulson, J. Lygeros, and F. Dörfler, "Data-enabled predictive control: In the shallows of the deepc,"in *2019 18th European Control Conference (ECC)*. IEEE, 2019, pp. 307–312.

[74] J. C. Willems, P. Rapisarda, I. Markovsky, and B. L. De Moor, "A note on persistency of excitation,"*Systems & Control Letters*, vol. 54, no. 4, pp. 325–329, 2005.

[75] J. Bongard, J. Berberich, J. Köhler, and F. Allgöwer, "Robust stability analysis of a simple data-driven model predictive control approach,"*IEEE Transactions on Automatic Control*, vol. 68, no. 5, pp. 2625–2637, 2022.

[76] J. Dong, M. Verhaegen, and E. Holweg, "Closed-loop subspace predictive control for fault tolerant mpc design,"*IFAC Proceedings Volumes*, vol. 41, no. 2, pp. 3216–3221, 2008.

[77] W. Favoreel, B. De Moor, and M. Gevers, "SPC: Subspace predictive control,"*IFAC Proceedings Volumes*, vol. 32, no. 2, pp. 4004–4009, 1999.

[78] M. Verhaegen and V. Verdult, *Filtering and system identification: a least squares approach*. Cambridge university press, 2007.

[79] J. Coulson, J. Lygeros, and F. Dörfler, "Distributionally robust chance constrained data-enabled predictive control,"*IEEE Transactions on Automatic Control*, vol. 67, no. 7, pp. 3289–3304, 2021.

[80] I. Markovsky, L. Huang, and F. Dörfler, "Data-driven control based on the behavioral approach: From theory to applications in power systems,"*IEEE Control Systems Magazine*, vol. 43, no. 5, pp. 28–68, 2023.

[81] E. Wong, "Active-set methods for quadratic programming,"Ph.D. dissertation, University of California, San Diego, 2011.

[82] J. Jonkman, "Definition of the floating system for phase iv of oc3,"National Renewable Energy Lab.(NREL), Golden, CO (United States), Tech. Rep., 2010.

[83] J. Jonkman, M. L. Buhl *et al.*, *FAST user's guide*, 2005.

[84] J. M. Jonkman, A. D. Wright, G. J. Hayman, and A. N. Robertson, "Full-system linearization for floating offshore wind turbines in openfast,"in *International Conference on Offshore Mechanics and Arctic Engineering*, vol. 51975. American Society of Mechanical Engineers, 2018, p. V001T01A028.

[85] "LIFEs50+ project,"https://lifes50plus.eu/wp-content/uploads/2015/11/D72_Design_Basis_Retyped-v1.1.pdf, accessed: 2024-01-18.

[86] B. Jonkman, "Turbsim user's guide v2. 00.00,"*Natl. Renew. Energy Lab*, 2014.

[87] K. Hasselmann, T. P. Barnett, E. Bouws, H. Carlson, D. E. Cartwright, K. Enke, J. Ewing, A. Gienapp, D. Hasselmann, P. Kruseman *et al.*, "Measurements of wind-wave growth and swell decay during the joint north sea wave project (jonswap)."*Ergaenzungsheft zur Deutschen Hydrographischen Zeitschrift, Reihe A*, 1973.

[88] A. Hegazy, P. Naaijen, V. Leroy, F. Bonnefoy, Y. Pérignon, and J.-W. van Wingerden, "The potential of wave feedforward control for floating wind turbines: A wave tank experiment," *Wind Energy Science Discussions*, vol. 2024, pp. 1–30, 2024.

[89] R. Dinkla, S. P. Mulders, J.-W. van Wingerden, and T. Oomen, "Closed-loop aspects of data-enabled predictive control,"*IFAC-PapersOnLine*, vol. 56, no. 2, pp. 1388–1393, 2023.

Glossary

List of Acronyms

FOWT	Floating offshore Wind Turbine
LCOE	Levelized Cost of Energy
TLP	Tension Leg Platform
SISO	Single-Input Single-Output
MIMO	Multiple-Input Multiple-Output
RNA	Rotor-Nacelle Assembly
CPC	Collective Pitch Control
IPC	Individual Pitch Control
GSPI	Gain Scheduled PI
DoF	Degree of Freedom
FB	feedback
FF	feedforward
LIDAR	LIght Detection And Ranging
LQR	Linear Quadratic Regulator
DAC	Disturbance Accommodating Control
LPV	Linear Parameter Varying
MPC	Model Predictive Control
NMPC	Nonlinear Model Predictive Control
LTI	Linear Time-Invariant
DDC	Data-Driven Control
DeePC	Data-enabled Predictive Control
SPC	Subspace Predictive Control
ROM	Reduced-Order Model
NREL	National Renewable Energy Laboratory

FAST	Fatigue, Aerodynamics, Structures, and Turbulence
QP	Quadratic Programming
RMSE	Root Mean Square Error
VAF	Variance Accounted For
PSD	Power Spectral Density
DEL	damage equivalent load
ADC	actuator duty cycle

List of Symbols

$\dot{\theta}_c$	Collective blade pitch rate
η_0	Wave elevation
$\Gamma^{(s)}$	Extended observability matrix
λ_i	Regularization weight of the slack variable i
$\mathcal{K}_{B_i}^{(s)}$	Extended controllability matrix
Ω	Rotor speed
ω_{g}	Generator speed
ω_e	Error between reference and measured generator speed
$\otimes$	Kronecker product
σ_i	Auxiliary slack variable for channel i
τ_{g}	Generator torque
θ_c	Collective blade pitch angle
Θ_{P}	Platform pitch angle
$^\circ$, deg	degree
d	Disturbance vector
D_d	Disturbance scaling matrix
D_u	Input scaling matrix
D_y	Output scaling matrix
e	Zero-mean, white noise vector
$E_{i,s,N}$	Hankel noise data matrix
f	Future window size

$F_{x,\mathrm{P}}$	Wave surge force acting on the platform
g	DeePC vector taking linear combinations of the data matrices
$H^{(s)}_{(B_i,D_i)}$	Block-Toeplitz matrix
I_n	Identity matrix of size $n \times n$
k_{opt}	Optimal mode gain
$M_{y,\mathrm{P}}$	Wave pitch moment acting on the platform
$M_{y,\mathrm{T}}$	Tower base fore-aft bending moment
N	Data batch size
O	Zero matrix
o	Zero vector
P	Electrical power
p	Past window size
P_{rel}	Relative performance
Q	Output weight
R	Input weight
r	Reference vector
T_s	Sampling period
u	Input vector
$U_{i,s,N}$	Hankel input data matrix
v	Wind speed
W	Watt
w	Measurable disturbance vector
$W_{i,s,N}$	Hankel disturbance data matrix
x	State vector
$X_{i,N}$	State block-row sequence
y	Output vector
$Y_{i,s,N}$	Hankel output data matrix
Z_N	Instrumental variable
hz	Hertz
rpm	rotations per minute
var	Variance